NASA TECHNICAL MEMORANDUM

NASA TM X-73,076

NASA TM X-73,076

WIND TUNNEL INVESTIGATION OF THE AERODYNAMIC CHARACTERISTICS OF FIVE FOREBODY MODELS AT HIGH ANGLES OF ATTACK AT MACH NUMBERS FROM 0.25 to 2

Earl R. Keener and Jamshid Taleghani

Ames Research Center
Moffett Field, California 94035

December 1975

1. Report No.	2. Government Accession No.	3. Recipient's Catalog No.
NASA TM X-73,076		

4. Title and Subtitle	5. Report Date
Wind Tunnel Investigation of the Aerodynamic Characteristics of Five Forebody Models at High Angles of Attack at Mach Numbers From 0.25 to 2	December 1975
	6. Performing Organization Code
7. Author(s)	8. Performing Organization Report No.
Earl R. Keener and Jamshid Taleghani	A-6280
	10. Work Unit No.
9. Performing Organization Name and Address	505-06-95
NASA-Ames Research Center Moffett Field, Ca. 94035	11. Contract or Grant No.
	13. Type of Report and Period Covered
12. Sponsoring Agency Name and Address	Technical Memorandum
	14. Sponsoring Agency Code

15. Supplementary Notes

16. Abstract

Five forebody models of various shapes were tested in the Ames 6- by 6-Foot Wind Tunnel to determine the aerodynamic characteristics at Mach numbers from 0.25 to 2 at a Reynolds number of 0.8×10^6 (nominal, based on base diameter). At a Mach number of 0.6 the Reynolds number was varied from 0.4 to 1.8×10^6 (nominal). Angle of attack was varied from -2° to 88° at zero sideslip. The purpose of the investigation was to determine the effect of Mach number on the side force that develops at low speeds and zero sideslip for all of these forebody models when the nose is pointed.

Test results show that with increasing Mach number the maximum side forces decrease to zero between Mach numbers of 0.8 and 1.5, depending on the nose angle; the smaller the nose angle the higher the Mach number at which the side force exists. At a Mach number of 0.6 there is some variation of side force with Reynolds number, the variation being the largest for the more slender tangent ogive ($\ell/d = 5$).

17. Key Words (Suggested by Author(s))	18. Distribution Statement
Aerodynamic Characteristics Transonic Bodies High Angle of Attack	Unlimited STAR Category 02

19. Security Classif. (of this report)	20. Security Classif. (of this page)	21. No. of Pages	22. Price*
Unclassified	Unclassified	101	

*For sale by the National Technical Information Service, Springfield, Virginia 22151

WIND TUNNEL INVESTIGATION OF THE AERODYNAMIC CHARACTERISTICS OF FIVE FOREBODY MODELS AT HIGH ANGLES OF ATTACK AT MACH NUMBERS FROM 0.25 TO 2

Earl R. Keener and Jamshid Taleghani*

Ames Research Center

SUMMARY

Five forebody models of various shapes were tested in the Ames 6- by 6-Foot Wind Tunnel to determine the aerodynamic characteristics at Mach numbers from 0.25 to 2 at a Reynolds number of 0.8×10^6 (nominal, based on base diameter). At a Mach number of 0.6 the Reynolds number was varied from 0.4 to 1.8×10^6 (nominal). Angle of attack was varied from -2° to 88° at zero sideslip. The purpose of the investigation was to determine the effect of Mach number on the side force that develops at low speeds and zero sideslip for all of these forebody models when the nose is pointed.

Test results show that with increasing Mach number the maximum side forces decrease to zero between Mach numbers of 0.8 and 1.5 depending on the nose angle; the smaller the nose angle the higher the Mach number at which the side force exists. At a Mach number of 0.6 there is some variation of side force with Reynolds number, the variation being the largest for the more slender tangent ogive ($\ell/d=5$).

INTRODUCTION

When bodies of revolution are pitched to high angles of attack, a side force can occur at zero sideslip angle. This side force results when the separation-induced vortex flow field on the lee side of the body becomes asymmetric. Although occurrence of asymmetric body vortex flow is well known, research on the phenomenon has increased considerably in recent years with the advent of highly maneuverable aircraft because the side force and yawing moment could contribute to the onset of aircraft spin (ref. 1). To date, much of the research on asymmetric forces has centered on studies of forces on long slender bodies. For example, references 2-4 present recent test results obtained at Ames for bodies with various nose shapes and cross sections. Results for forebody models tested at low speed and low Reynolds number (ref. 5) showed that the configuration of the forebody might play an important role in the spin characteristics of the

* Project engineer, ARO, Inc.

aircraft. Accordingly a comprehensive wind tunnel test program was undertaken to obtain static aerodynamic data for forebody-alone models, covering a wide range of forebody shapes and a wide range of Reynolds numbers and Mach numbers. The objective was to determine the effect of forebody on the forces and moments so that design criteria could be established for aircraft and missiles with good high angle-of-attack aerodynamic characteristics. Selected results of tests at low subsonic speeds have been presented in reference 6.

This report presents static aerodynamic data for the same five forebody models of reference 6 at transonic and supersonic Mach numbers. The data obtained from the tests are presented with a minimum of analysis.

NOMENCLATURE

The axis system and sign convention are presented in figure 1. Except for lift and drag coefficients, the data are presented in the body axis coordinate system with the moment center located at the base of the forebody models. Because the data were computer plotted, the corresponding plot symbol, where used, is given together with the conventional symbol.

Symbol	Plot Symbol	Definition
b	B	span of elliptic forebody at base (major or minor axis of base depending on the orientation of the model; major or minor axis horizontal)
C_A	CA	axial-force coefficient; axial force/qS
C_{AF}	CAF	axial-force coefficient adjusted for base pressure equal to free stream static pressure, $[C_A + C_{pb}$ (base area/S)]
C_m	CLM	pitching-moment coefficient, pitching moment/qSd
$C_{m,R}$	CRM	resultant-moment coefficient, $C_n \sin \Psi + C_m \cos \Psi$
C_N	CN	normal-force coefficient, normal force/qS
$\lvert C_N \rvert$	ACN	absolute value of C_N
C_n	CYN	yawing-moment coefficient, yawing moment/qSd

Symbol	Plot Symbol	Definition
CP_R	CPR	resultant-force center of pressure location, fraction of length, ℓ, from nose tip, $1-(C_{m,R}/C_R)\ (d/\ell)$
$C_{p,b}$	CPB	base pressure coefficient, $(p_b - p)/q$
C_R	CR	resultant-force coefficient in body axis system, $\sqrt{C_N^2 + C_Y^2}$
C_Y	CY	side-force coefficient; side force/qS
$\lvert C_Y \rvert$	ACY	absolute value of C_Y
d	D	reference base diameter (for elliptic body it is taken to be the span, b, at the base)
ℓ	L	reference length (length of forebodies with pointed noses, except reference length of paraboloid is with parabolic nose)
M	MACH	free stream Mach number
p		free stream static pressure
p_b		base pressure
q		free stream dynamic pressure
R	R	Reynolds number, based on base diameter
R/d		unit Reynolds number, 10^6/m
S	S	area of base (elliptic body: area of an equivalent circular base with a diameter equal to the span of the base)
α	ALPHA	angle of attack
β	BETA	angle of sideslip
δ_N		nose semiapex angle
Ψ	PSI	angle between the resultant and normal forces, resultant force inclined to the right is positive angle looking upstream, $\tan^{-1}(C_Y/C_N)$

MODEL CONFIGURATION CODE

Symbol	Definition
FC1	conical forebody with pointed nose
FEH	elliptic tangent ogive forebody with pointed nose; major axis horizontal
FEV	elliptic tangent ogive forebody with pointed nose; major axis vertical
FP	parabolic forebody with pointed nose
FT3.5	tangent ogive forebody with pointed nose; $\ell/d=3.5$
FT5	tangent ogive forebody with pointed nose; $\ell/d=5.0$

TEST FACILITY

The models were tested in the Ames Research Center 6- by 6-Foot Supersonic Wind Tunnel, which is a variable pressure, continuous flow facility. The nozzle leading to the test section is of the asymmetric sliding-block type which permits a continuous variation of Mach number from 0.6 to 2.3. A Mach number of 0.25 was obtained with special speed control settings; however, this Mach number is not generally used in test programs because of relatively rough air flow. Limited data, therefore, were obtained at this Mach number. The test section has a perforated floor and ceiling with provisions for boundary layer removal.

MODEL DESCRIPTION

Figure 2 is a sketch of the five forebody models designed to represent forebodies of aircraft fuselages or missiles; Table 1 lists the dimensions. Photographs of one of the models and the wind tunnel installation are shown in figure 3. Four of the forebodies were bodies of revolution: two tangent ogives with fineness ratios of 3.5 and 5.0, a paraboloid, and a cone. Although all of these bodies had removable nose sections of various nose radii, only the pointed nose tips were used in the present investigation. The paraboloid was provided with a pointed nose with an apex angle (32.9°) identical to that of the $\ell/d = 3.5$ tangent ogive (see Table 1 for apex angles of the other bodies). The fifth body was designed with an elliptic cross section that could be tested with either

the major or the minor axis perpendicular to the crossflow velocity. The major and minor axes of the base were selected so that the respective ℓ/d values were 3.5 and 5.0 to coincide with the circular tangent ogive values.

TESTING AND PROCEDURES

The investigation was conducted over a Mach number range of 0.6 to 2.0 at a unit Reynolds number of 5×10^6/m. At a Mach number of 0.6 the unit Reynolds number was varied from 2.5×10^6 to 12×10^6/m. Some limited test data were obtained at M = 0.25. Three model-support setups were required to cover the angle of attack ranges: -2° to 28°, 28° to 58° and 58° to 88°. The model support shown in figures 3(a) and 3(b) is a straight sting with a 45° offset support, resulting in an angle of attack range of 28° to 58°. The lower and higher angle ranges were obtained with a sting-bent joint of 30°, bent down for α = -2° to 28° (fig. 3(c)) and bent up for α = 58° to 88°. The angle of sideslip was zero. Aerodynamic forces and moments on the model were measured using an internal six-component strain-gage balance. The model base pressure was measured using one pressure tube attached to the sting and open at the base of the model. The ℓ/d = 3.5 tangent ogive forebody was tested over the maximum angle of attack range of α = -2° to 88°. All other models were tested with the straight sting at α = 28° to 58°. The elliptic tangent ogive was tested with its major axis both horizontal and vertical.

PRESENTATION OF RESULTS

Table 2 is an index of the figures in which the data for each of the five forebody models are presented. In figures 4 to 6 the effects of Mach number and Reynolds number are presented for the angle of attack range of -2° to 88° for the ℓ/d = 3.5 tangent ogive. In figures 7 to 15 the effects of Mach number and Reynolds number are presented for α = 28° to 58° for the ℓ/d = 5 tangent ogive, the paraboloid, the 20 degree cone and the elliptic tangent ogive tested with the major axis horizontal and vertical. The following coefficients are plotted and faired as a function of angle of attack using an automatic data plotting system: C_Y, C_N, $|C_Y|/|C_N|$, $(C_R - C_N)$, C_n, C_m, C_{AF}, CP_R, Ψ, $C_{m,R}$ and $C_{p,b}$. (Note that the results for $|C_Y|/|C_N|$ and CP_R are naturally spurious at angles of attack near zero, because these parameters are undefined at α = 0).

DISCUSSION

The purpose of this investigation was to determine the effect of Mach number on the side force that develops at low speed and zero sideslip for

all of the forebody models when the nose is pointed. Previous tests at subsonic speeds in the Ames 12-Foot Wind Tunnel (ref. 6) showed that the side forces were as large as 1.5 times the normal force and varied considerably with Reynolds number. It was shown in reference 6 that the angle of attack at the onset of side force can be correlated with the nose semiapex angle by a simple formula: onset $\alpha \simeq 2\ \delta_N$. Further, it was found that these side forces can be reduced or eliminated by bluntness or nose strakes.

The present investigation included tests at $M = 0.25$ and $R/d = 5 \times 10^6/m$ for both circular tangent ogives and the cone. The results shown in figures 4, 7, and 10 are similar to the results obtained for the same test conditions in the Ames 12-Foot Tunnel (ref. 6), in that large side forces develop at zero sideslip. Test results for all of the pointed forebodies show that with increasing Mach number the maximum side forces decrease to zero between $M = 0.8$ and 1.5, depending on the nose angle; the smaller the nose angle the higher the Mach number at which the side force exists. Test results at $M = 0.6$ show some variation of side force with Reynolds number. The variation is the largest for the more slender $\ell/d = 5$ tangent ogive.

Ames Research Center
National Aeronautics and Space Administration
Moffett Field, California 94035

November 28, 1975

REFERENCES

1. Chambers, J. R.; Anglin, E. L.; and Bowman, J. S., Jr.: Effects of a Pointed Nose on Spin Characteristics of a Fighter Airplane Model Including Correlation with Theoretical Calculations. NASA TN D-5921, 1970.

2. Jorgensen, Leland H.; and Nelson, Edgar R.: Experimental Aerodynamic Characteristics for a Cylindrical Body of Revolution With Various Noses at Angles of Attack from 0 to 58° and Mach Numbers From 0.6 to 2.0. NASA TM X-3128, 1974.

3. Jorgensen, Leland H.; and Nelson, Edgar R.: Experimental Aerodynamic Characteristics for a Cylindrical Body of Revolution With Side Strakes and Various Noses at Angles of Attack From 0 to 58° and Mach Numbers From 0.6 to 2.0. NASA TM X-3130, 1975.

4. Jorgensen, Leland H.; and Nelson, Edgar R.: Experimental Aerodynamic Characteristics for Bodies of Elliptic Cross Section at Angles of Attack From 0 to 58° and Mach Numbers From 0.6 to 2.0. NASA TM X-3129, 1975

5. Coe, P. L., Jr.; Chambers, J. R.; and Letko, W.: Asymmetric Lateral-Directional Characteristics of Pointed Bodies of Revolution at High Angles of Attack. NASA TN D-7095, 1973.

6. Keener, Earl R.; and Chapman, Gary T.: Onset of Aerodynamic Side Forces at Zero Sideslip on Symmetric Forebodies at High Angles of Attack. AIAA Paper 74-770, 1974.

TABLE 1. - MODEL GEOMETRY

Forebody Shape						
Planform	Crossection	$\frac{\ell}{d}$	ℓ,cm	d,cm	S,cm^2	Sharp nose apex angle, deg
Tangent ogive	Circular	3.5	53.3	15.24	182.4	32.9
Tangent ogive	Circular	5.0	76.2	15.24	182.4	22.8
Tangent ogive	Elliptic					
Major Axis-Horizontal		3.5	66.0	18.87	279.6	32.9
Major Axis-Vertical		5.0	66.0	13.21	137.0	22.8
Cone	Circular	2.84	53.3	18.82	278.2	20.0
Paraboloid	Circular	3.5	53.3	15.24	182.4	32.9

Reference diameter (d) and area (S):

Circular bodies: Base diameter and base area

Elliptic bodies: Span at the base and area of an equivalent circular base with a diameter equal to base span.

TABLE 2. - INDEX OF DATA FIGURES

Notes:

1. Positive directions of force coefficients, moment coefficients, and angles are indicated by arrows
2. For clarity, origins of wind and stability axes have been displaced from the center of gravity

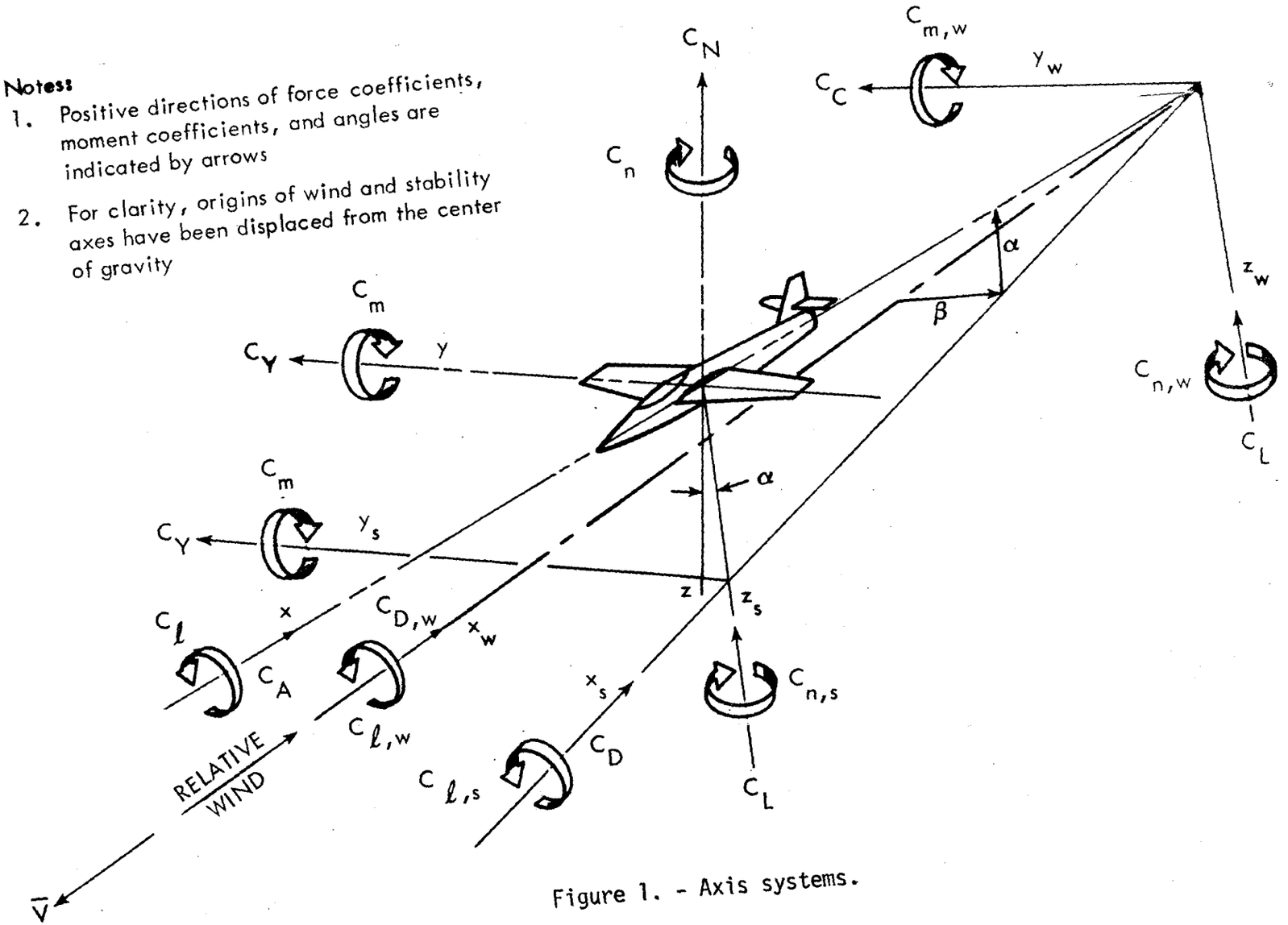

Figure 1. - Axis systems.

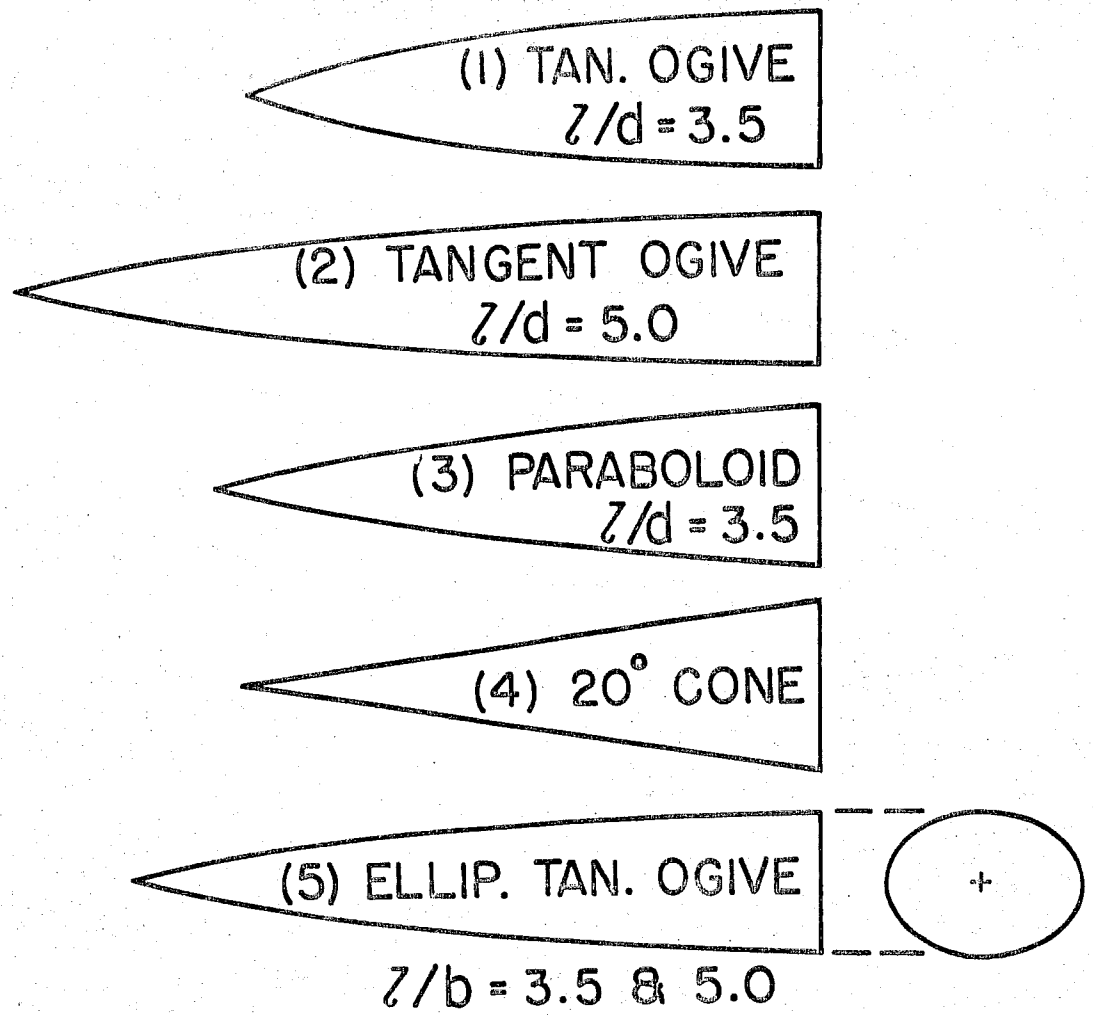

Figure 2. - Sketches of models.

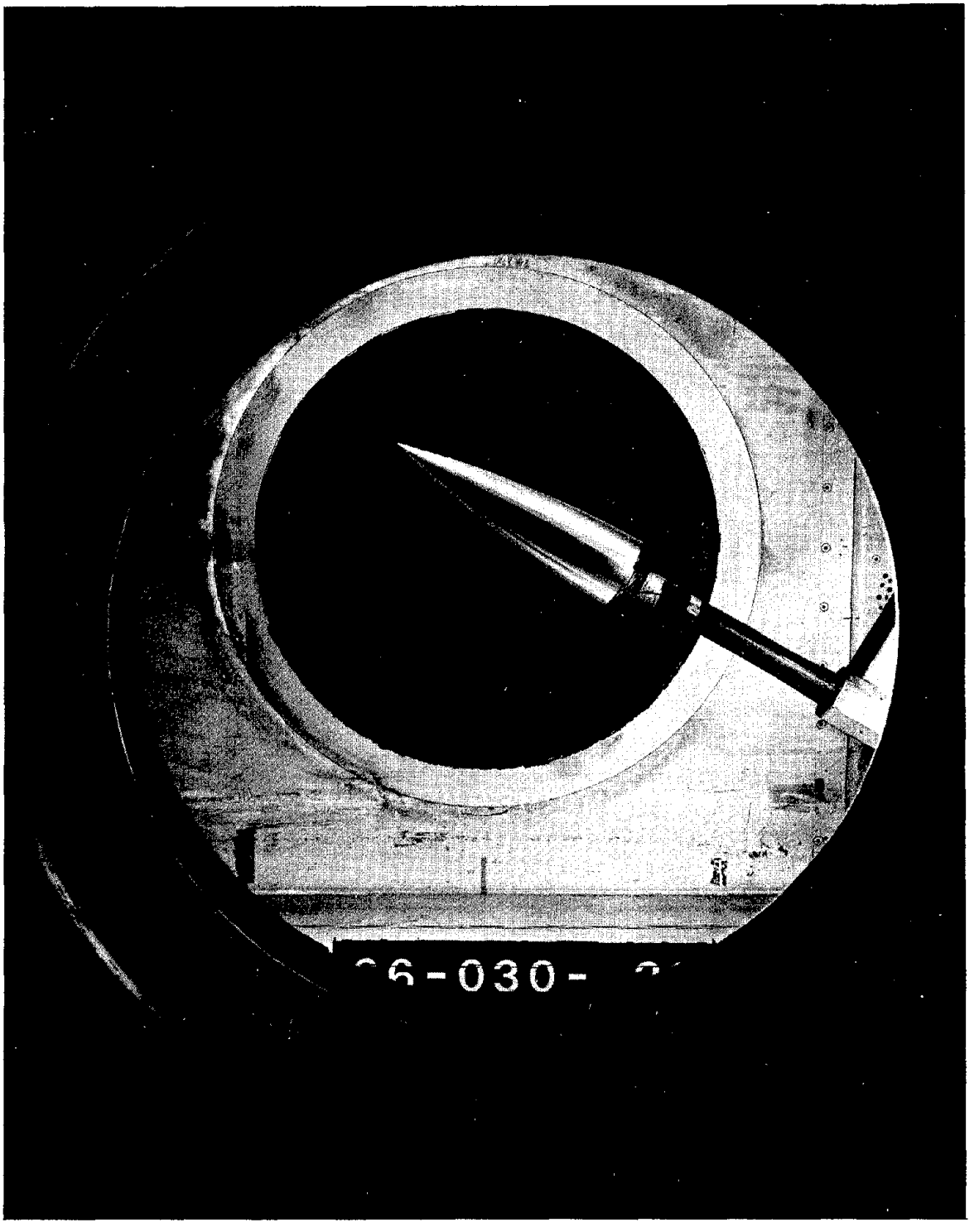

(a) Side View of straight sting support setup for α = 28° to 58°

Figure 3. - Photographs of typical model-support set-ups in the Ames 6- by 6-Foot Wind Tunnel

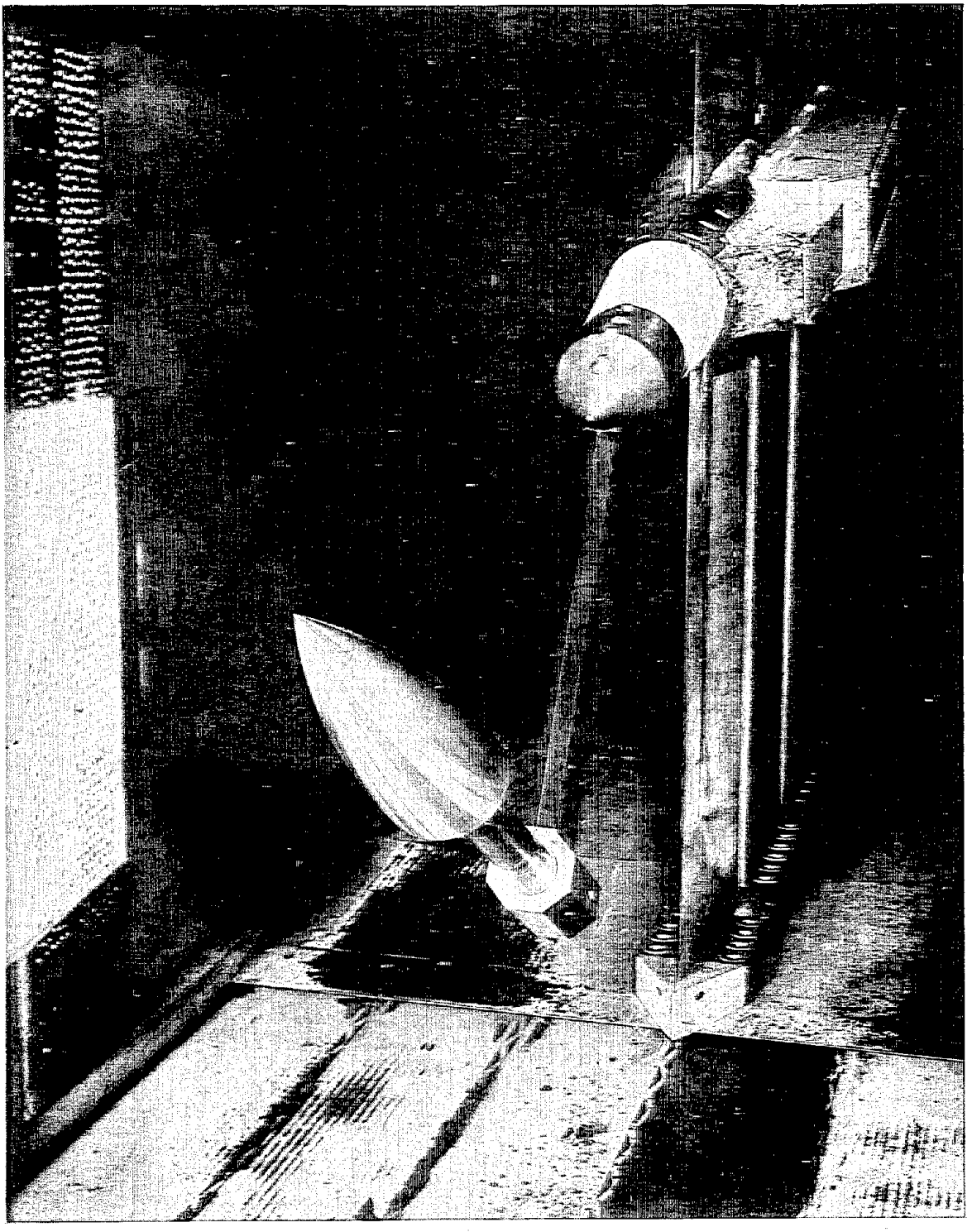

(b) Three-quarter front view of straight sting support setup for α = 28° to 58°

Figure 3. - Continued

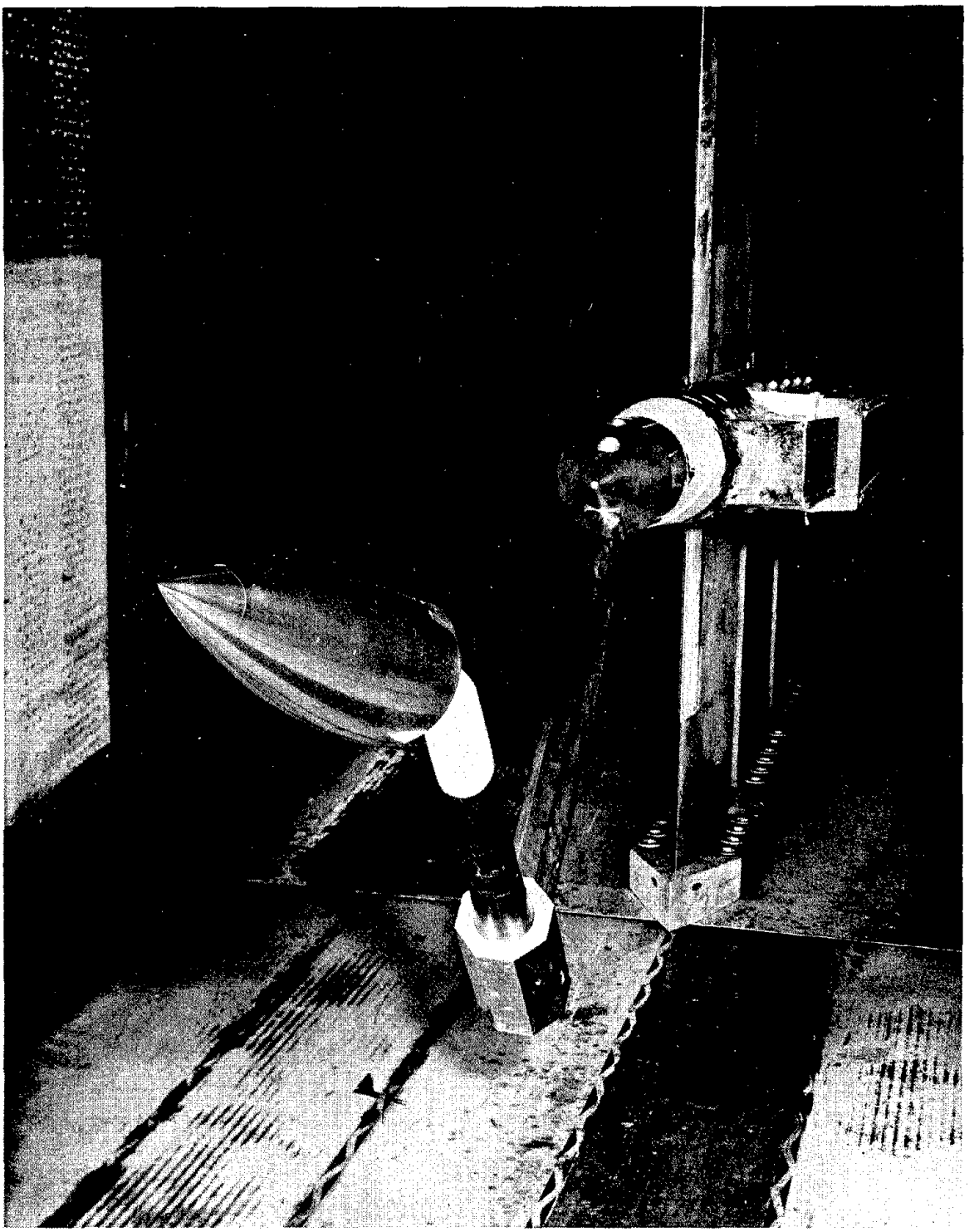

(c) Three-quarter front view of 30° bent sting support setup for α = -2° to 28°

Figure 3. - Concluded

DATA

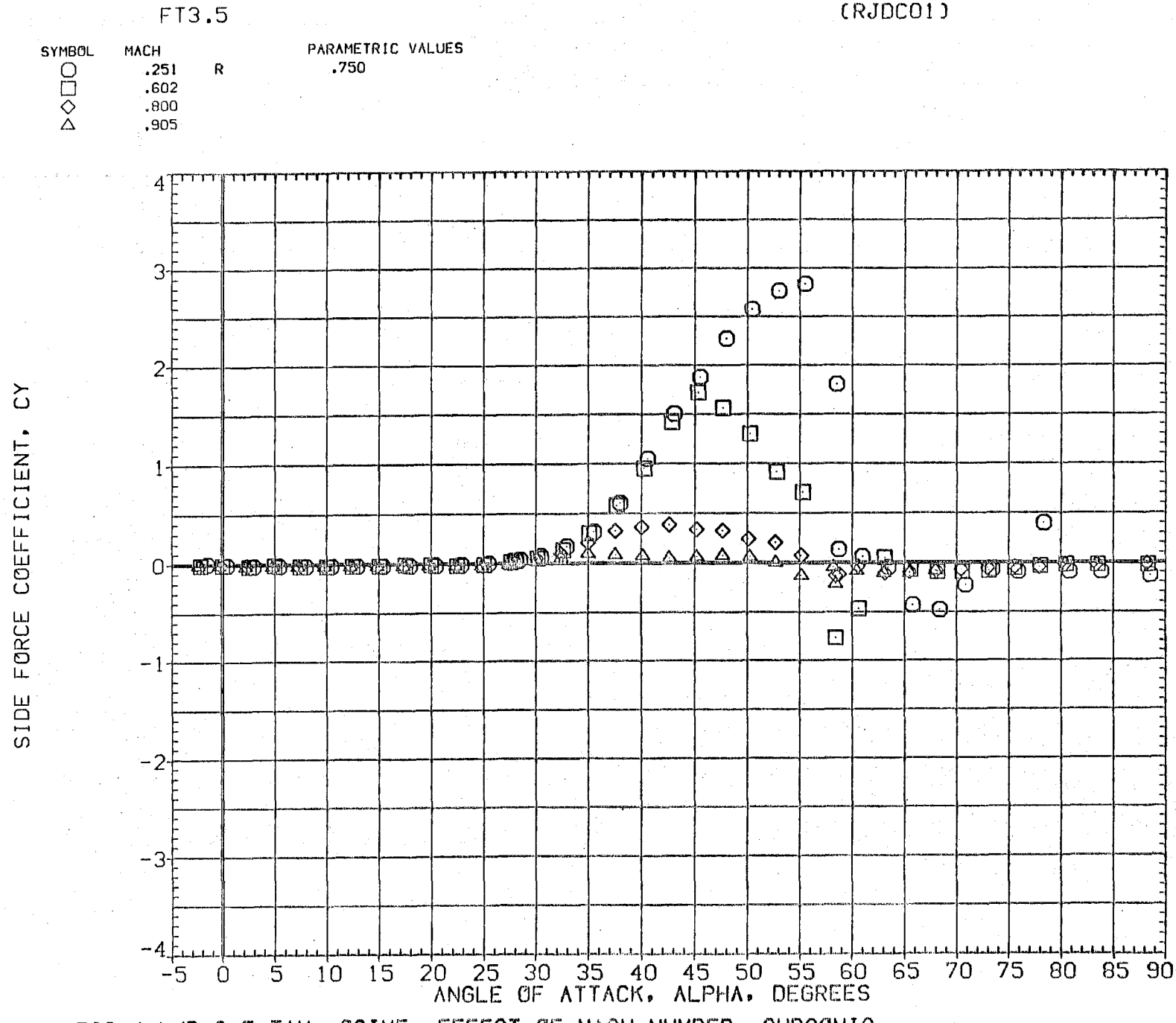

FIG.4 L/D=3.5 TAN. OGIVE, EFFECT OF MACH NUMBER, SUBSONIC

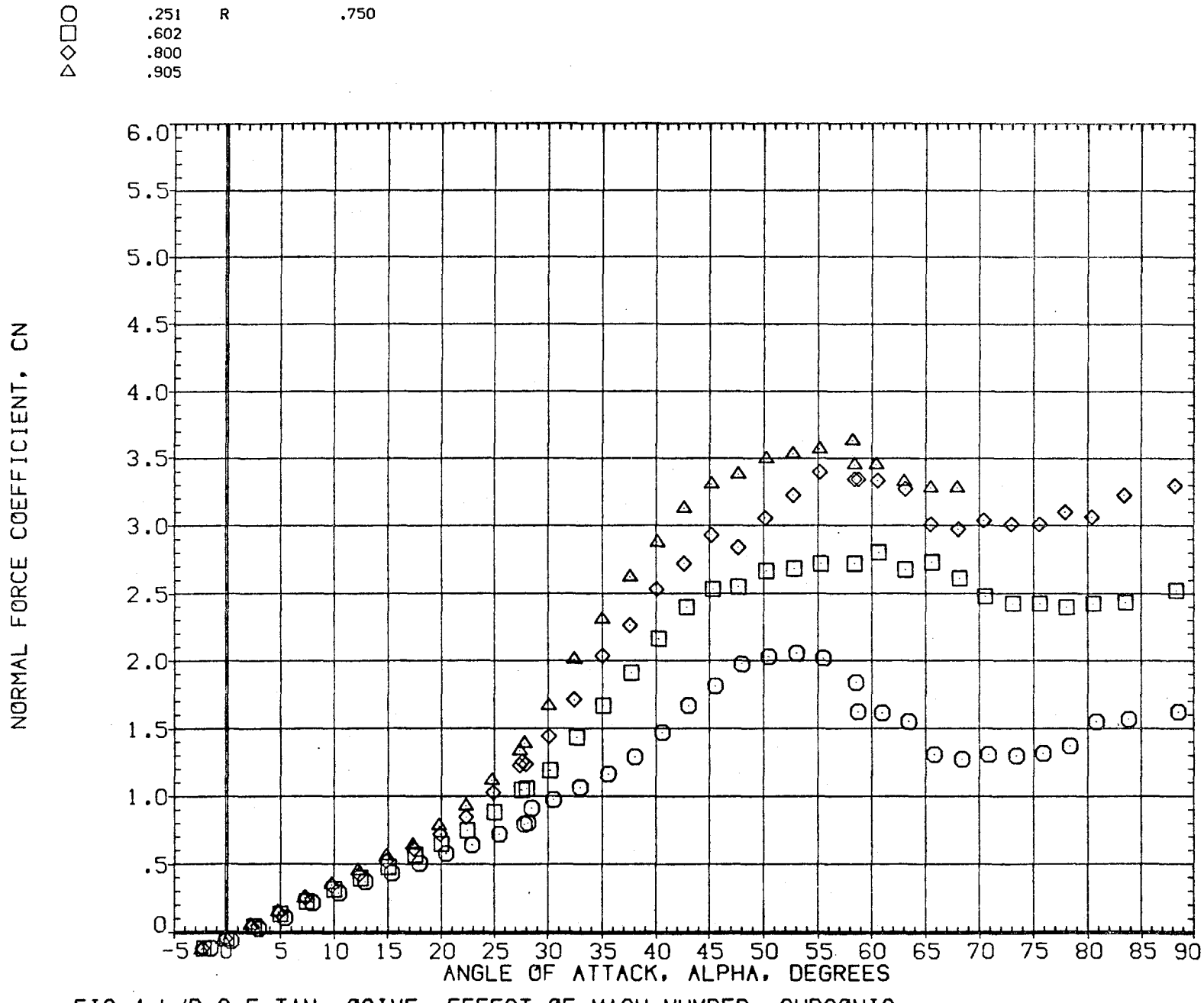

FIG.4 L/D=3.5 TAN. OGIVE, EFFECT OF MACH NUMBER, SUBSONIC

FT3.5 (RJDC01)

SYMBOL	MACH		PARAMETRIC VALUES
○	.251	R	.750
□	.602		
◇	.800		
△	.905		

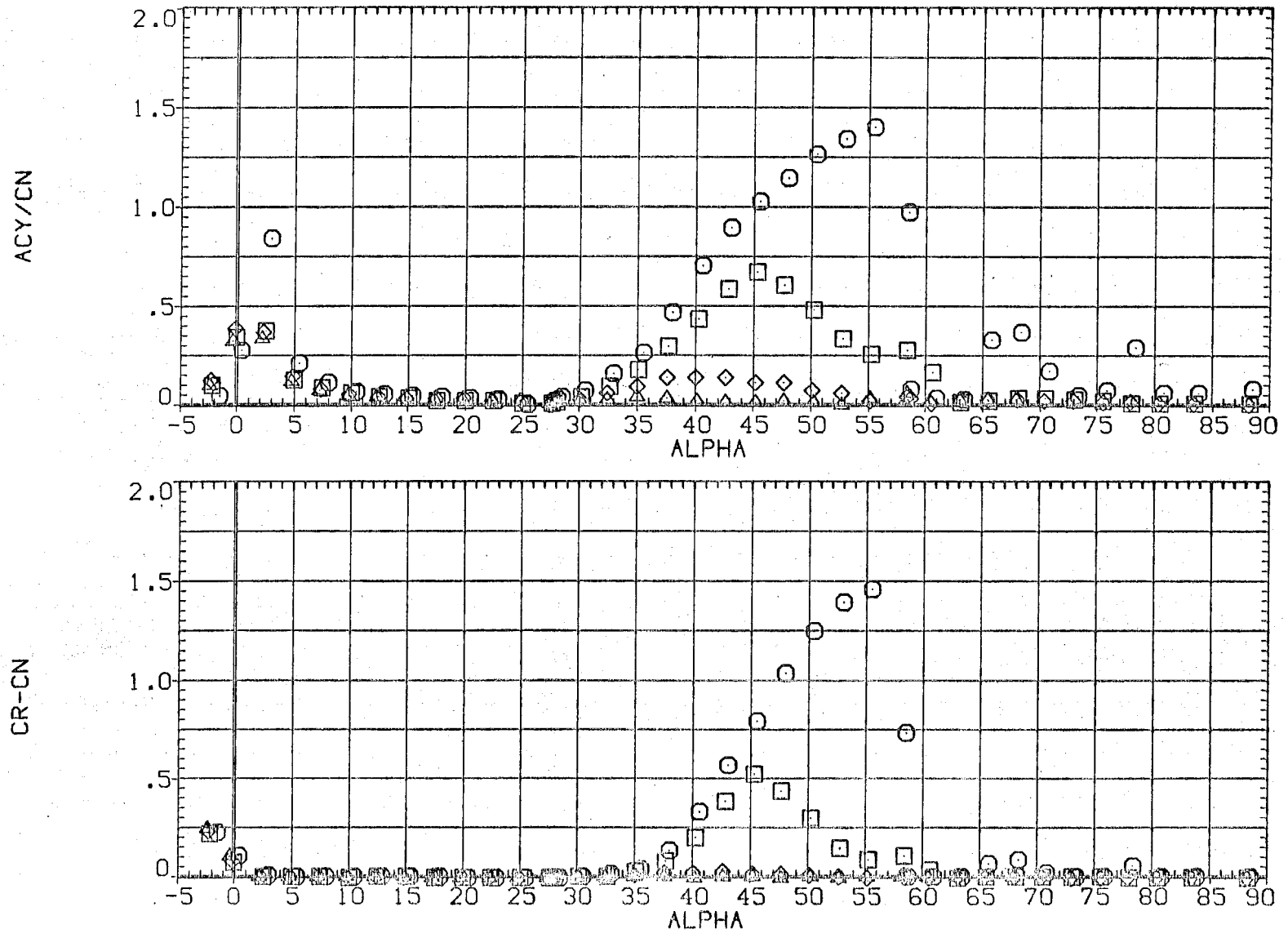

FIG.4 L/D=3.5 TAN. OGIVE, EFFECT OF MACH NUMBER, SUBSONIC

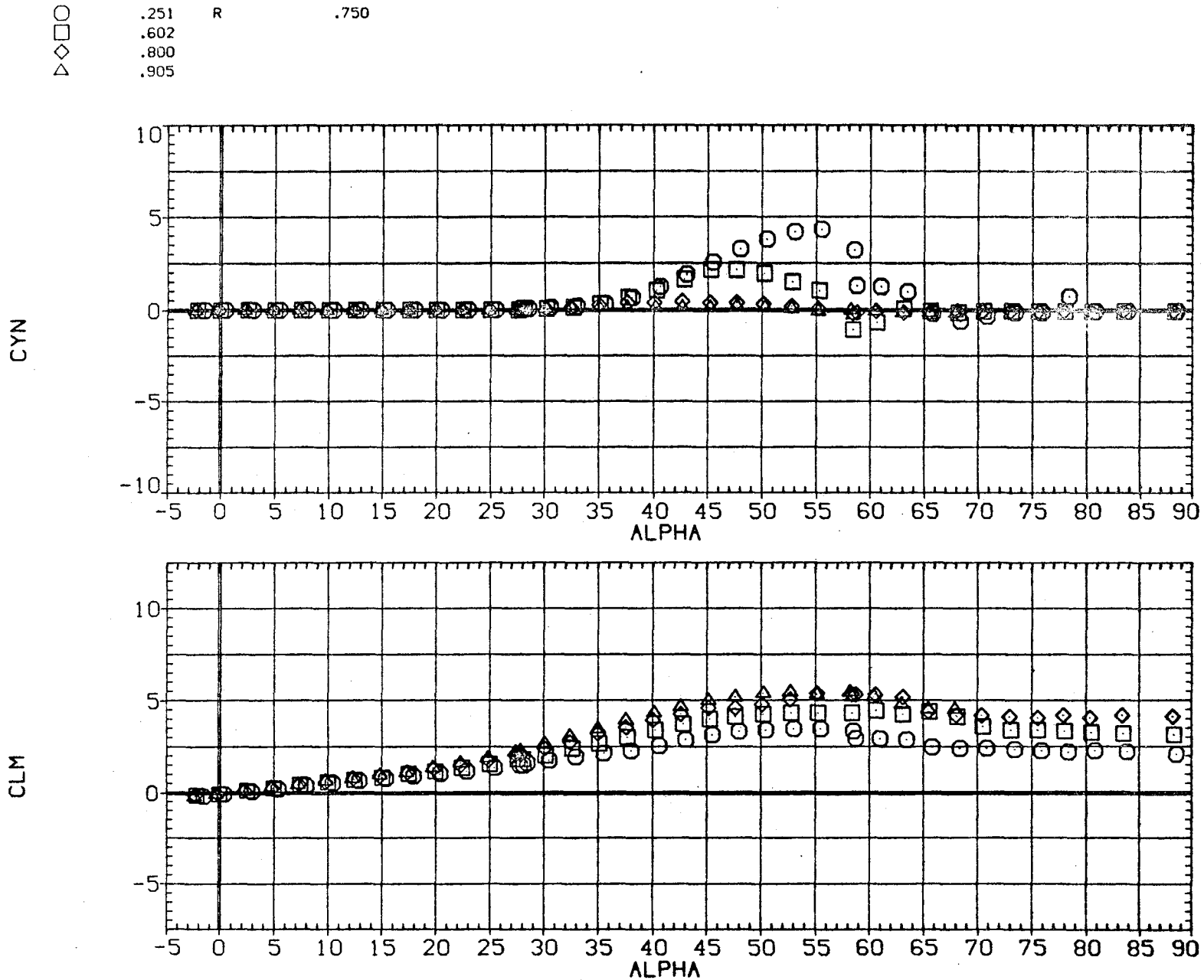

FIG.4 L/D=3.5 TAN. OGIVE, EFFECT OF MACH NUMBER, SUBSONIC

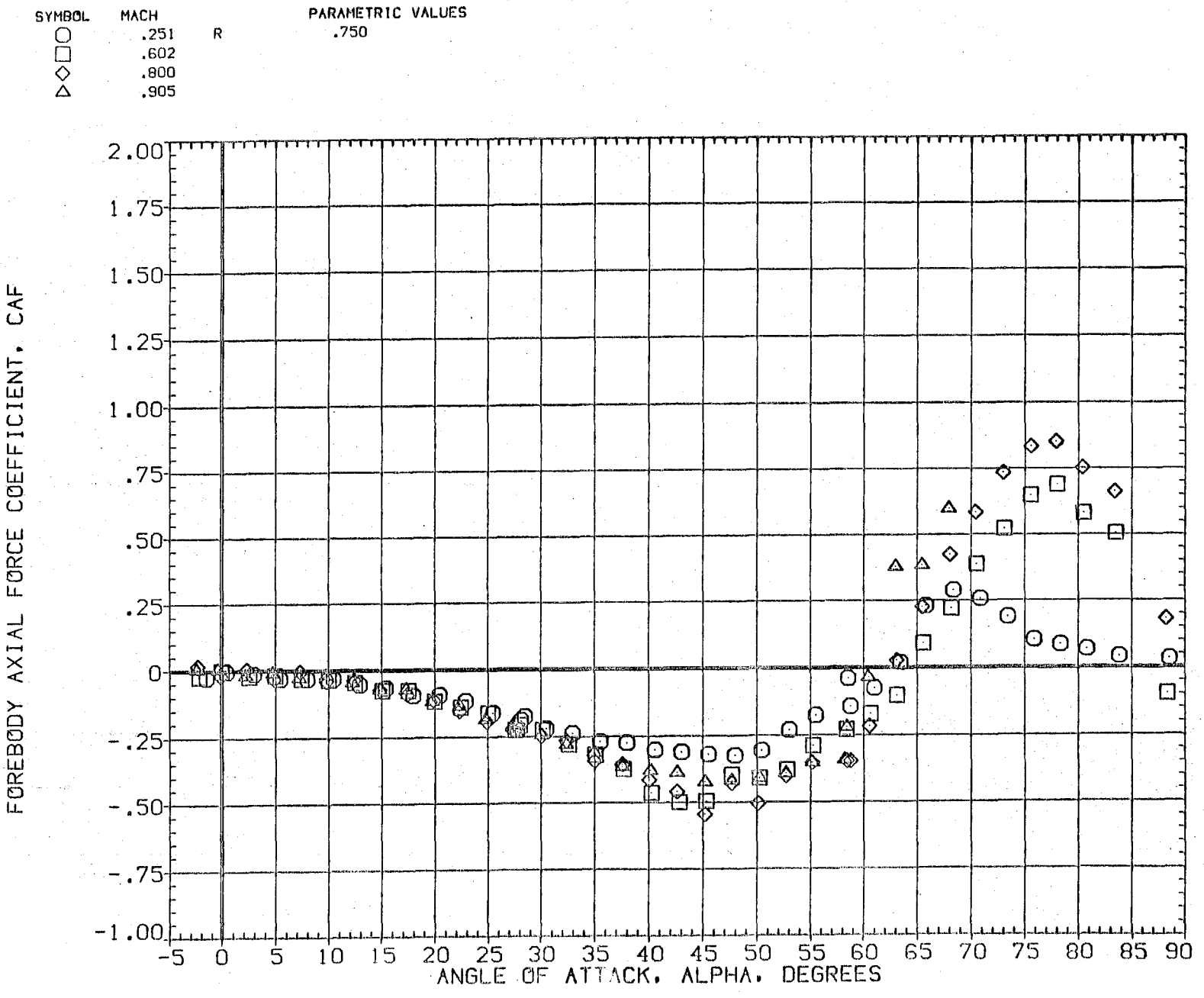

FIG.4 L/D=3.5 TAN. OGIVE, EFFECT OF MACH NUMBER, SUBSONIC

SYMBOL	MACH		PARAMETRIC VALUES
○	.251	R	.750
□	.602		
◇	.800		
△	.905		

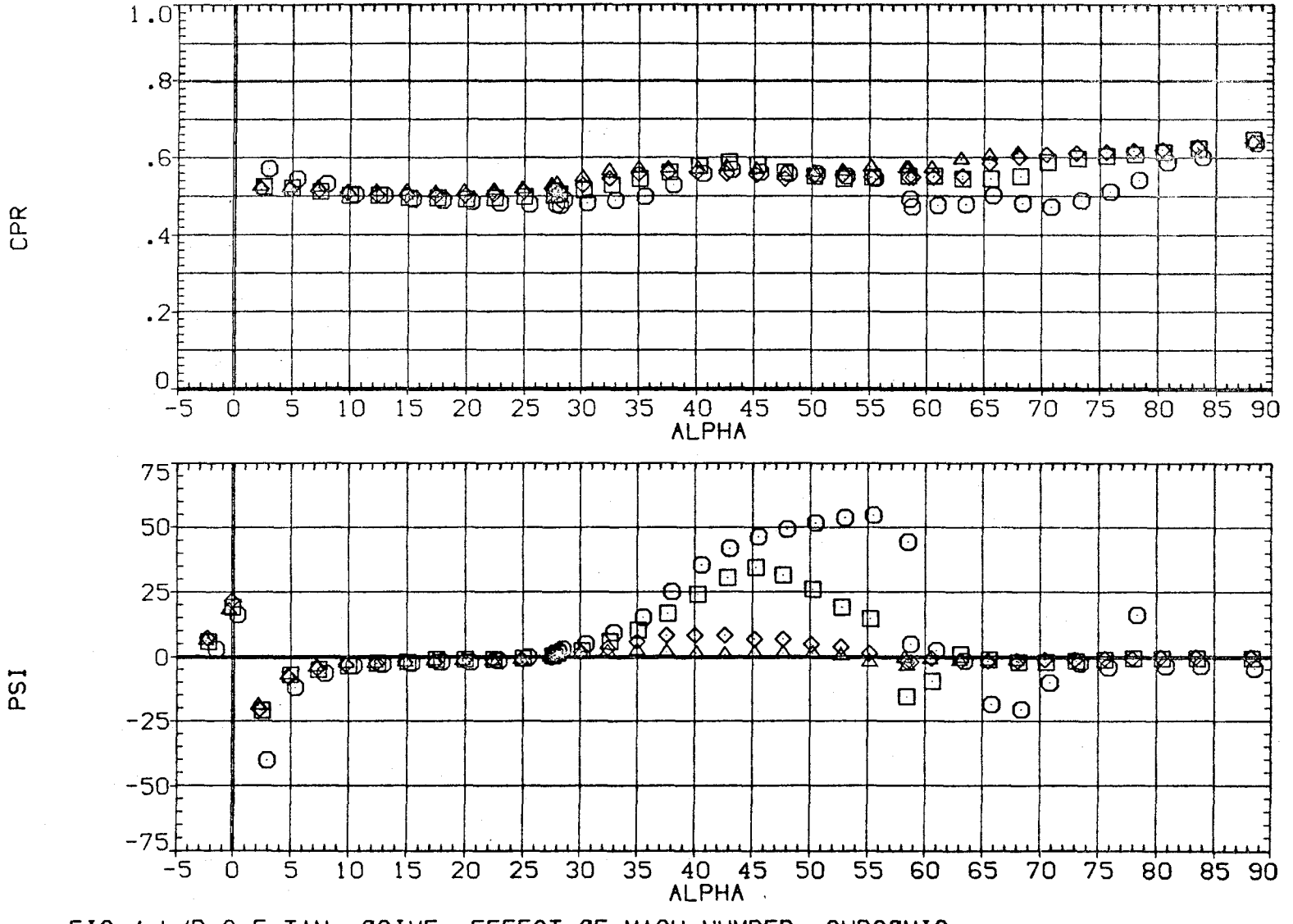

FIG.4 L/D=3.5 TAN. OGIVE, EFFECT OF MACH NUMBER, SUBSONIC

SYMBOL	MACH		PARAMETRIC VALUES
○	.251	R	.750
□	.602		
◇	.800		
△	.905		

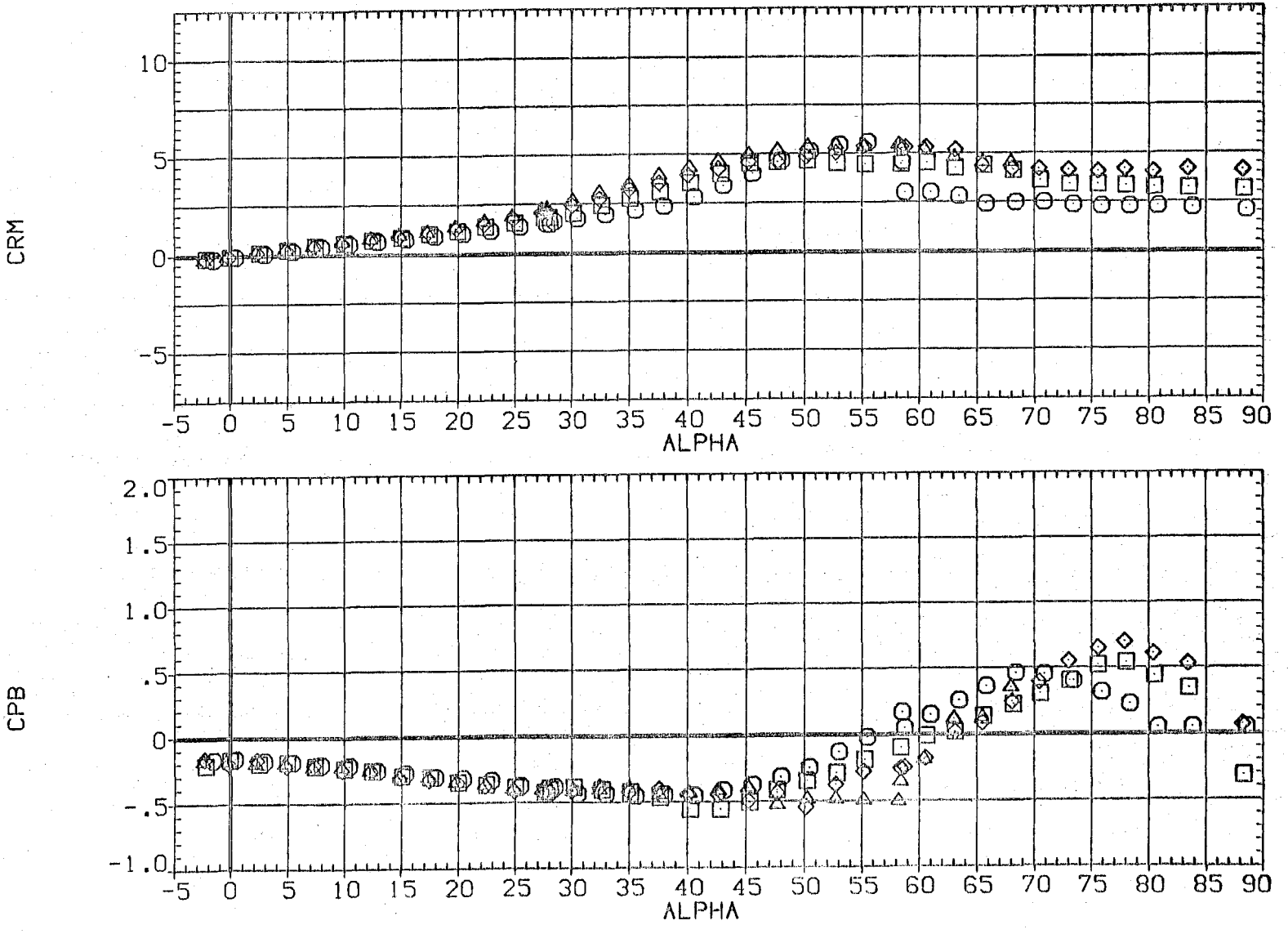

FIG.4 L/D=3.5 TAN. OGIVE, EFFECT OF MACH NUMBER, SUBSONIC.

SYMBOL	MACH		PARAMETRIC VALUES
○	1.195	R	.750
□	1.506		
◇	1.993		

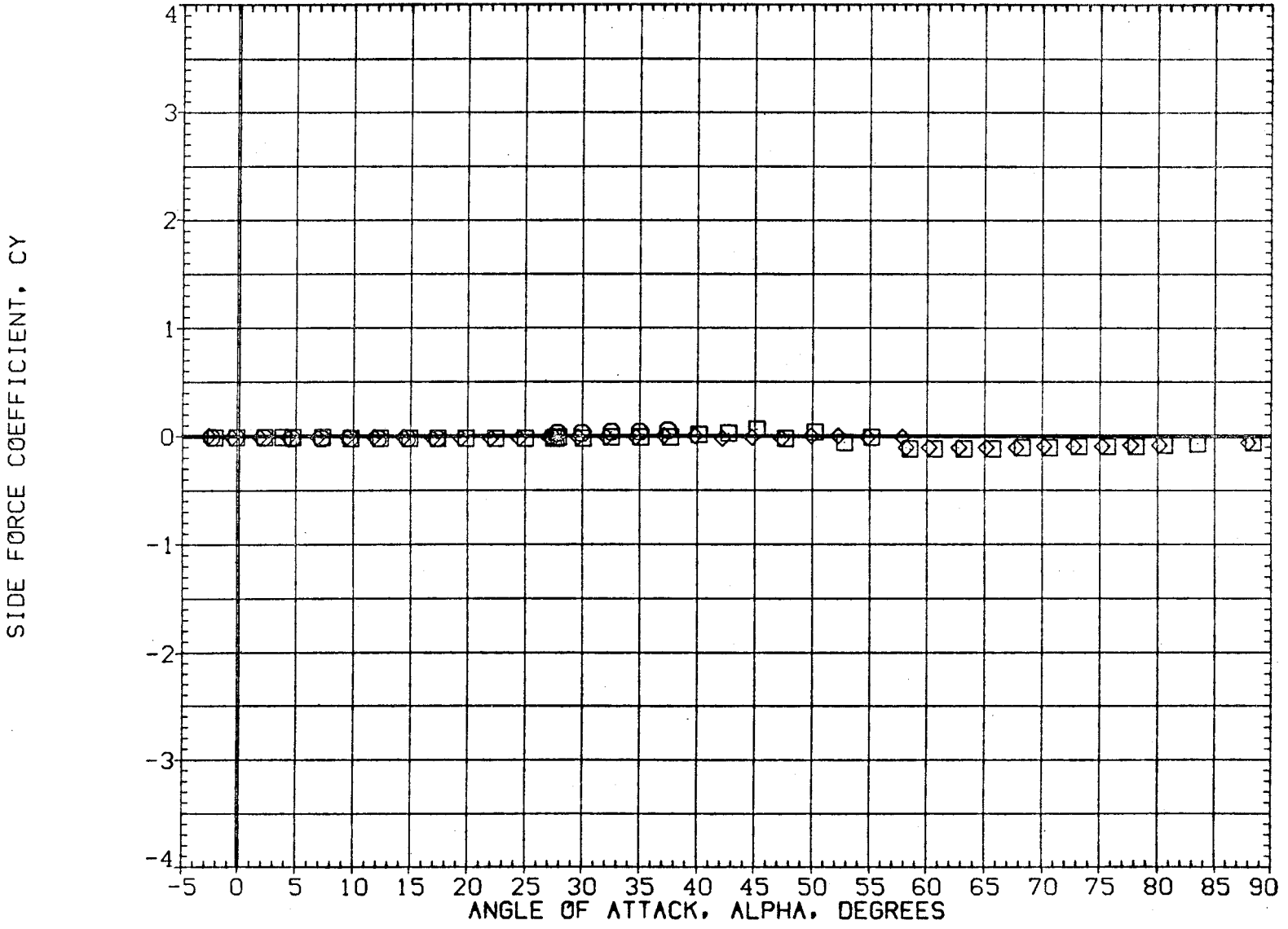

FIG.5 L/D=3.5 TAN. OGIVE, EFFECT OF MACH NUMBER, SUPERSONIC

SYMBOL	MACH		PARAMETRIC VALUES
○	1.195	R	.750
□	1.506		
◇	1.993		

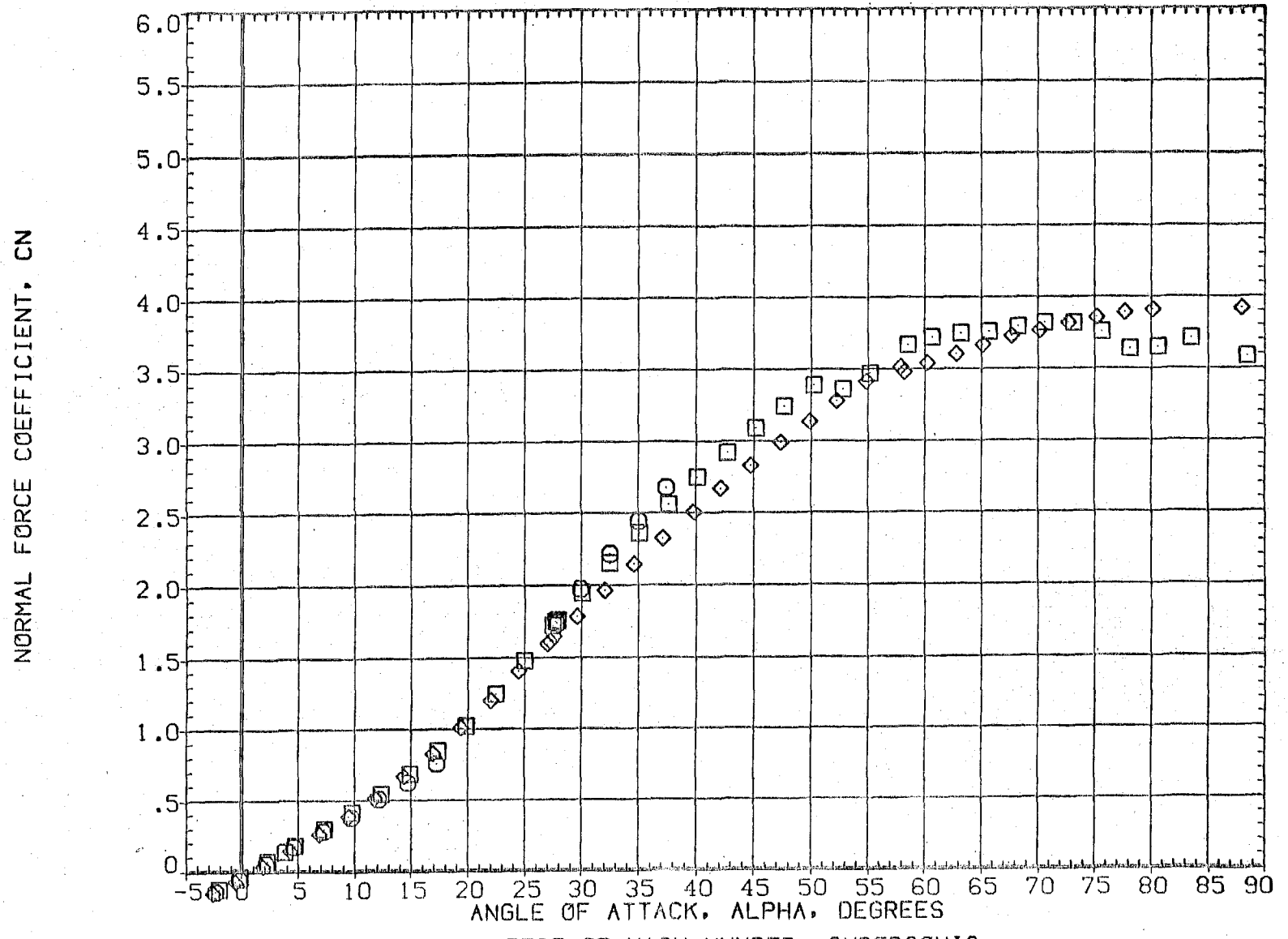

FIG.5 L/D=3.5 TAN. OGIVE, EFFECT OF MACH NUMBER, SUPERSONIC

SYMBOL	MACH		PARAMETRIC VALUES
○	1.195	R	.750
□	1.506		
◇	1.993		

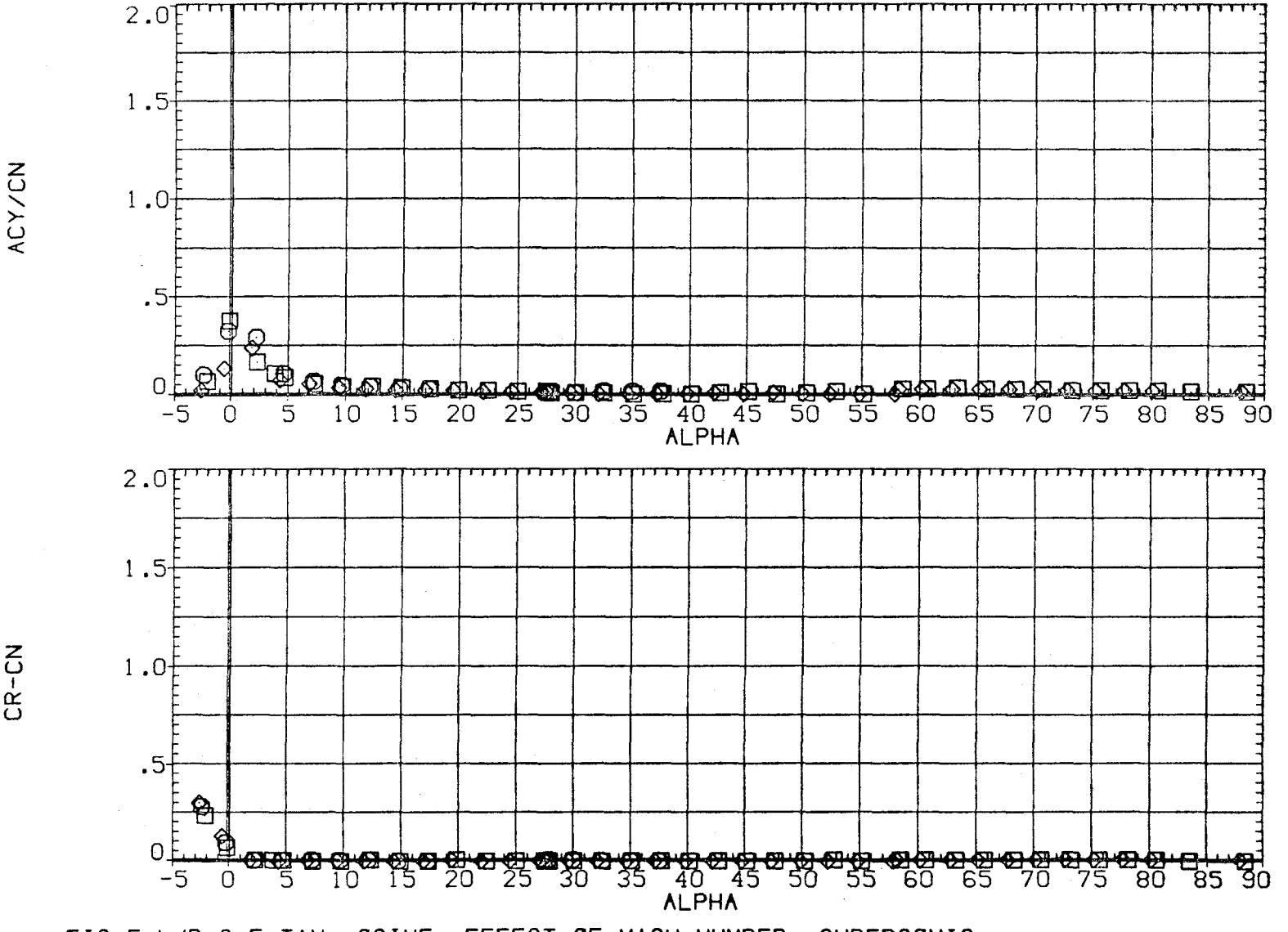

FIG.5 L/D=3.5 TAN. OGIVE, EFFECT OF MACH NUMBER, SUPERSONIC

SYMBOL	MACH		PARAMETRIC VALUES
○	1.195	R	.750
□	1.506		
◇	1.993		

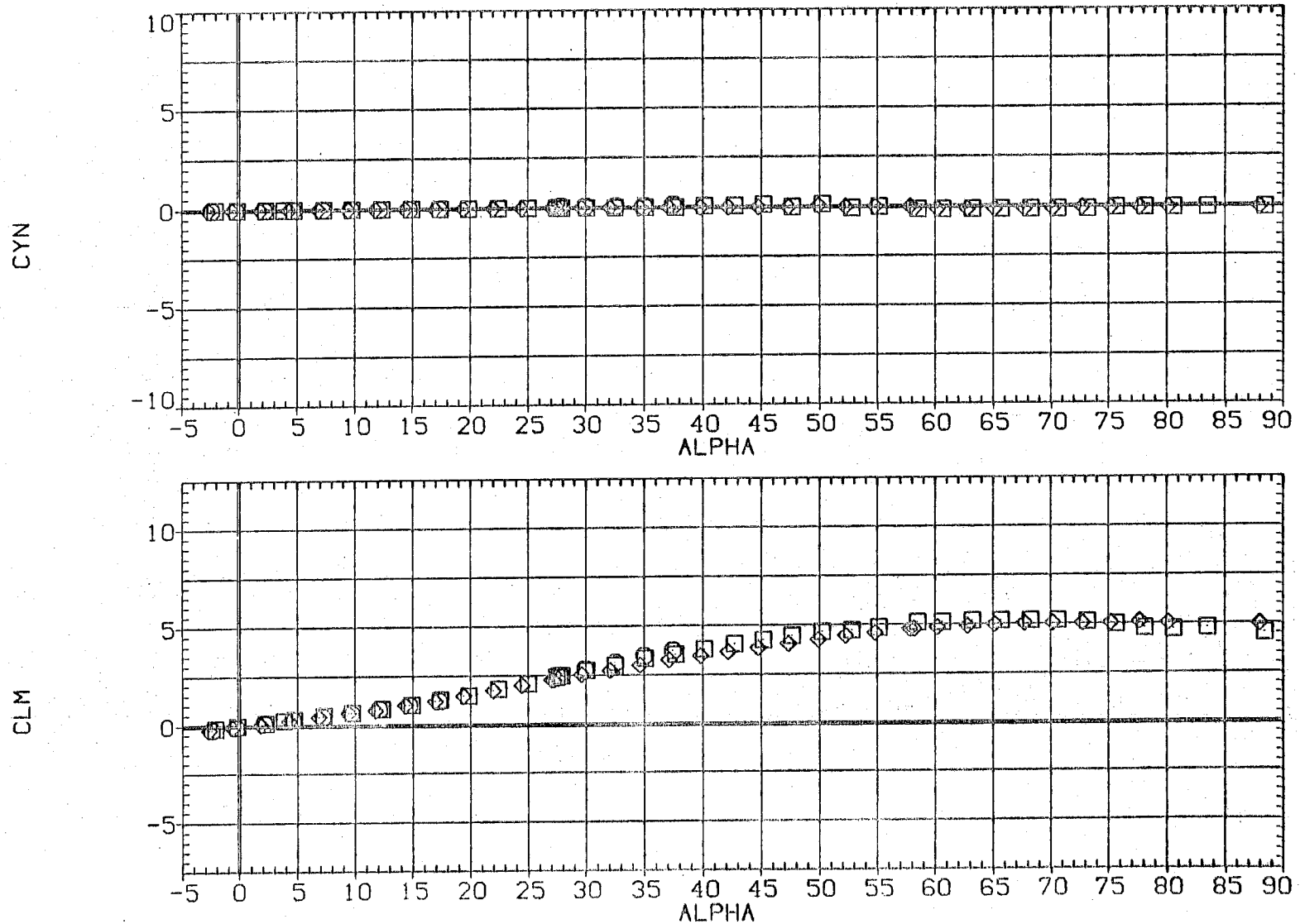

FIG.5 L/D=3.5 TAN. OGIVE, EFFECT OF MACH NUMBER, SUPERSONIC

SYMBOL	MACH		PARAMETRIC VALUES
○	1.195	R	.750
□	1.506		
◇	1.993		

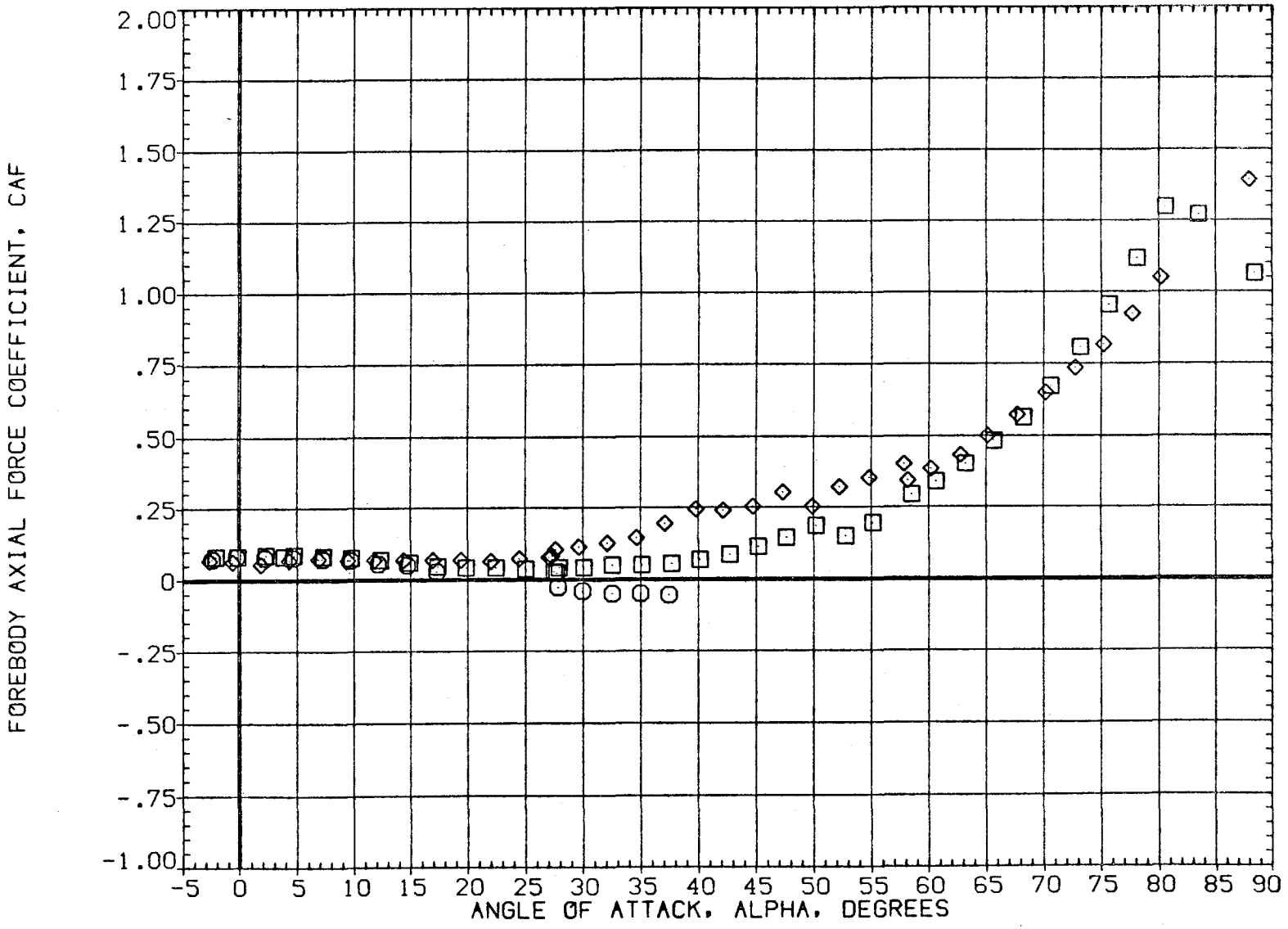

FIG.5 L/D=3.5 TAN. OGIVE, EFFECT OF MACH NUMBER, SUPERSONIC

FT2.5 (AJDC01)

SYMBOL	MACH		PARAMETRIC VALUES
○	1.195	R	.750
□	1.506		
◇	1.993		

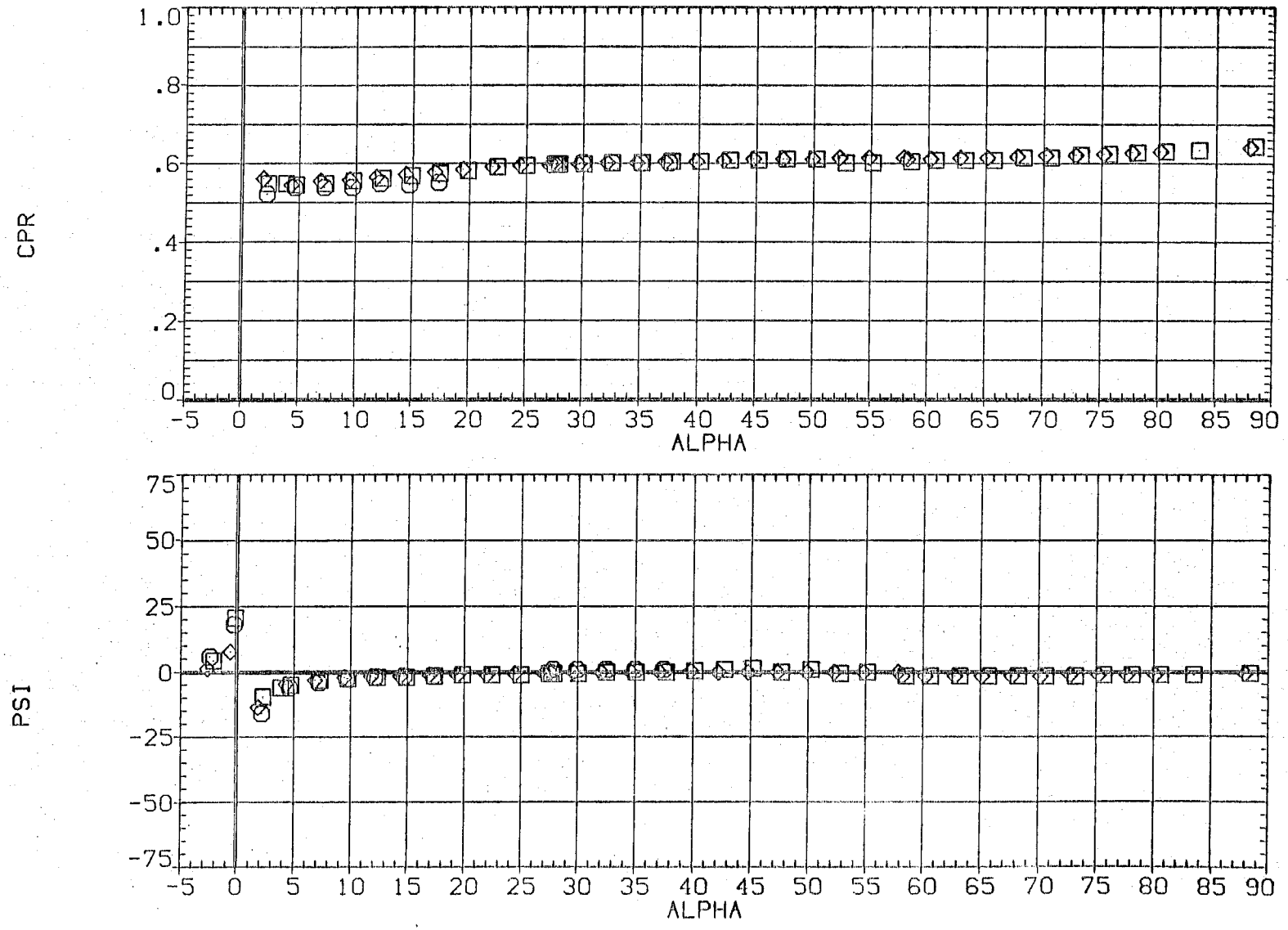

FIG.5 L/D=3.5 TAN. OGIVE, EFFECT OF MACH NUMBER, SUPERSONIC

SYMBOL	MACH		PARAMETRIC VALUES
○	1.195	R	.750
□	1.506		
◇	1.993		

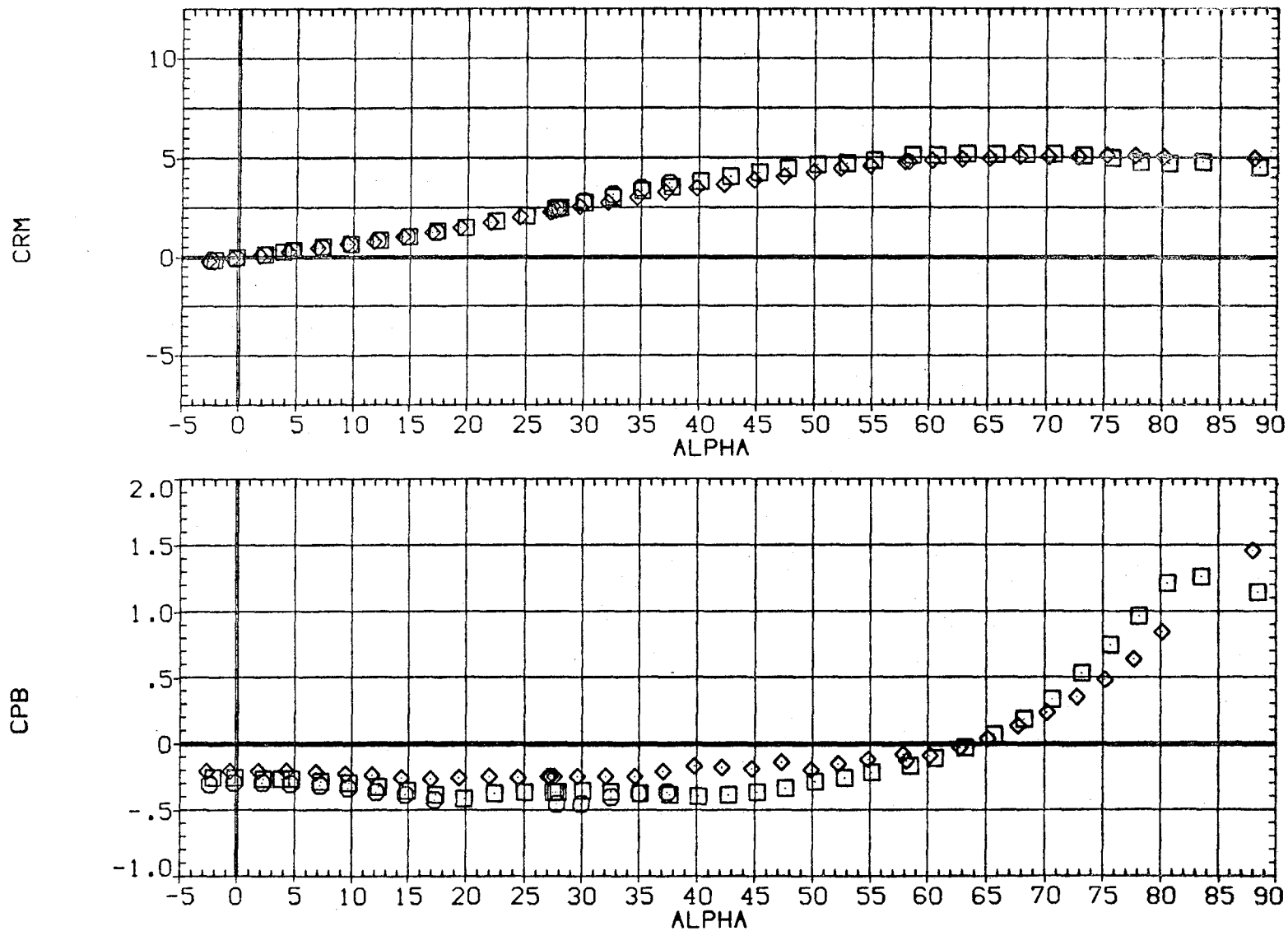

FIG.5 L/D=3.5 TAN. OGIVE, EFFECT OF MACH NUMBER, SUPERSONIC

DATA SET	SYMBOL	CONFIGURATION DESCRIPTION	R	BETA
(RJDA13)	○	FT3.5	.400	.000
(RJDA14)	□	FT3.5	.750	.000
(RJDA12)	◇	FT3.5	1.750	.000

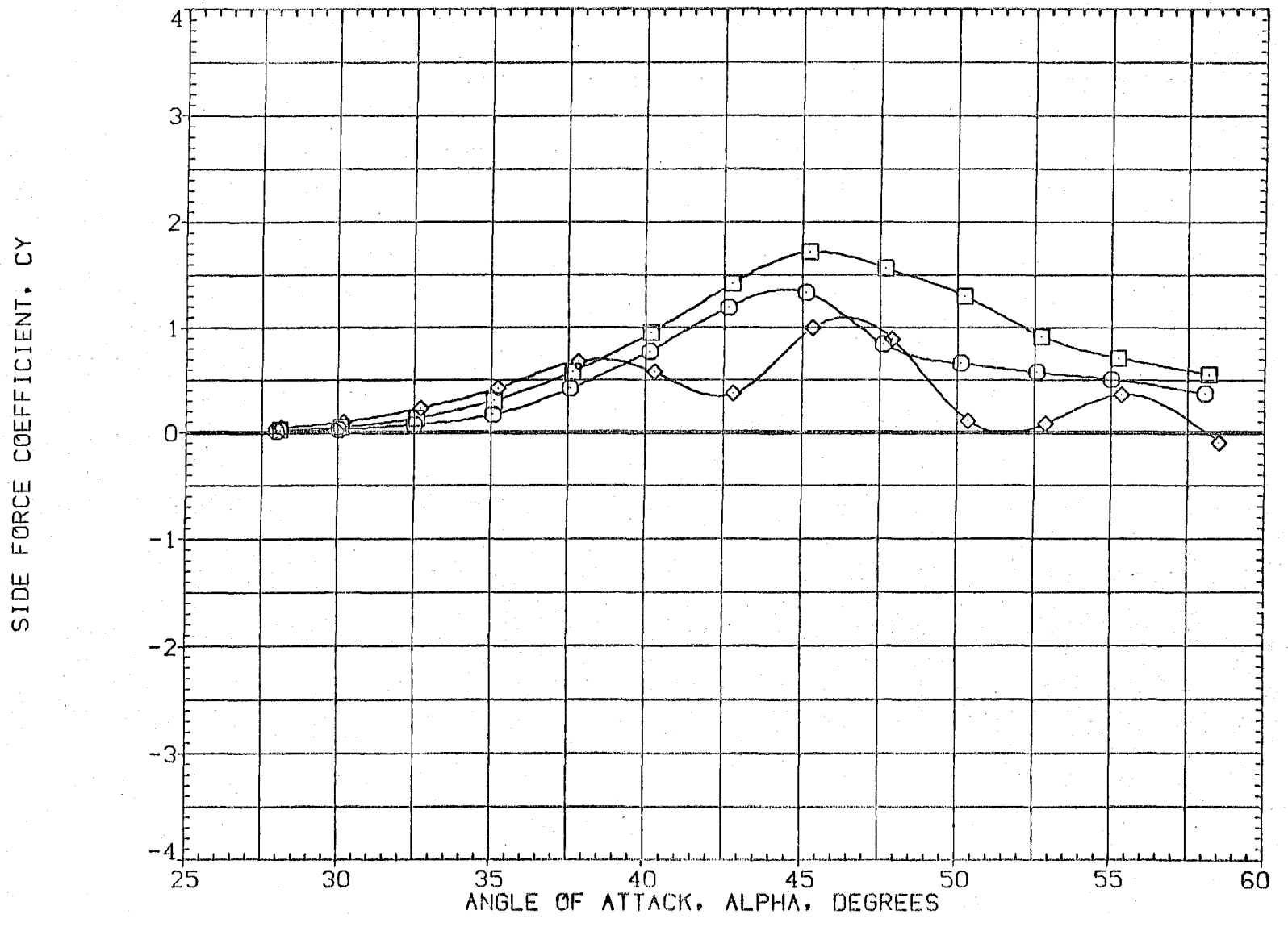

FIG.6 L/D=3.5 TAN. OGIVE, EFFECT OF REYNOLDS NUMBER

(A)MACH = .60

DATA SET	SYMBOL	CONFIGURATION DESCRIPTION	R	BETA
(RJDA13)	○	FT3.5	.400	.000
(RJDA14)	□	FT3.5	.750	.000
(RJDA12)	◇	FT3.5	1.750	.000

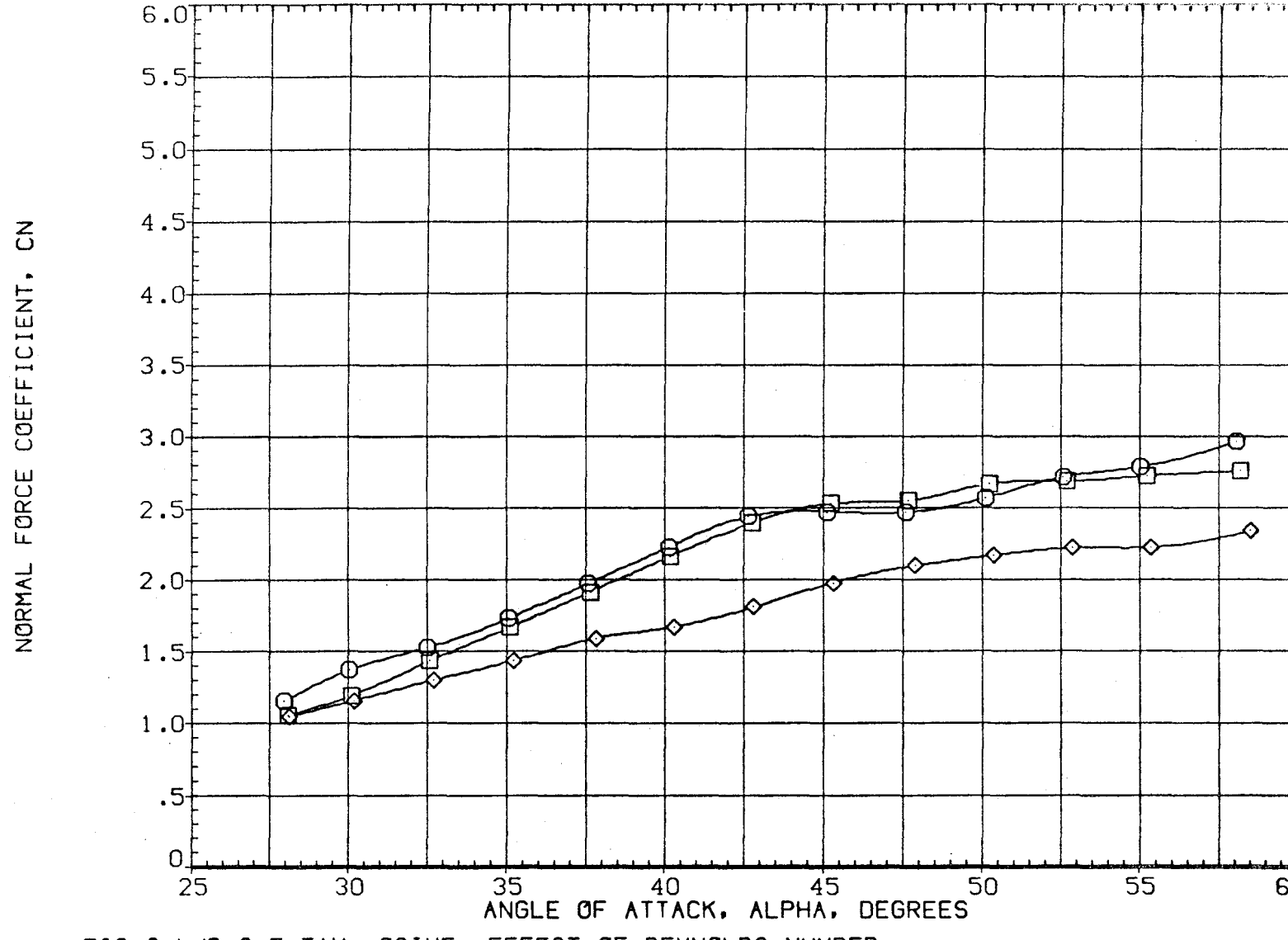

FIG.6 L/D=3.5 TAN. OGIVE, EFFECT OF REYNOLDS NUMBER

(A)MACH = .60

DATA SET	SYMBOL	CONFIGURATION DESCRIPTION	R	BETA
(RJDA13)	○	FT3.5	.400	.000
(RJDA14)	□	FT3.5	.750	.000
(RJDA12)	◇	FT3.5	1.750	.000

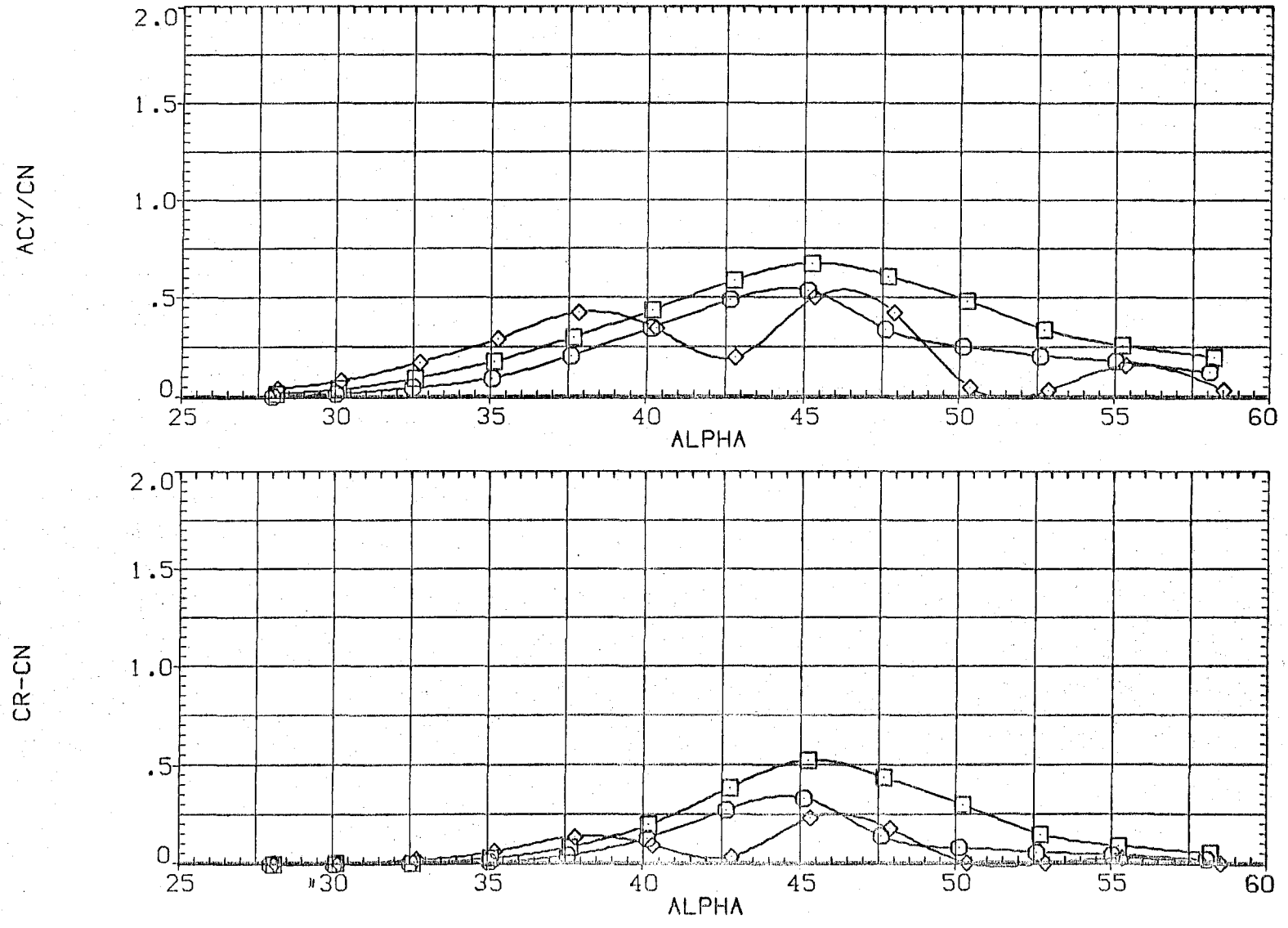

FIG.6 L/D=3.5 TAN. OGIVE, EFFECT OF REYNOLDS NUMBER

(A)MACH = .60

DATA SET	SYMBOL	CONFIGURATION DESCRIPTION	R	BETA
(RJDA13)	○	FT3.5	.400	.000
(RJDA14)	□	FT3.5	.750	.000
(RJDA12)	◇	FT3.5	1.750	.000

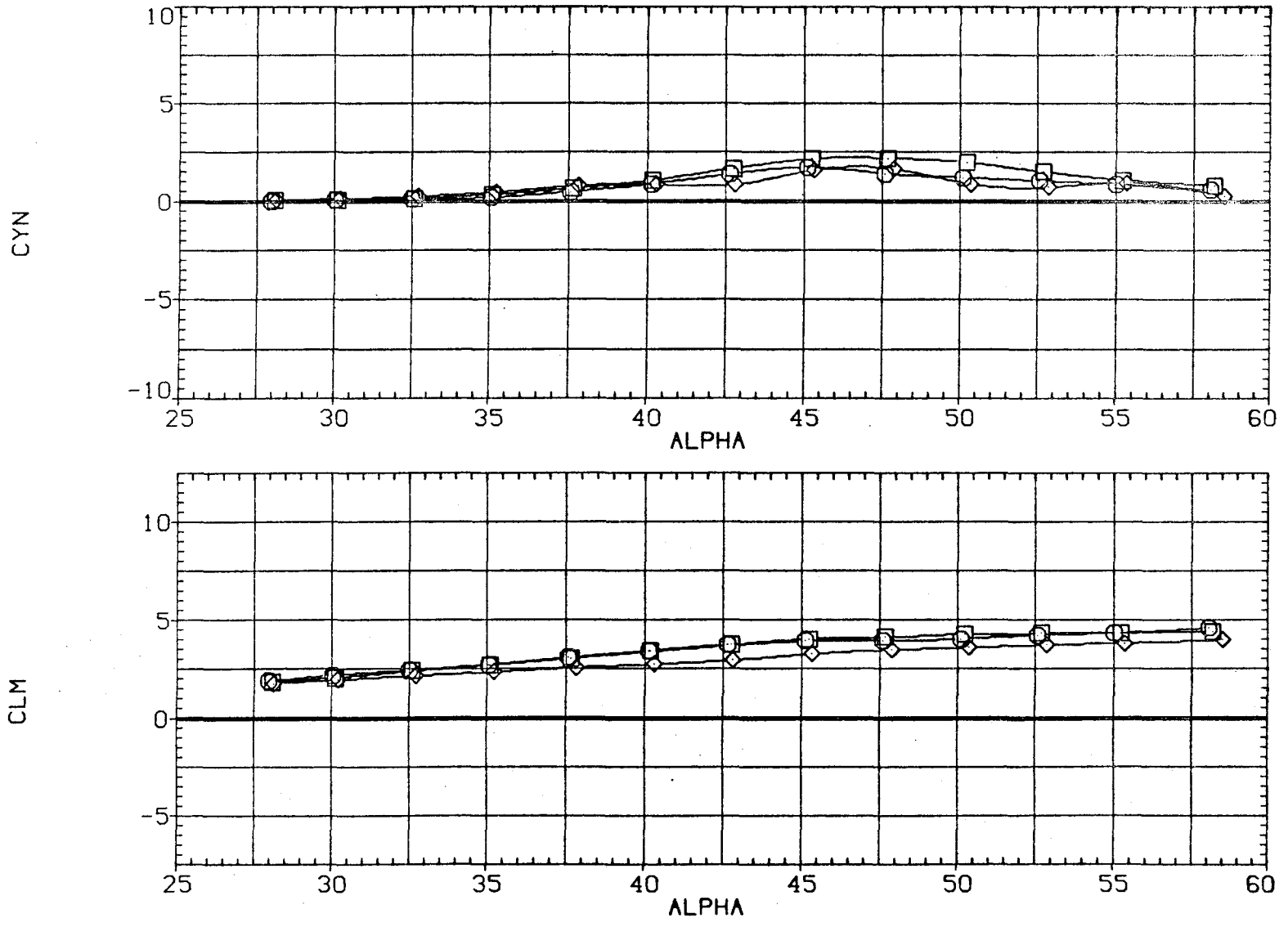

FIG.6 L/D=3.5 TAN. OGIVE, EFFECT OF REYNOLDS NUMBER

(A)MACH = .60

DATA SET	SYMBOL	CONFIGURATION DESCRIPTION	R	BETA
(RJDA13)		FT3.5	.400	.000
(RJDA14)		FT3.5	.750	.000
(RJDA12)		FT3.5	1.750	.000

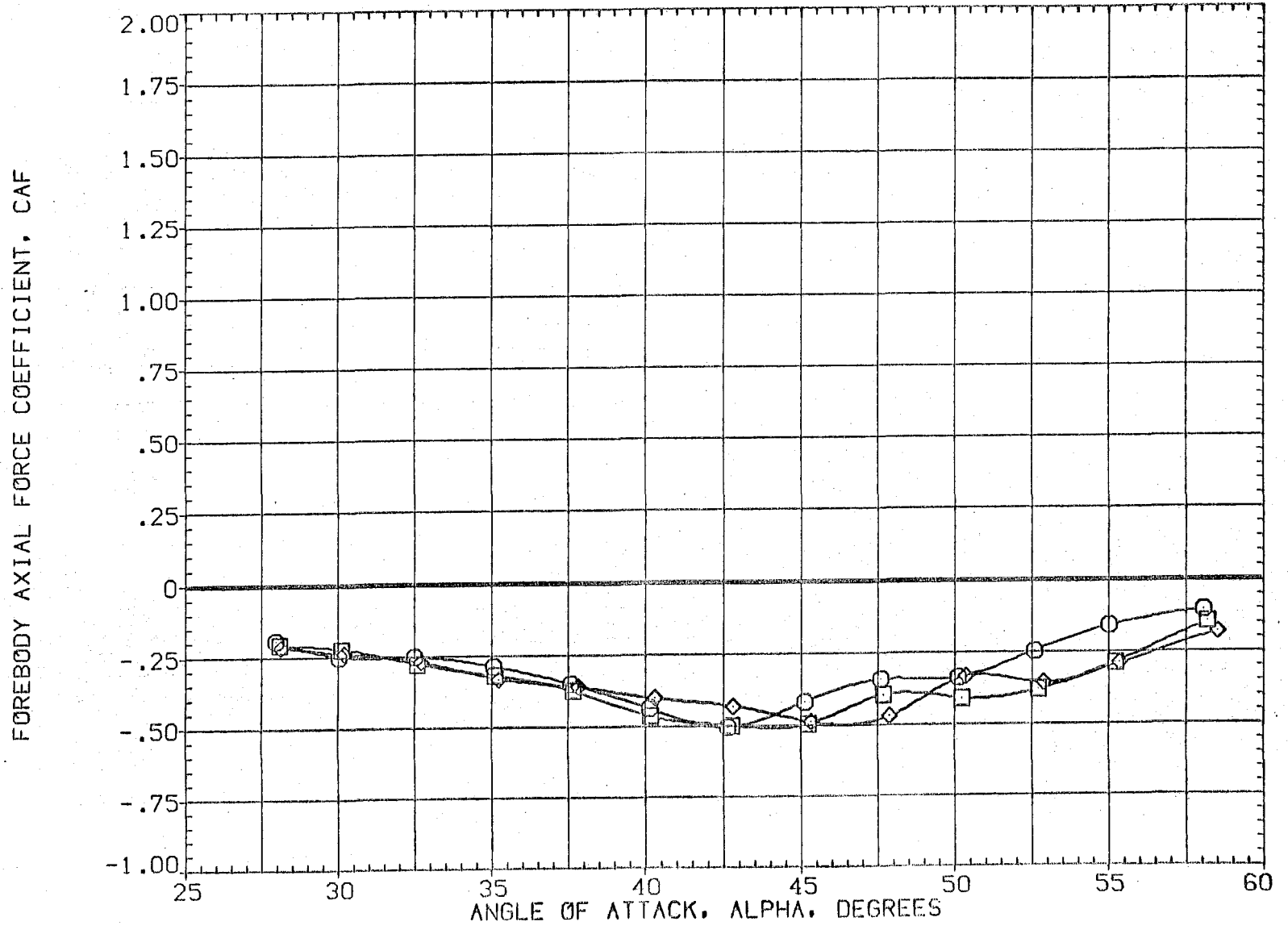

FIG.6 L/D=3.5 TAN. OGIVE, EFFECT OF REYNOLDS NUMBER

DATA SET	SYMBOL	CONFIGURATION DESCRIPTION	R	BETA
(AJD013)	○	FT3.5	.400	.000
(AJD014)	□	FT3.5	.750	.000
(AJD012)	◇	FT3.5	1.750	.000

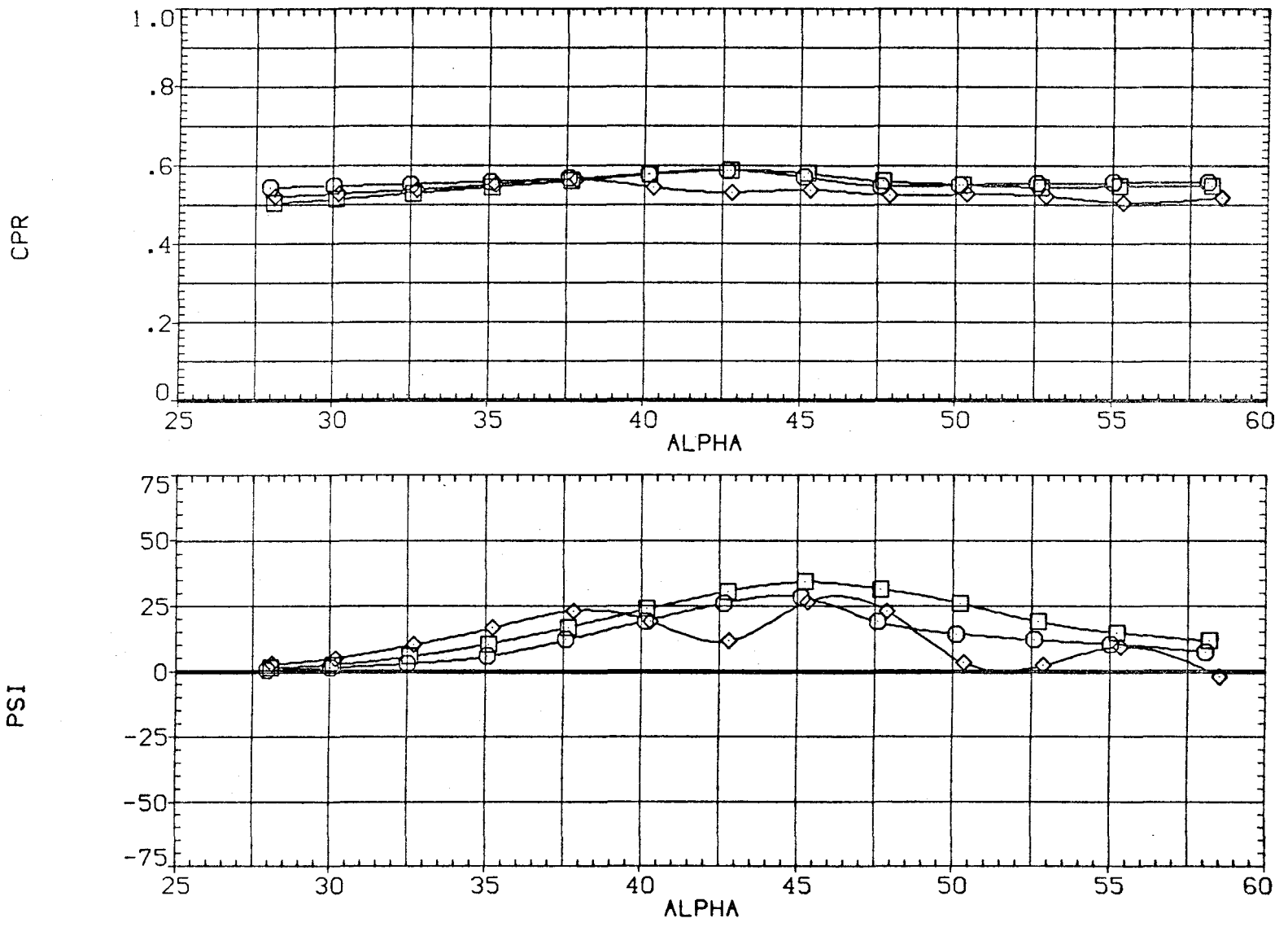

FIG.6 L/D=3.5 TAN. OGIVE, EFFECT OF REYNOLDS NUMBER

(A)MACH = .60

DATA SET	SYMBOL	CONFIGURATION DESCRIPTION	R	BETA
(AJD013)		FT3.5	.400	.000
(AJD014)		FT3.5	.750	.000
(AJD012)		FT3.5	1.750	.000

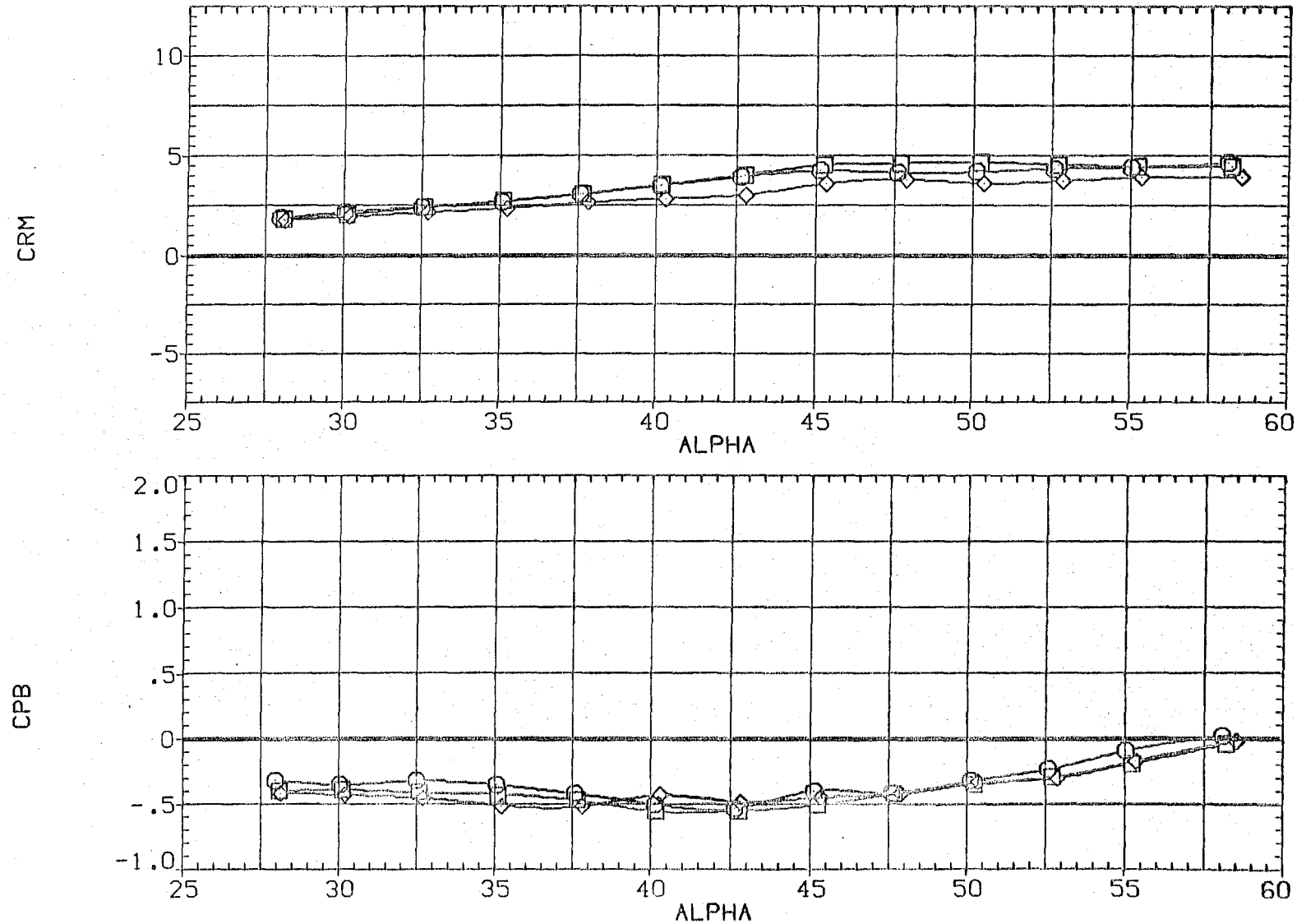

FIG.6 L/D=3.5 TAN. OGIVE, EFFECT OF REYNOLDS NUMBER

(A)MACH = .60

SYMBOL	MACH		PARAMETRIC VALUES		
○	.253	BETA	.000	R	.750
□	.600				
◇	.800				
△	.904				

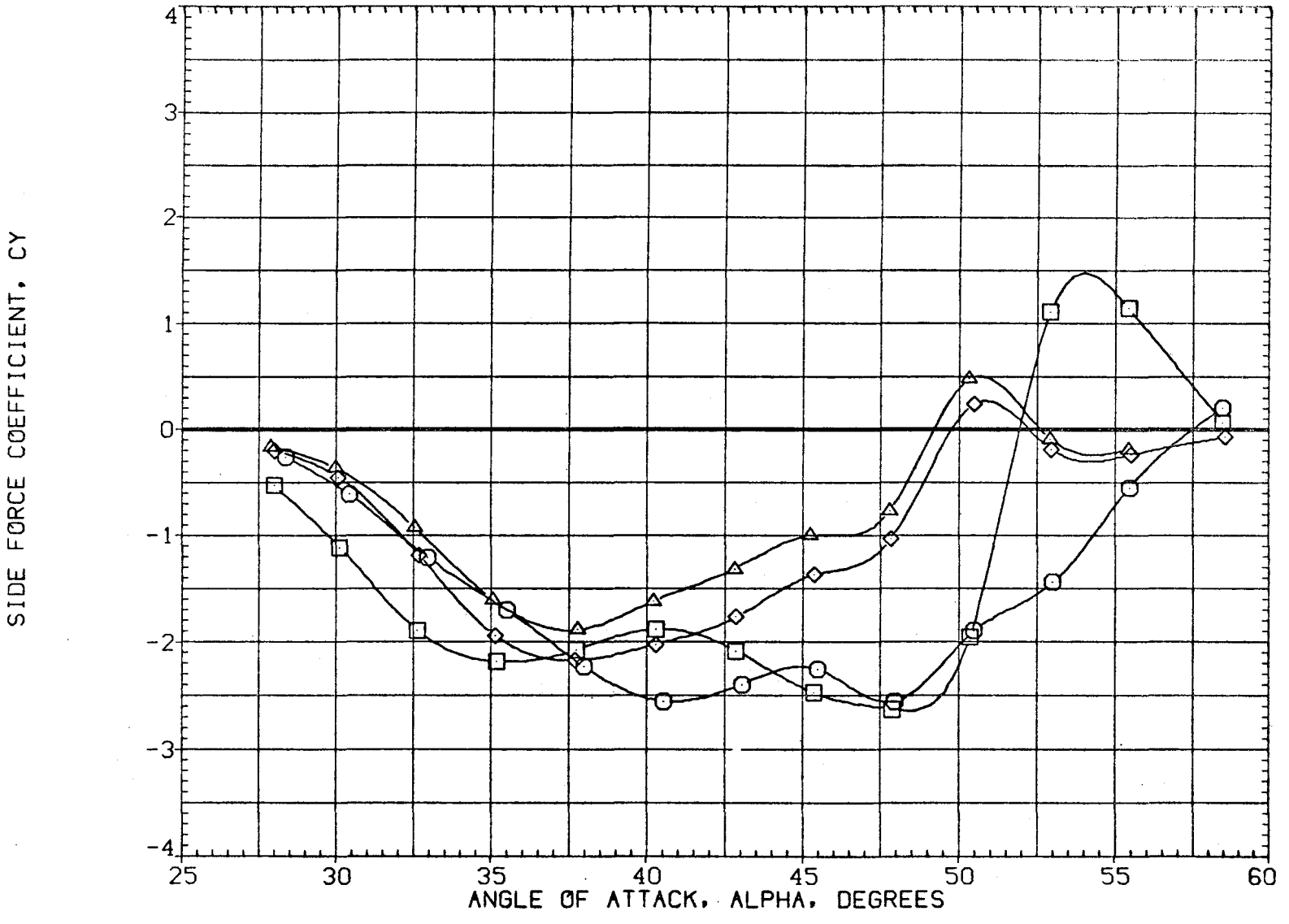

FIG.7 L/D=5 TAN. OGIVE, EFFECT OF MACH NUMBER, SUBSONIC

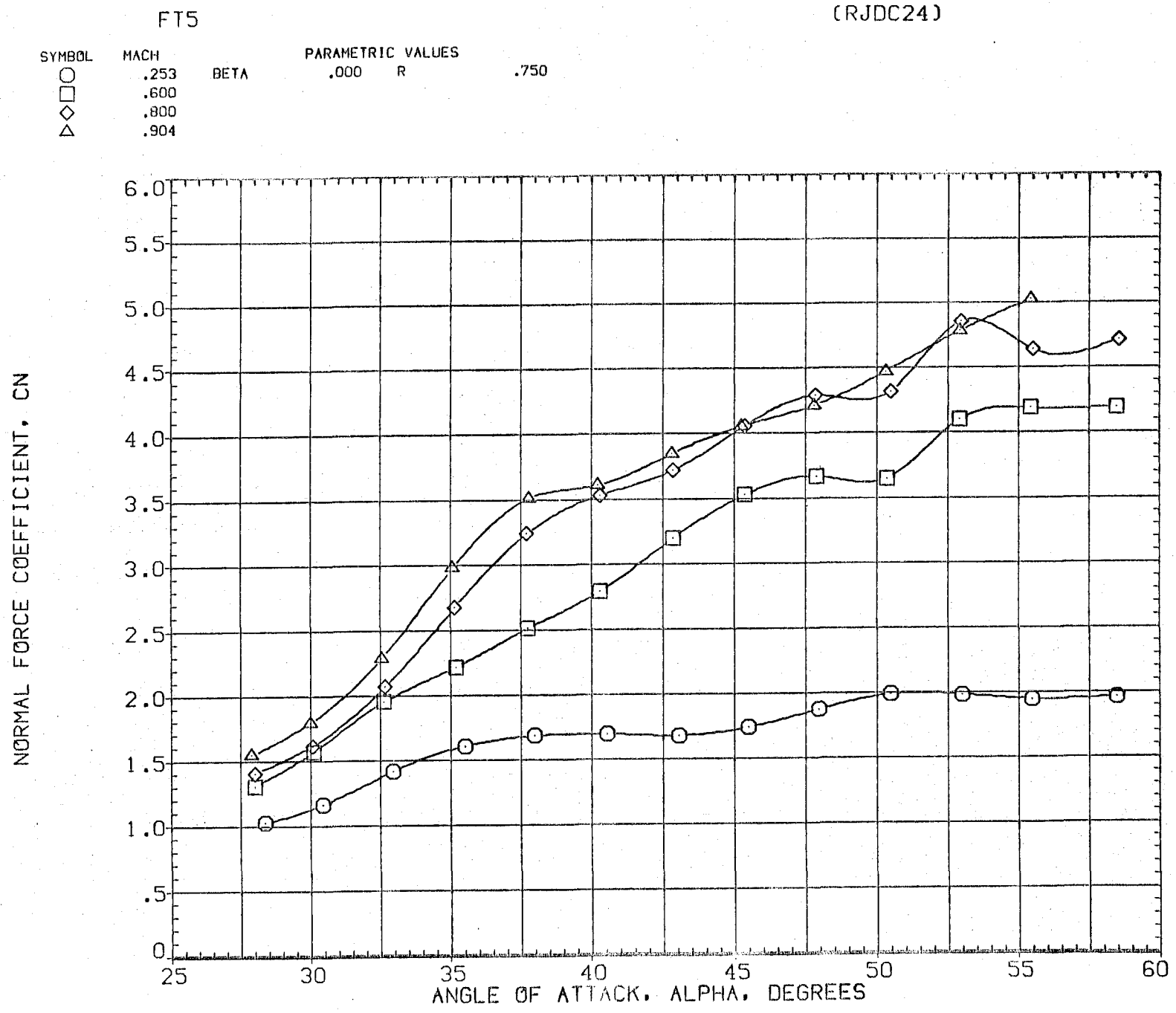

FIG.7 L/D=5 TAN. OGIVE, EFFECT OF MACH NUMBER, SUBSONIC

SYMBOL	MACH		PARAMETRIC VALUES		
○	.253	BETA	.000	R	.750
□	.600				
◇	.800				
△	.904				

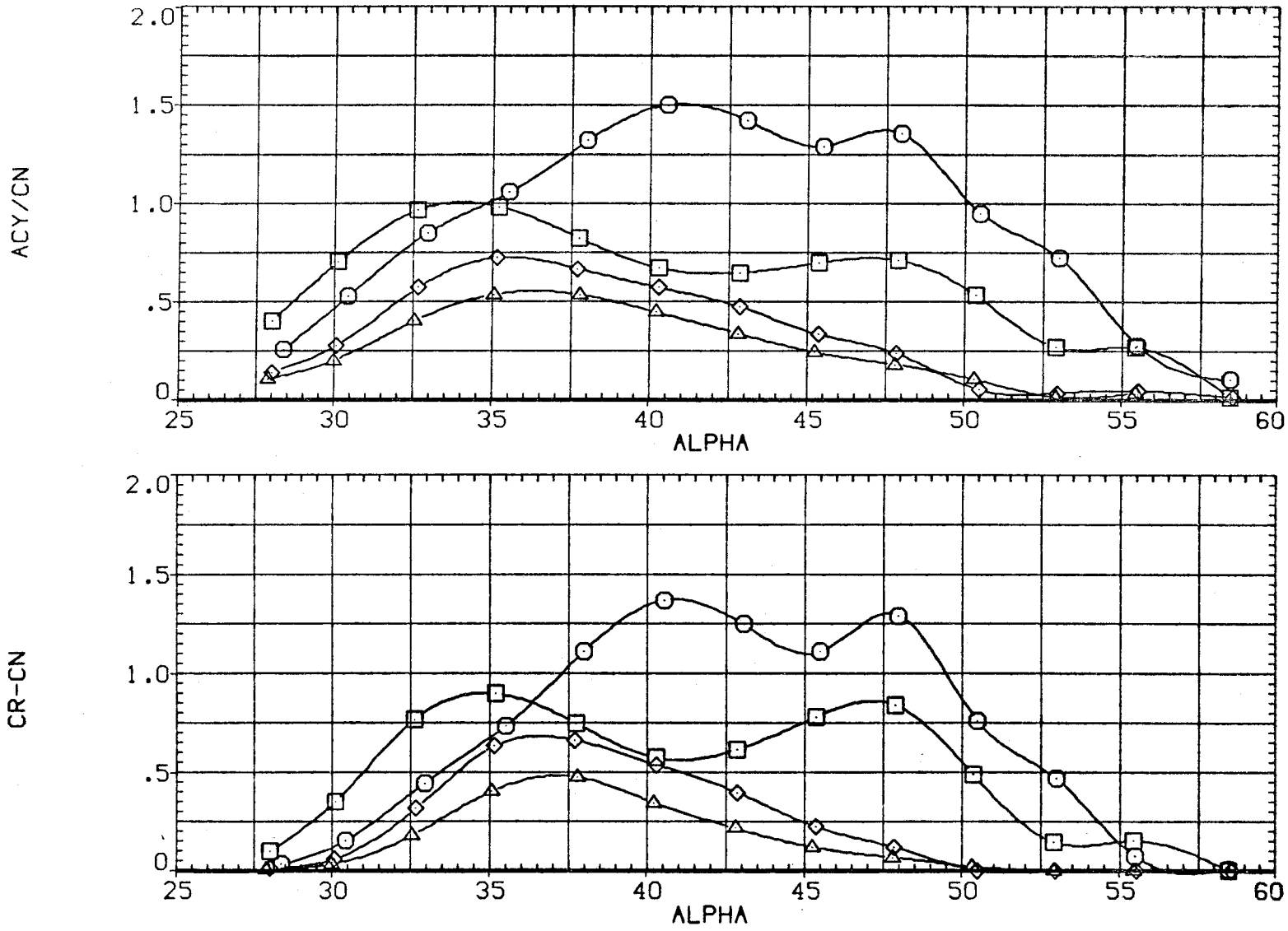

FIG.7 L/D=5 TAN. OGIVE, EFFECT OF MACH NUMBER, SUBSONIC

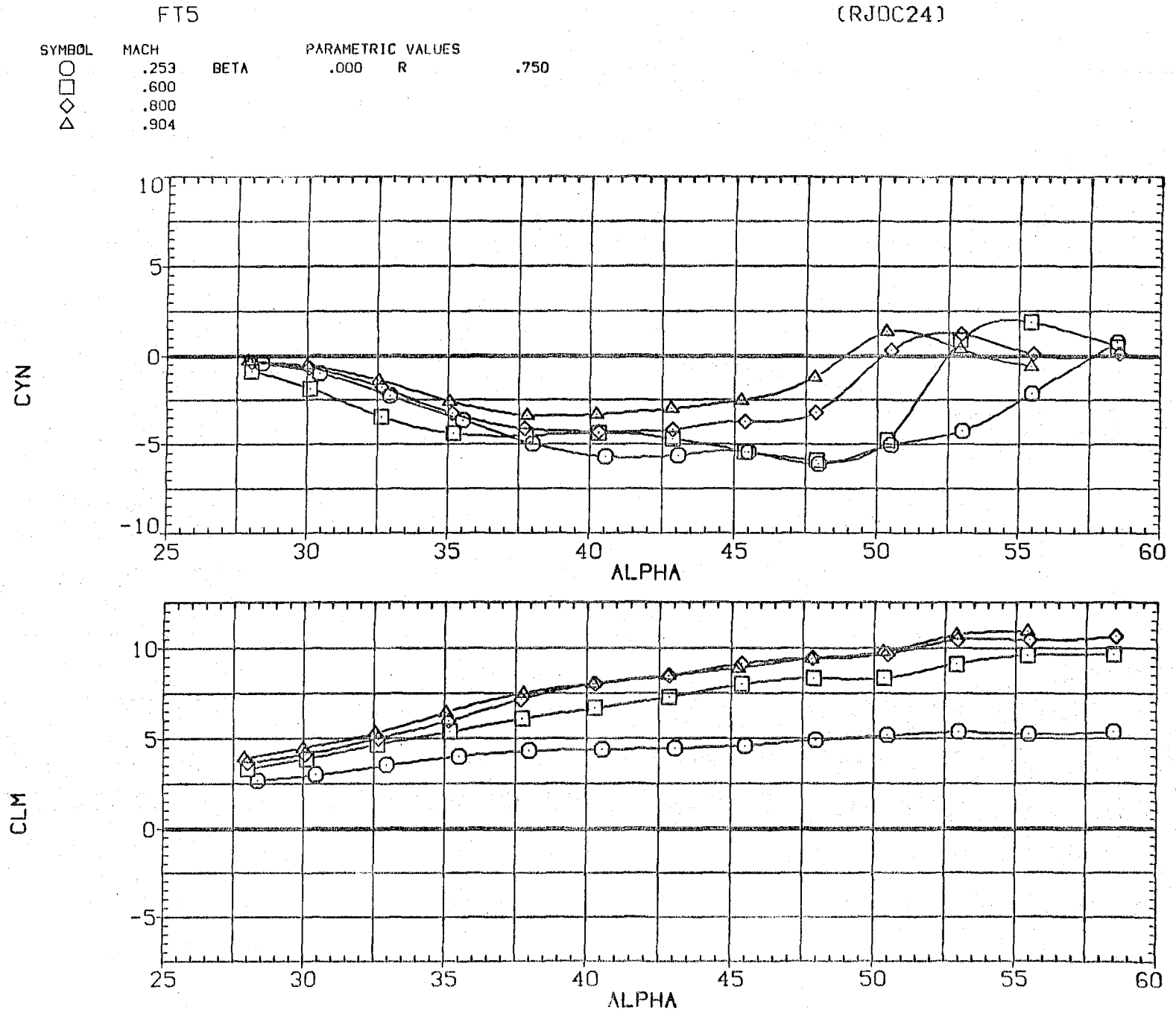

FIG.7 L/D=5 TAN. OGIVE, EFFECT OF MACH NUMBER, SUBSONIC

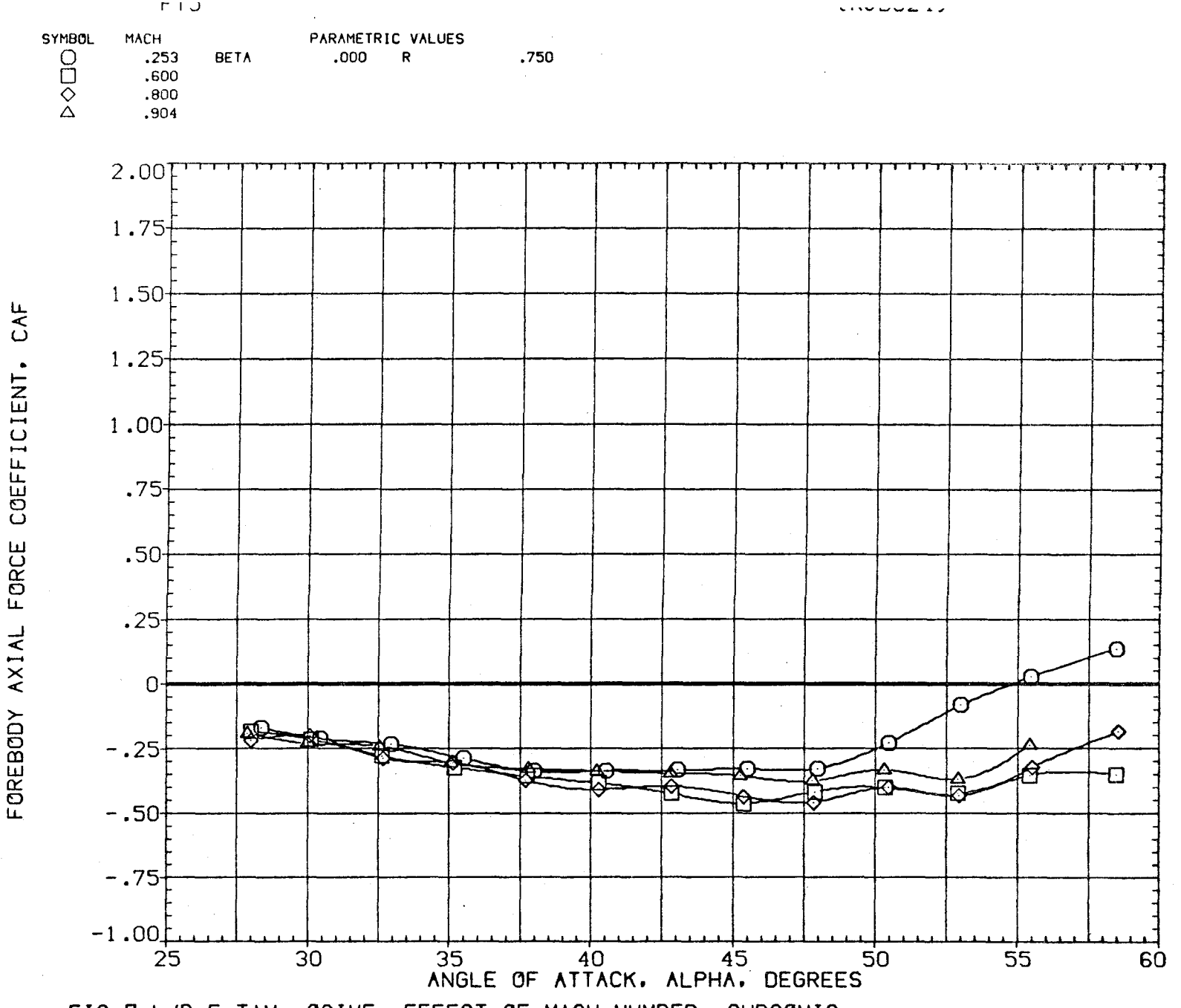

FIG.7 L/D=5 TAN. OGIVE, EFFECT OF MACH NUMBER, SUBSONIC

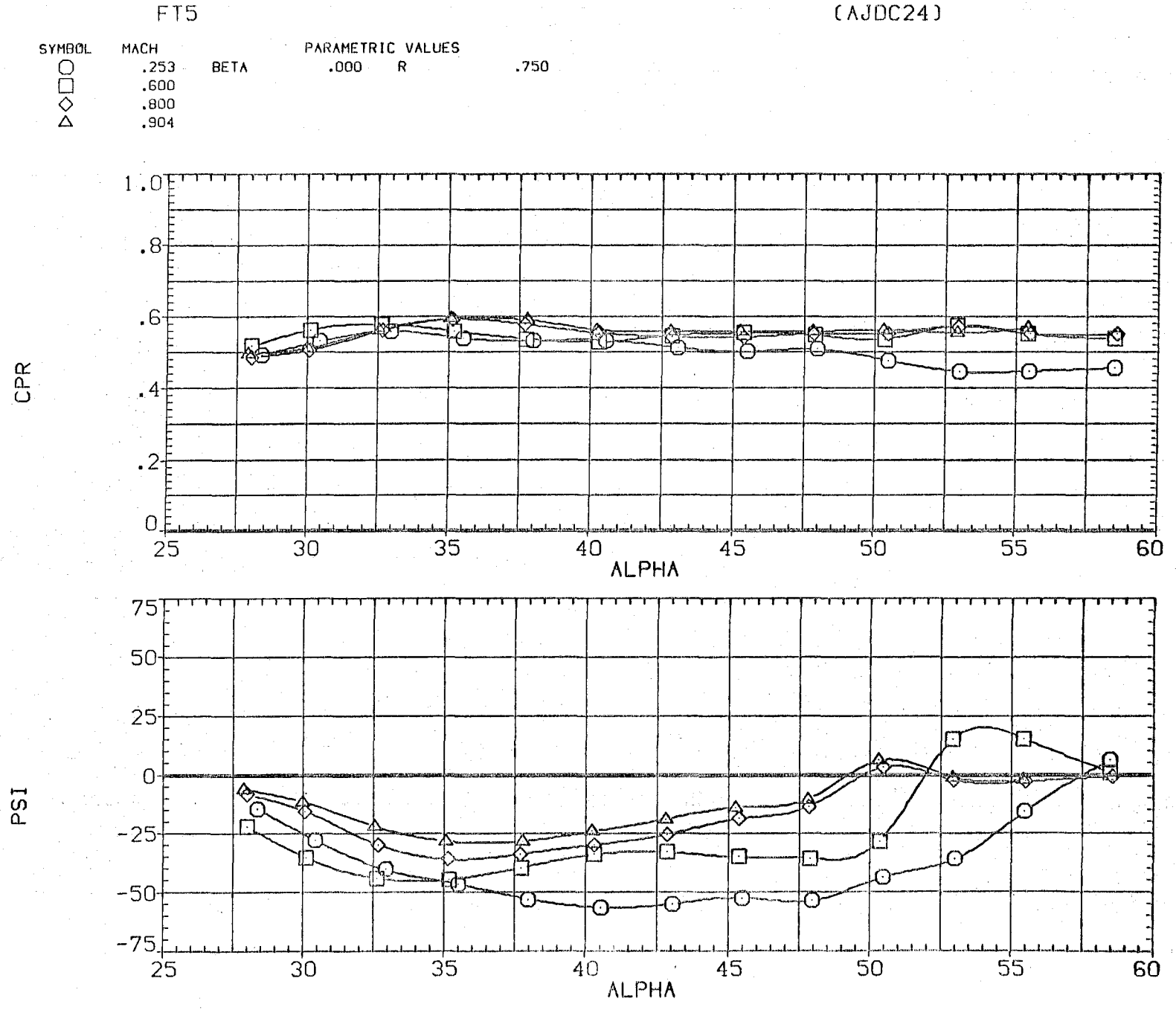

FIG.7 L/D=5 TAN. OGIVE, EFFECT OF MACH NUMBER, SUBSONIC

SYMBOL	MACH		PARAMETRIC VALUES		
○	.253	BETA	.000	R	.750
□	.600				
◇	.800				
△	.904				

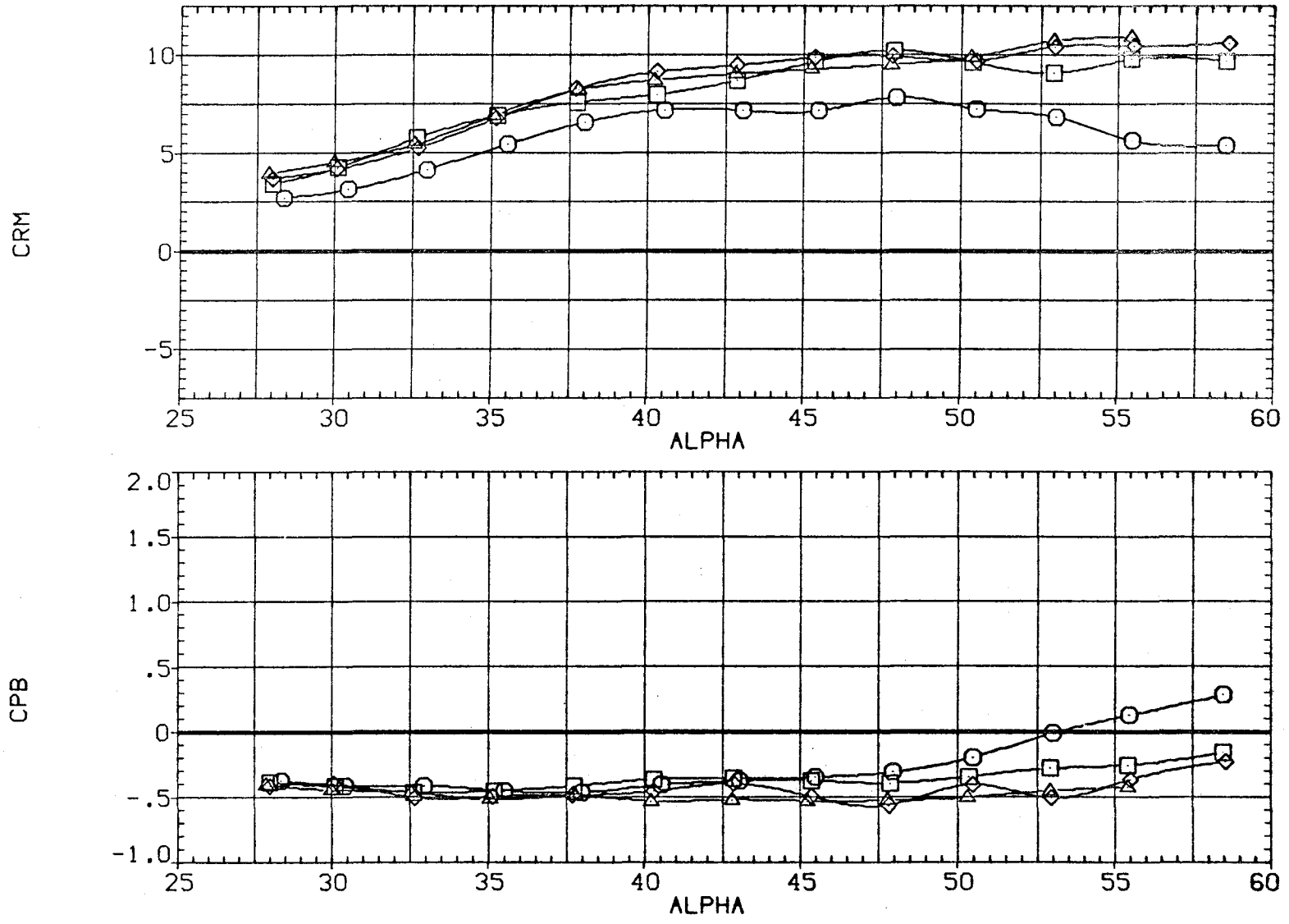

FIG.7 L/D=5 TAN. OGIVE, EFFECT OF MACH NUMBER, SUBSONIC

FT5 (RJDC24)

SYMBOL	MACH		PARAMETRIC VALUES		
○	1.201	BETA	.000	R	.750
□	1.504				
◇	1.995				

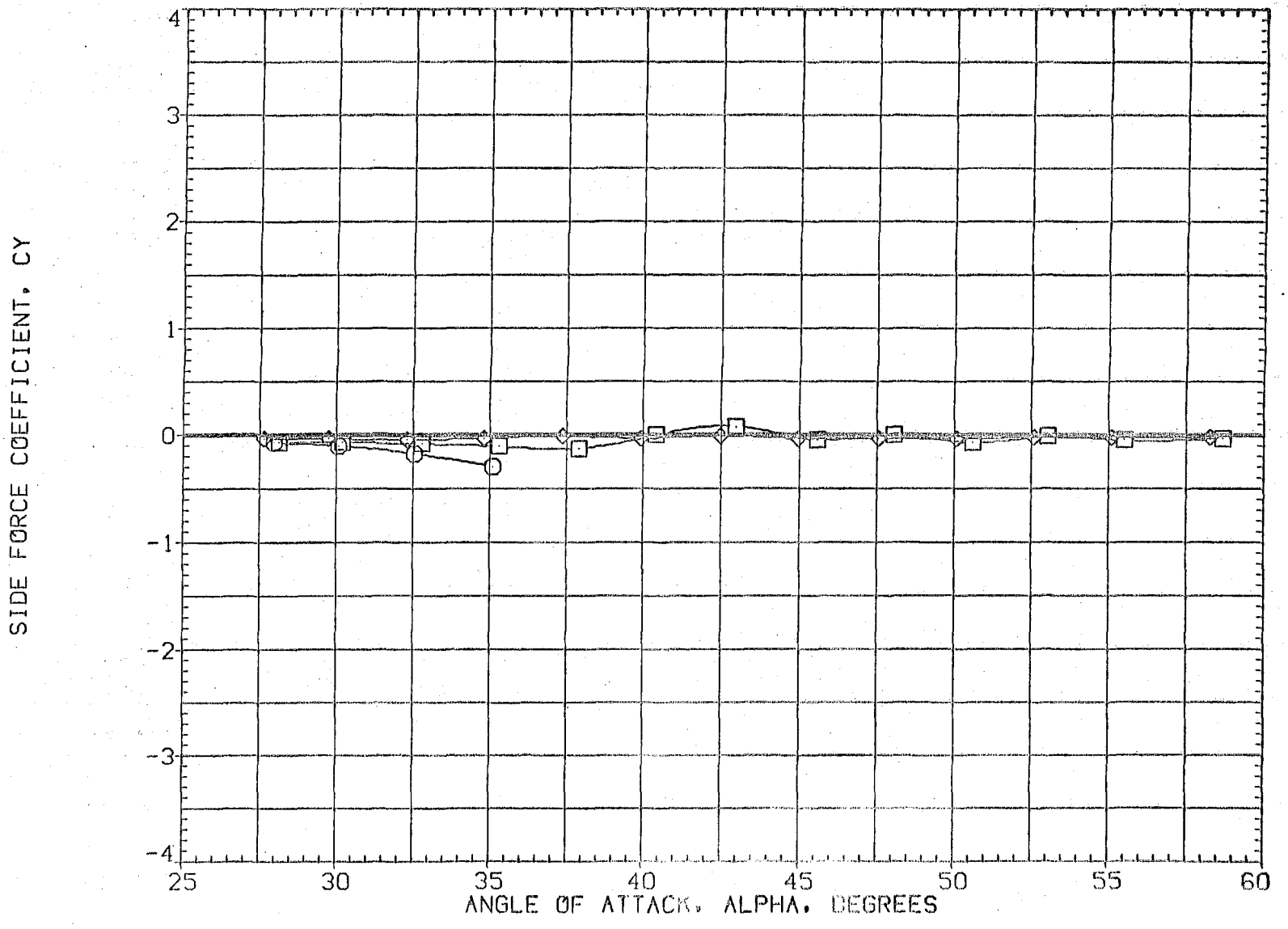

FIG.8 L/D=5 TAN. OGIVE, EFFECT OF MACH NUMBER, SUPERSONIC

SYMBOL	MACH		PARAMETRIC VALUES		
○	1.201	BETA	.000	R	.750
□	1.504				
◇	1.995				

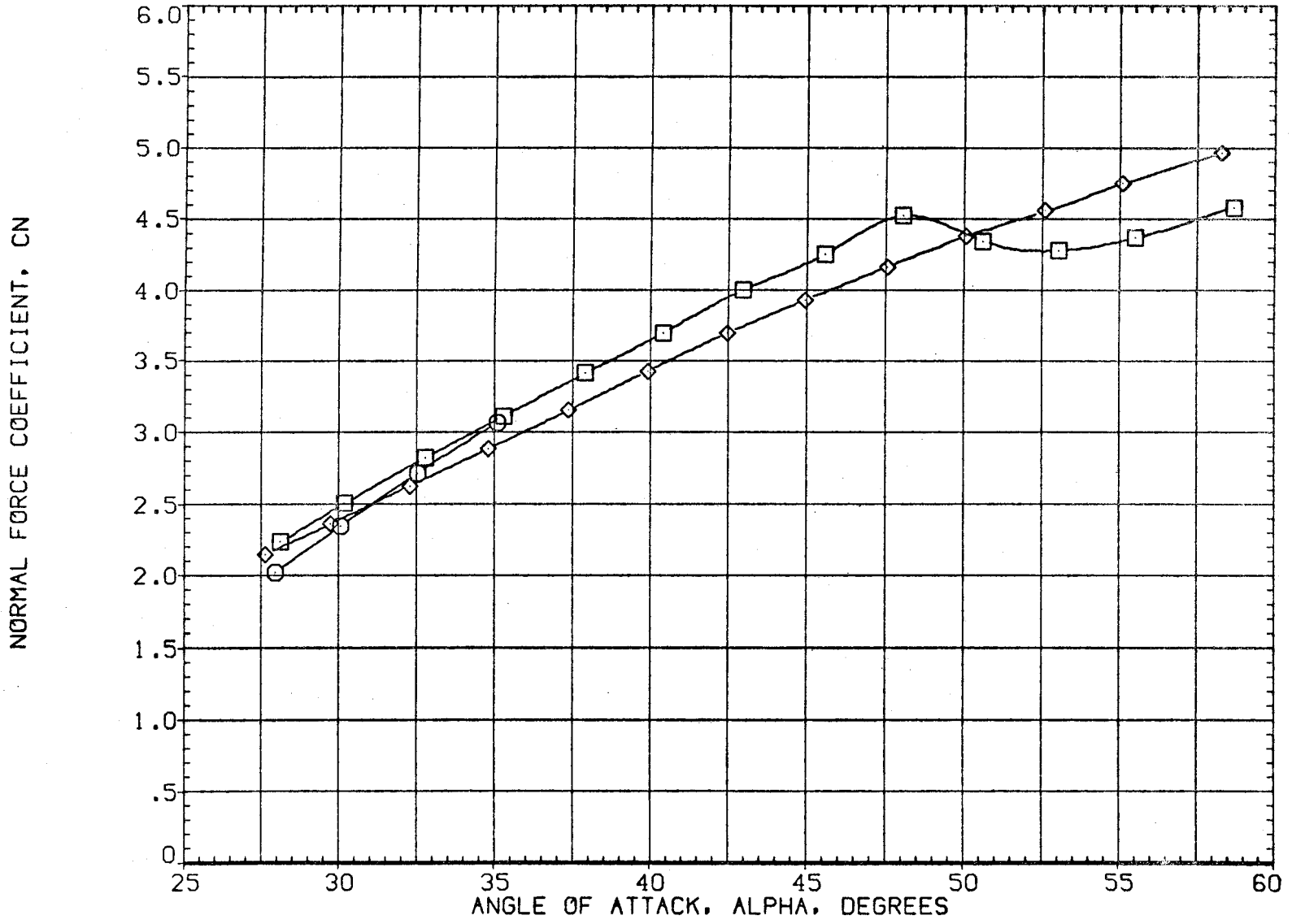

FIG.8 L/D=5 TAN. OGIVE, EFFECT OF MACH NUMBER, SUPERSONIC

SYMBOL	MACH		PARAMETRIC VALUES		
○	1.201	BETA	.000	R	.750
□	1.504				
◇	1.995				

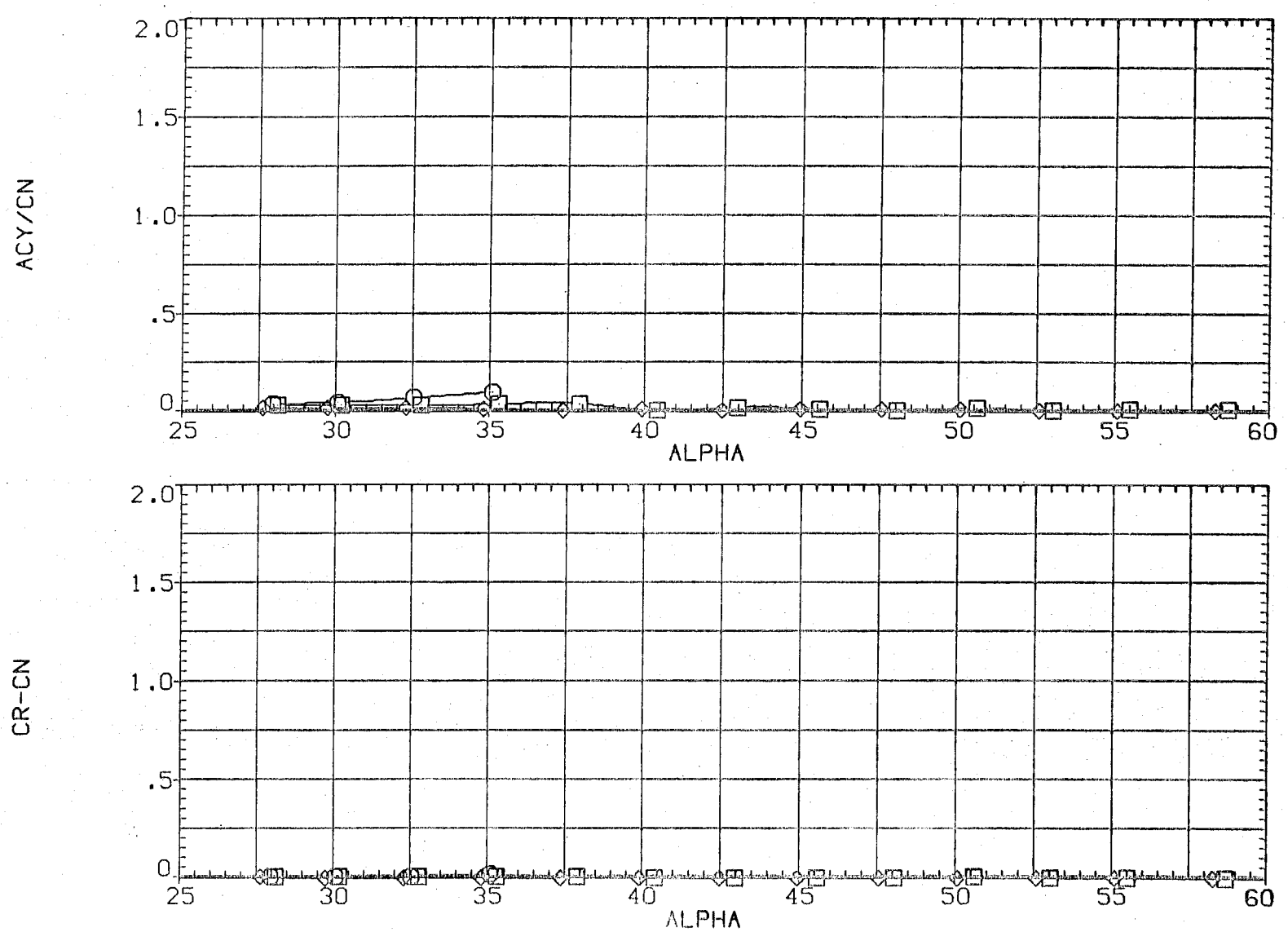

FIG.8 L/D=5 TAN. OGIVE, EFFECT OF MACH NUMBER, SUPERSONIC

SYMBOL	MACH		PARAMETRIC VALUES		
○	1.201	BETA	.000	R	.750
□	1.504				
◇	1.995				

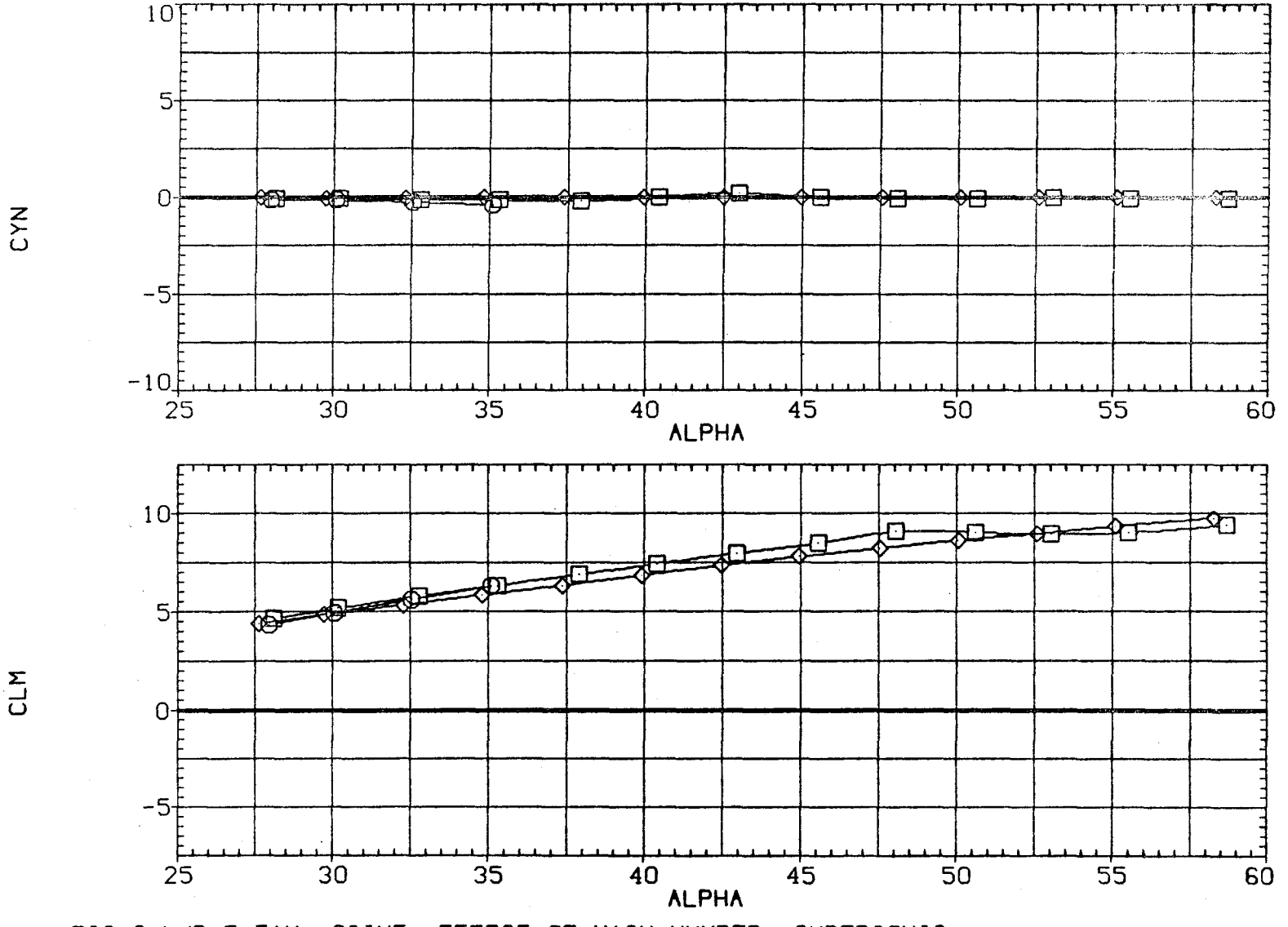

FIG.8 L/D=5 TAN. OGIVE, EFFECT OF MACH NUMBER, SUPERSONIC

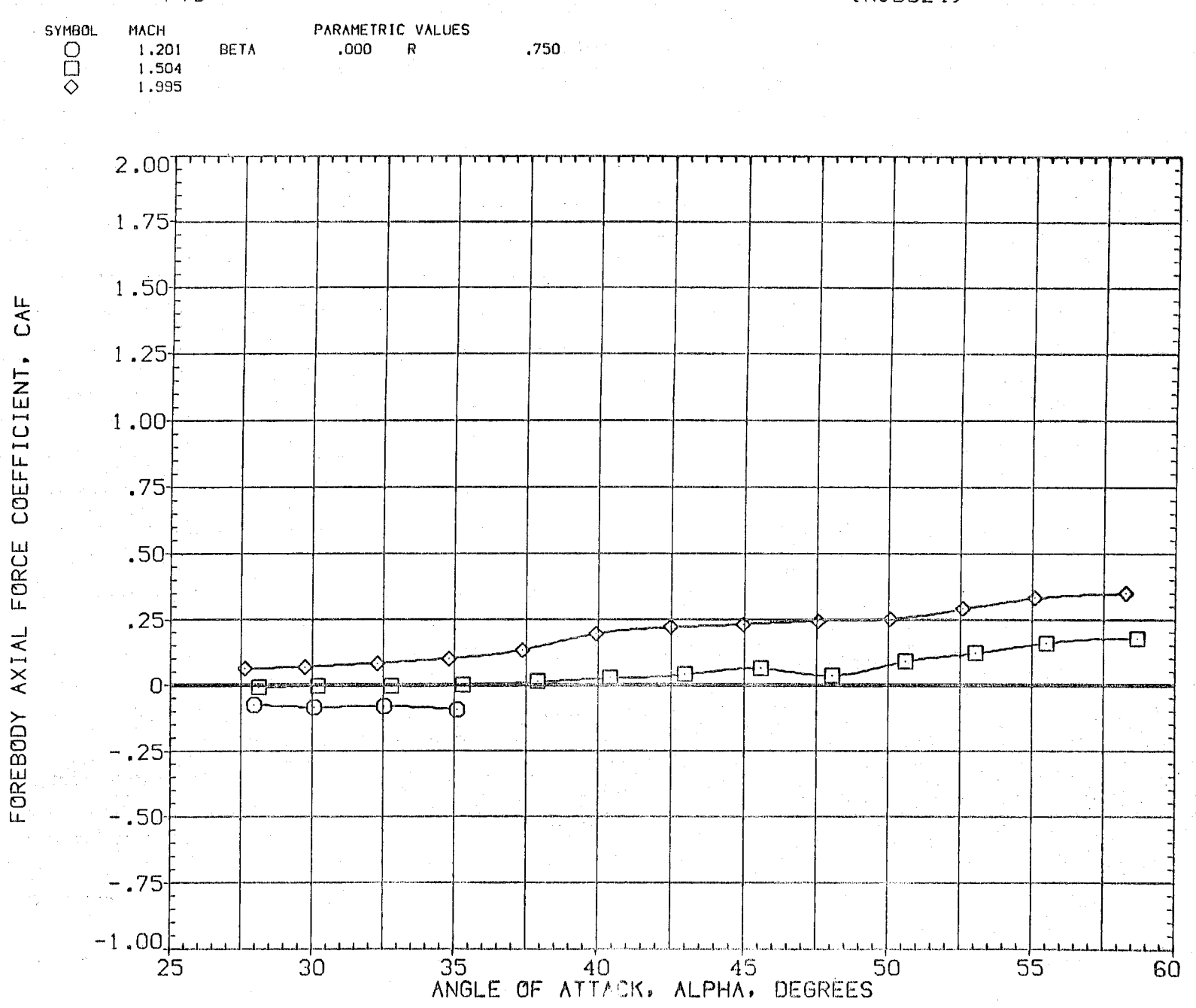

FIG.8 L/D=5 TAN. OGIVE, EFFECT OF MACH NUMBER, SUPERSONIC

SYMBOL	MACH		PARAMETRIC VALUES		
○	1.201	BETA	.000	R	.750
□	1.504				
◇	1.995				

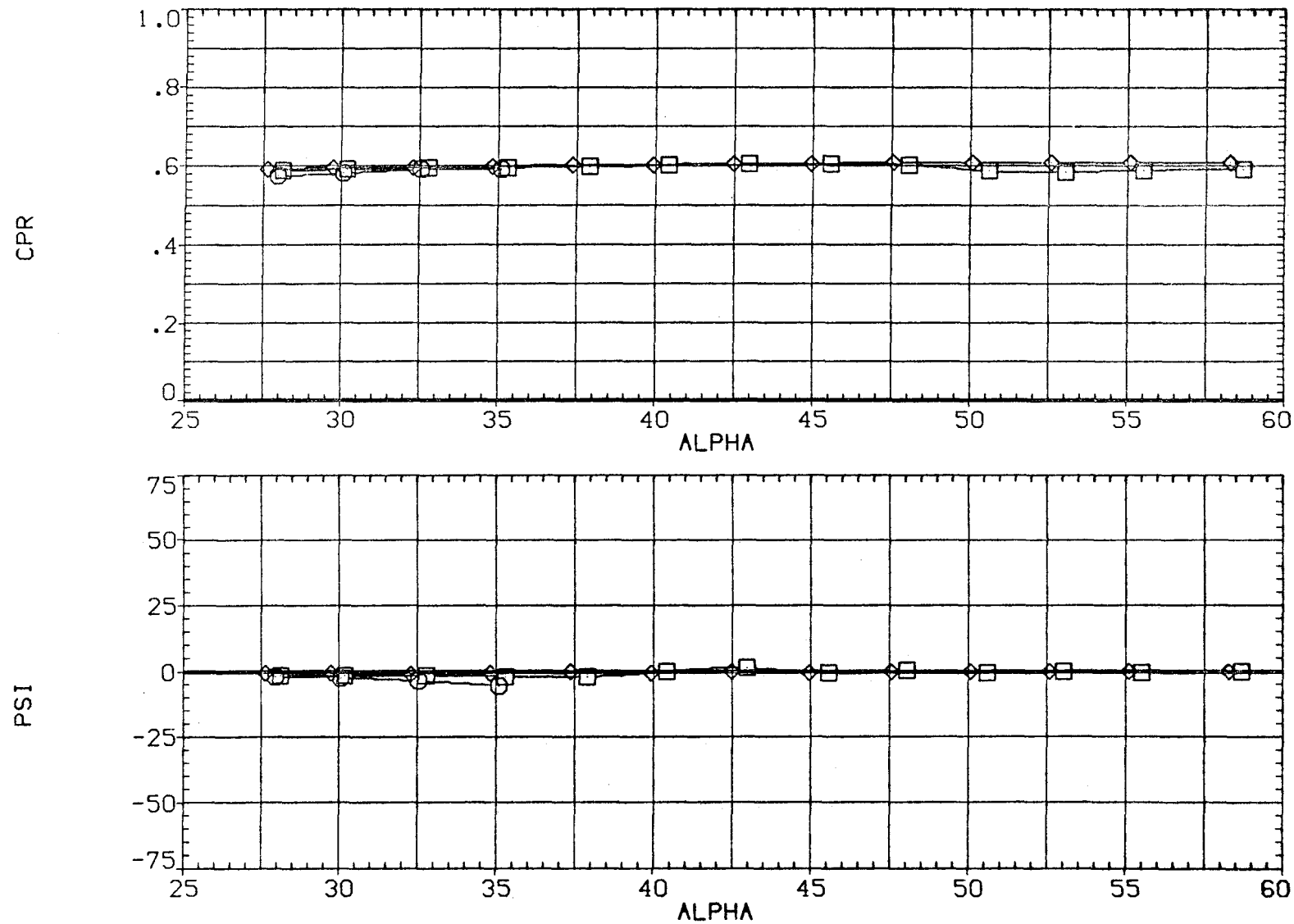

FIG.8 L/D=5 TAN. OGIVE, EFFECT OF MACH NUMBER, SUPERSONIC

SYMBOL	MACH		PARAMETRIC VALUES		
○	1.201	BETA	.000	R	.750
□	1.504				
◇	1.995				

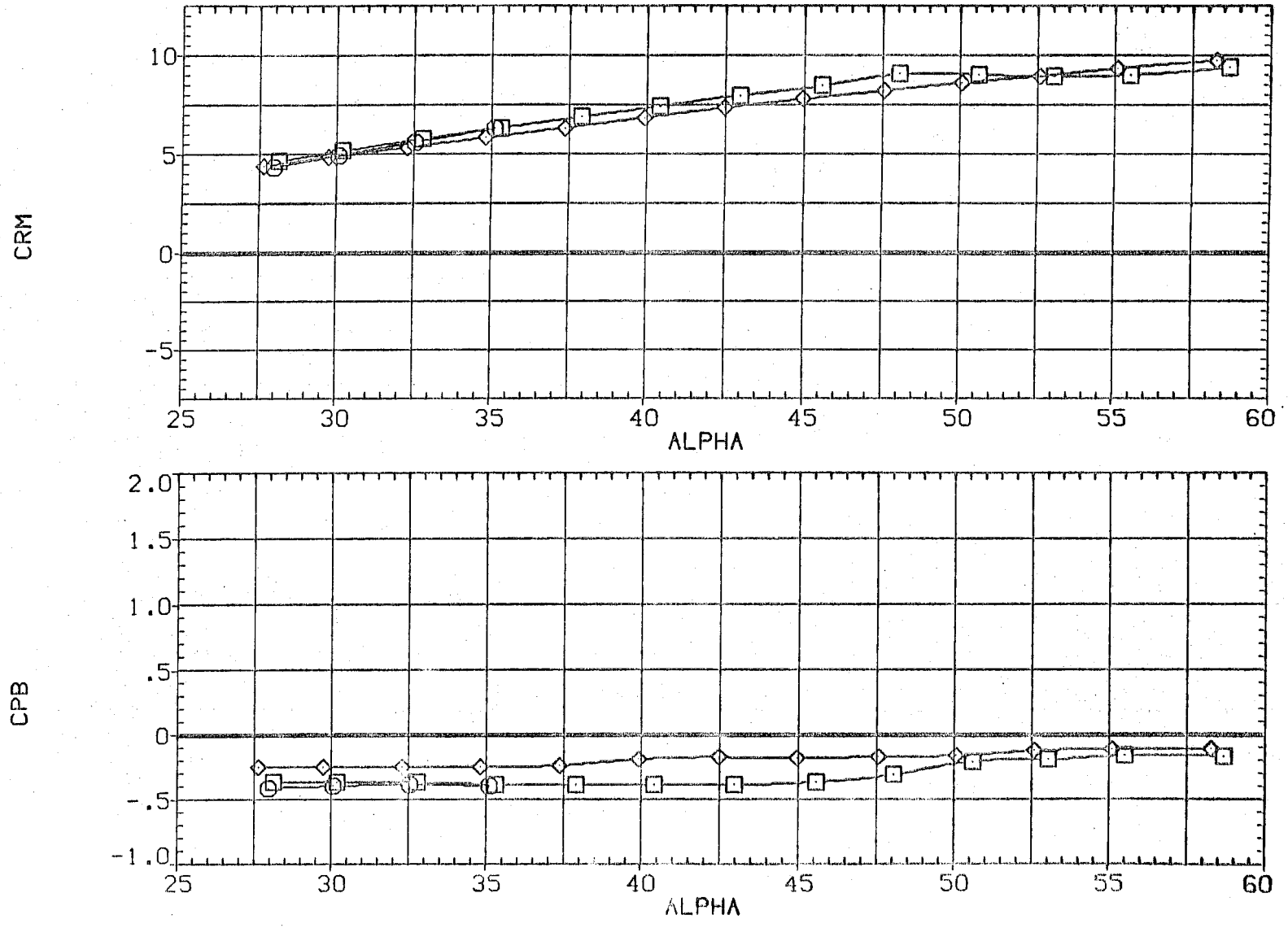

FIG.8 L/D=5 TAN. OGIVE, EFFECT OF MACH NUMBER, SUPERSONIC

DATA SET	SYMBOL	CONFIGURATION DESCRIPTION	R	BETA
(RJDA25)	○	FT5	.400	.000
(RJDC24)	□	FT5	.750	.000
(RJDA26)	◇	FT5	1.750	.000

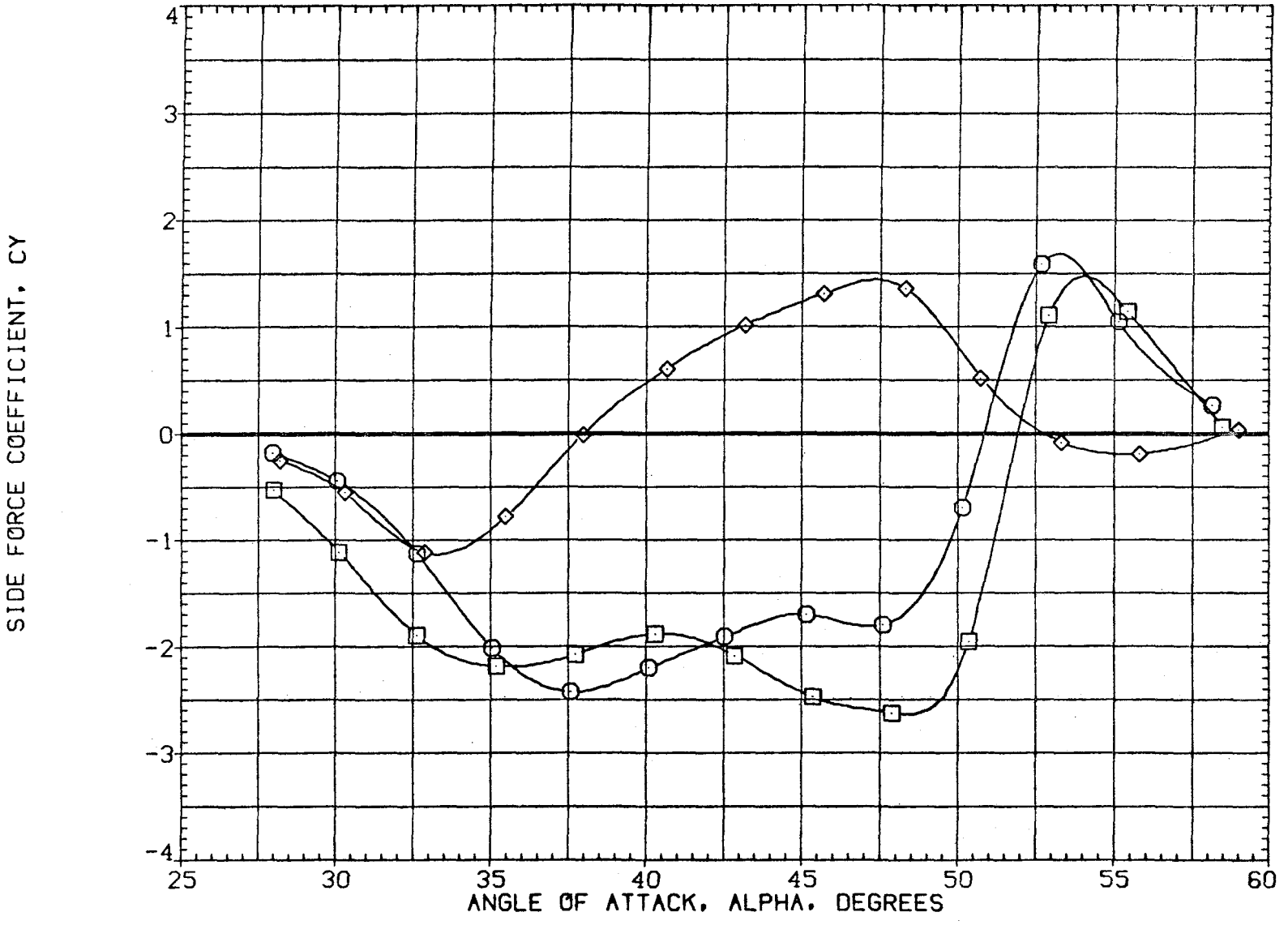

FIG.9 L/D=5 TAN. OGIVE, EFFECT OF REYNOLDS NUMBER

(A)MACH = .60

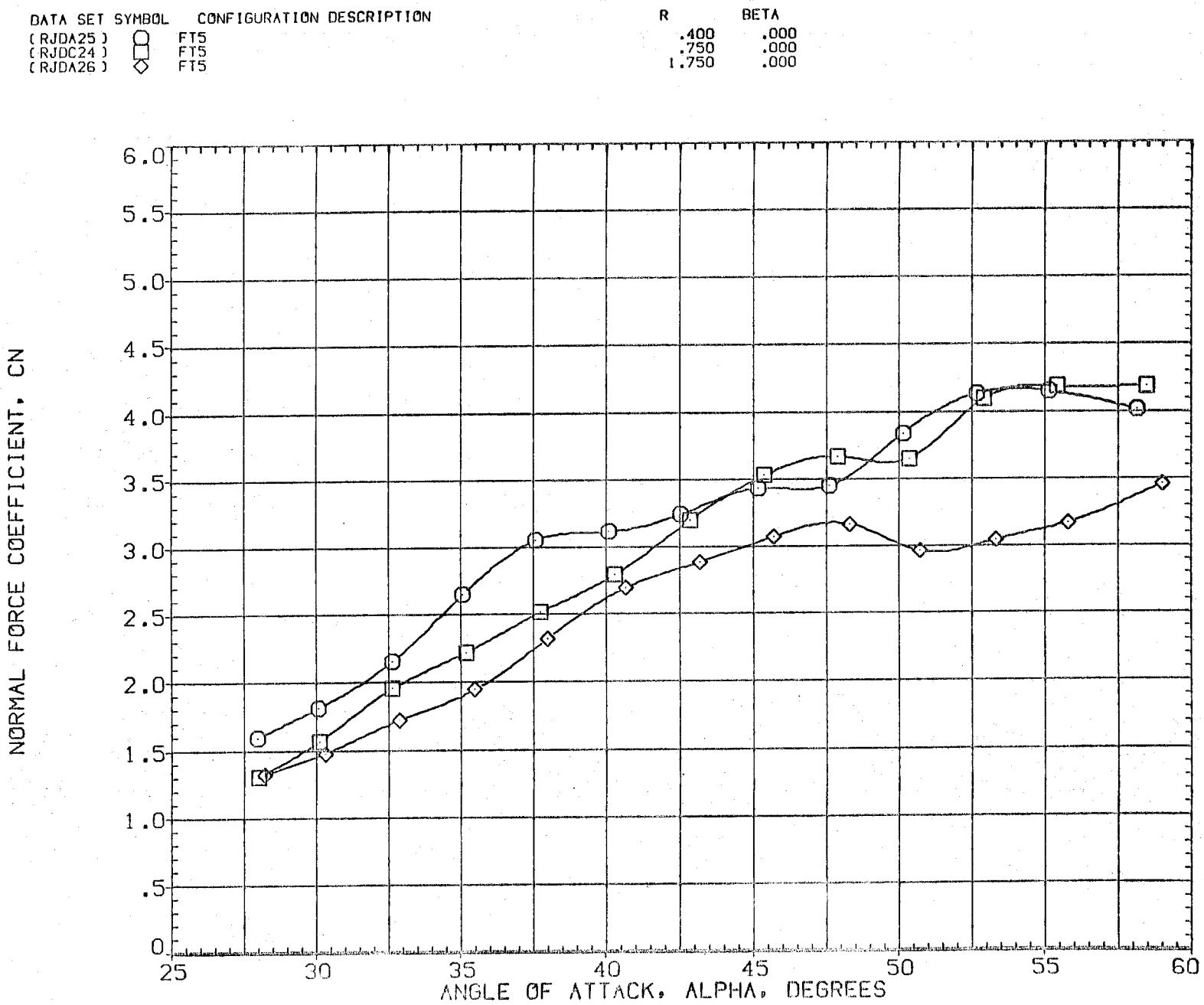

FIG.9 L/D=5 TAN. OGIVE, EFFECT OF REYNOLDS NUMBER

DATA SET	SYMBOL	CONFIGURATION DESCRIPTION	R	BETA
(RJDA25)	○	FT5	.400	.000
(RJDC24)	□	FT5	.750	.000
(RJDA26)	◇	FT5	1.750	.000

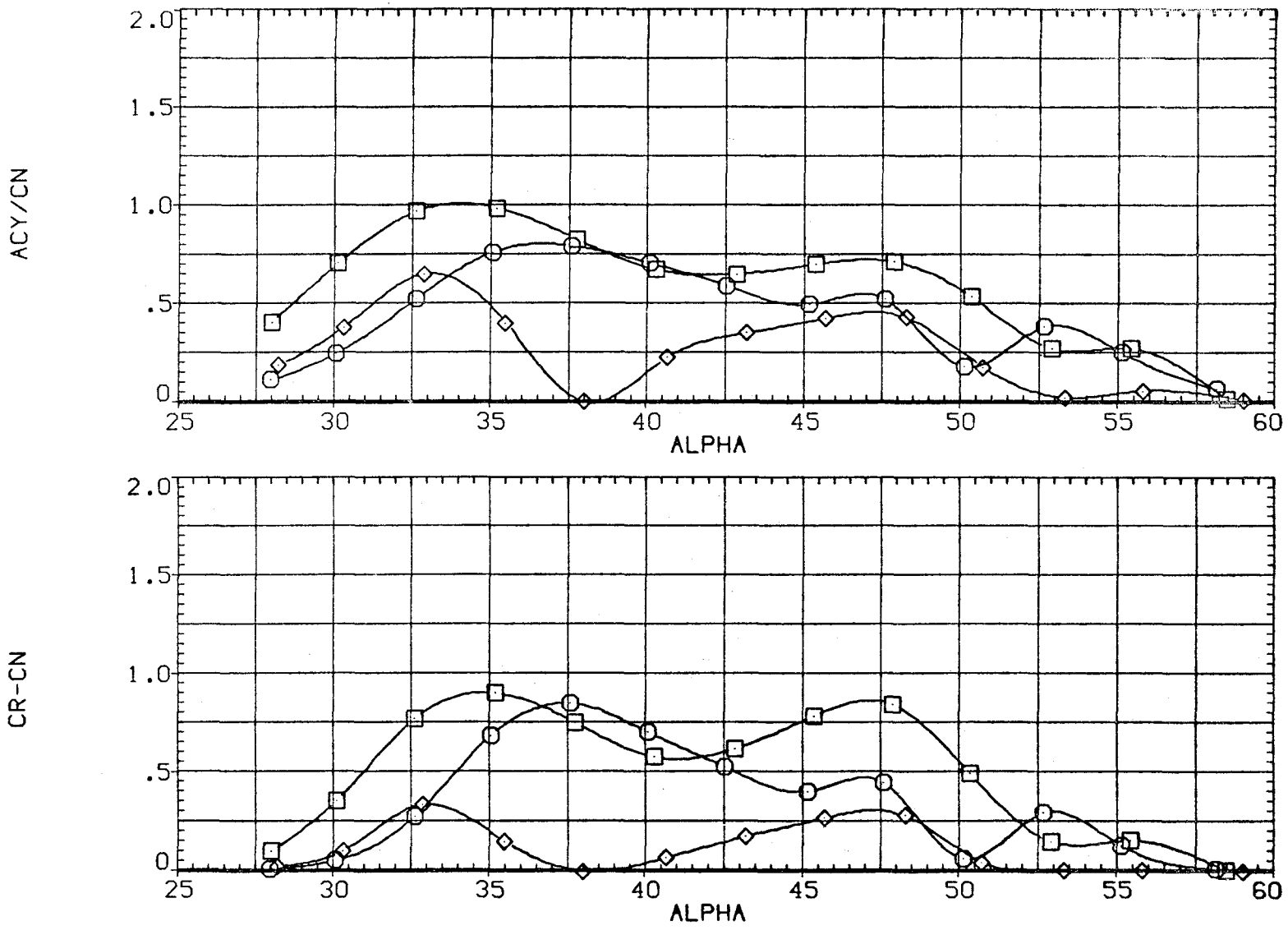

FIG.9 L/D=5 TAN. OGIVE, EFFECT OF REYNOLDS NUMBER

(A)MACH = .60

DATA SET	SYMBOL	CONFIGURATION DESCRIPTION	R	BETA
(RJDA25)		FT5	.400	.000
(RJDC24)		FT5	.750	.000
(RJDA26)		FT5	1.750	.000

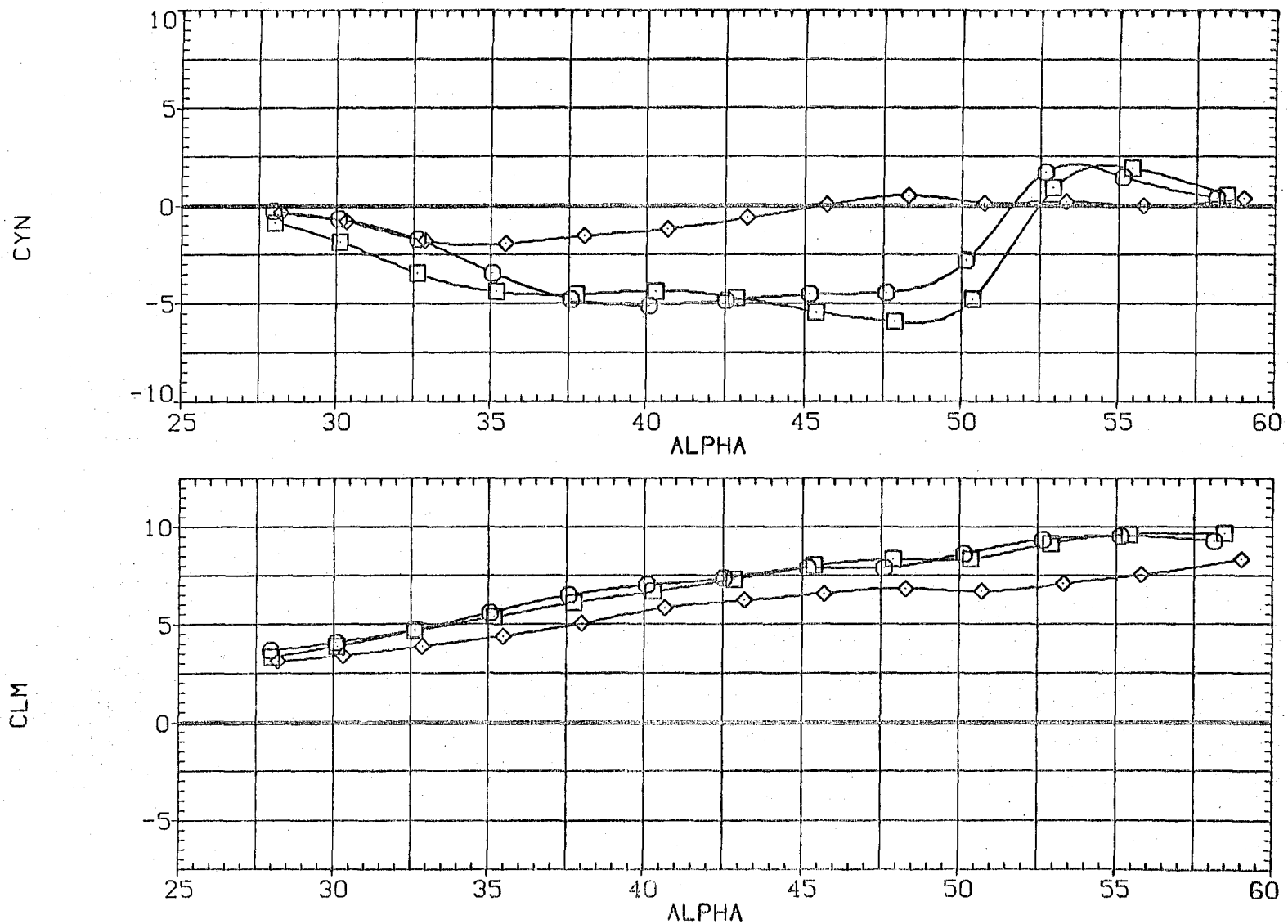

FIG.9 L/D=5 TAN. OGIVE, EFFECT OF REYNOLDS NUMBER

(A)MACH = .60

DATA SET SYMBOL	CONFIGURATION DESCRIPTION	R	BETA
(RJDA25)	FT5	.400	.000
(RJDC24)	FT5	.750	.000
(RJDA26)	FT5	1.750	.000

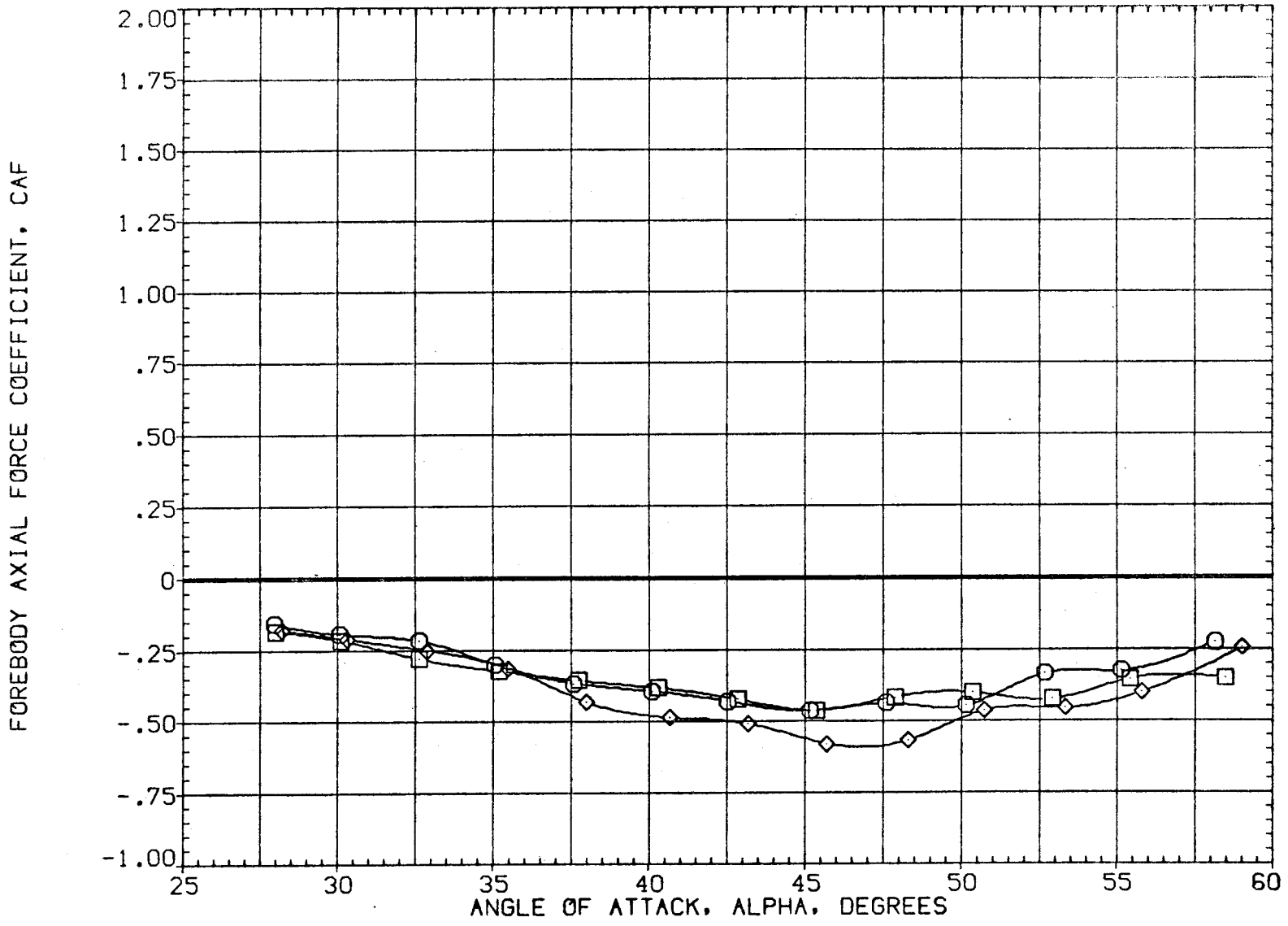

FIG.9 L/D=5 TAN. OGIVE, EFFECT OF REYNOLDS NUMBER

(A)MACH = .60

DATA SET	SYMBOL	CONFIGURATION DESCRIPTION	R	BETA
(AJD025)	○	FT5	.400	.000
(AJD024)	□	FT5	.750	.000
(AJD026)	◇	FT5	1.750	.000

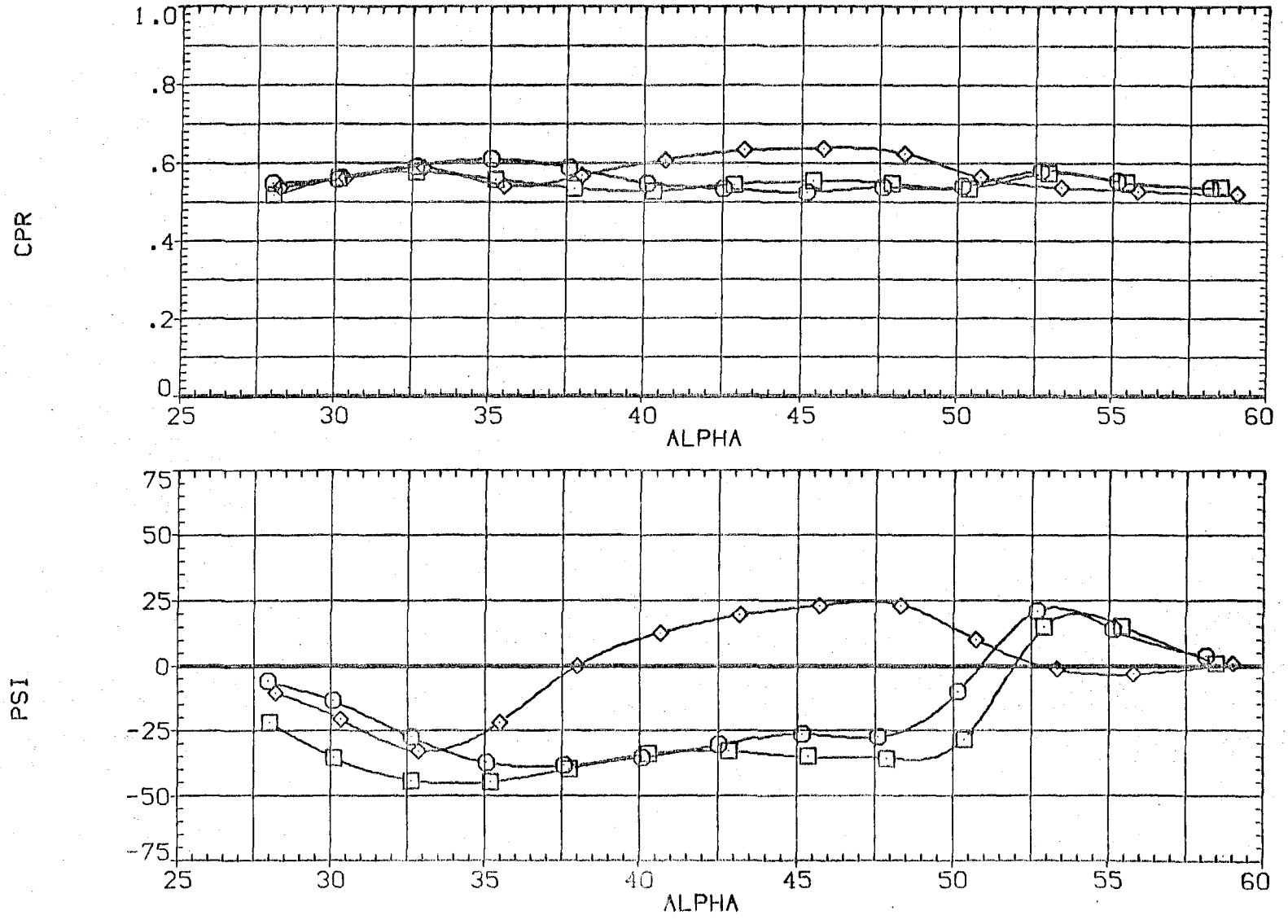

FIG.9 L/D=5 TAN. OGIVE, EFFECT OF REYNOLDS NUMBER

DATA SET	SYMBOL	CONFIGURATION DESCRIPTION	R	BETA
(AJD025)	○	FT5	.400	.000
(AJDC24)	□	FT5	.750	.000
(AJD026)	◇	FT5	1.750	.000

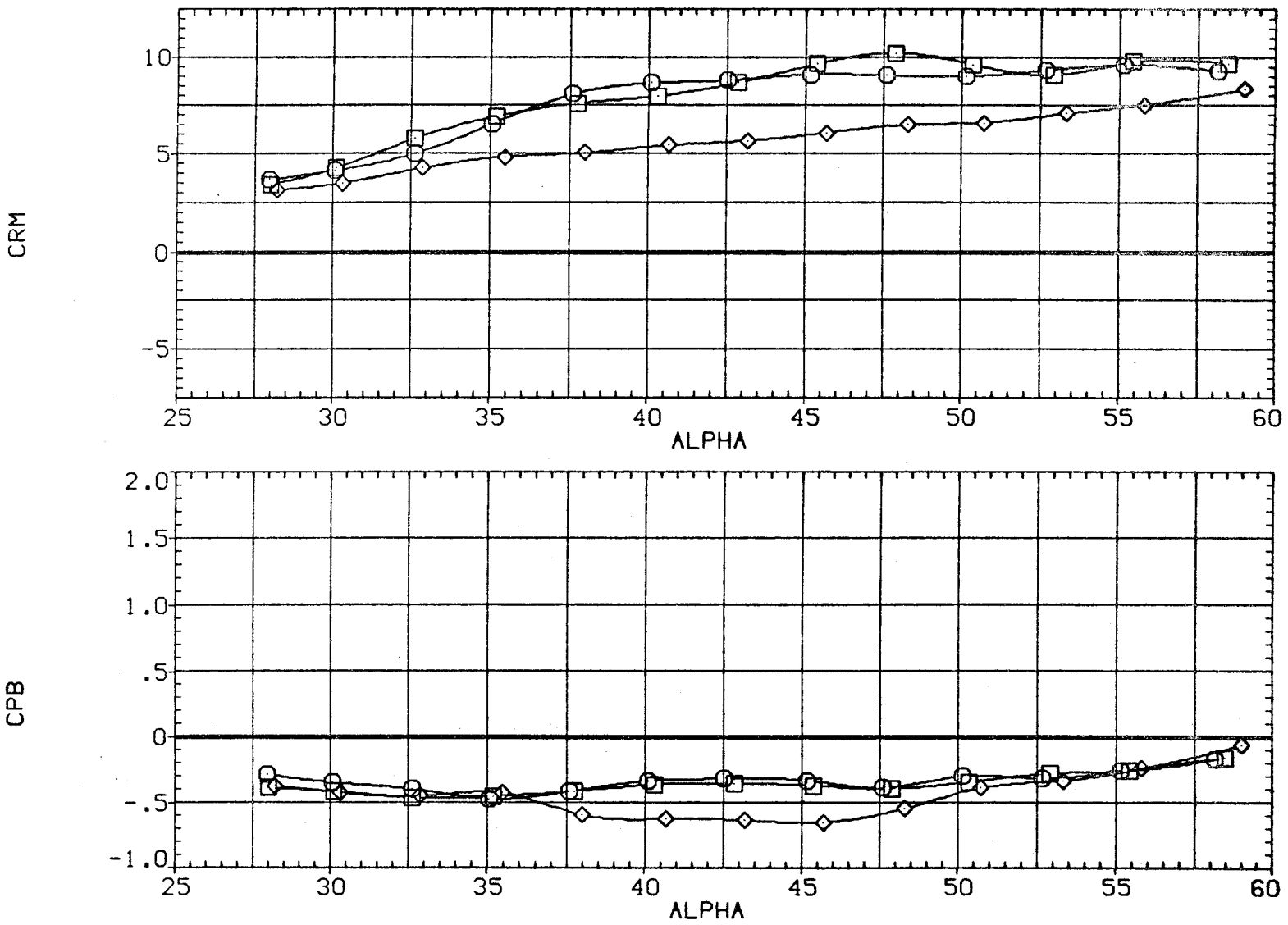

FIG.9 L/D=5 TAN. OGIVE, EFFECT OF REYNOLDS NUMBER

(A)MACH = .60

SYMBOL	MACH		PARAMETRIC VALUES		
○	.600	BETA	.000	R	.750
□	.795				
◇	1.497				
△	1.981				

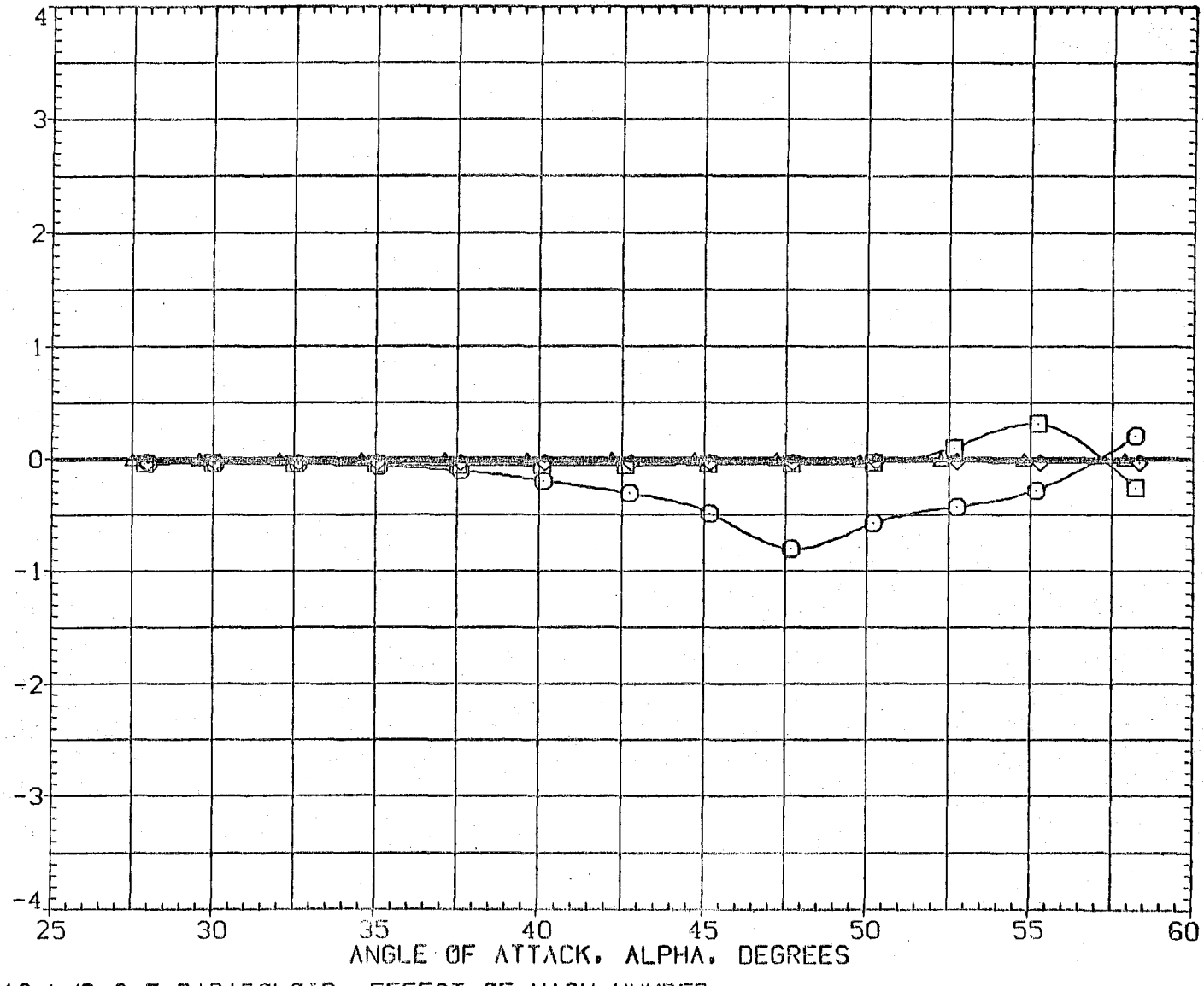

FIG.10 L/D=3.5 PARABOLOID, EFFECT OF MACH NUMBER

SYMBOL	MACH		PARAMETRIC VALUES		
○	.600	BETA	.000	R	.750
□	.795				
◇	1.497				
△	1.981				

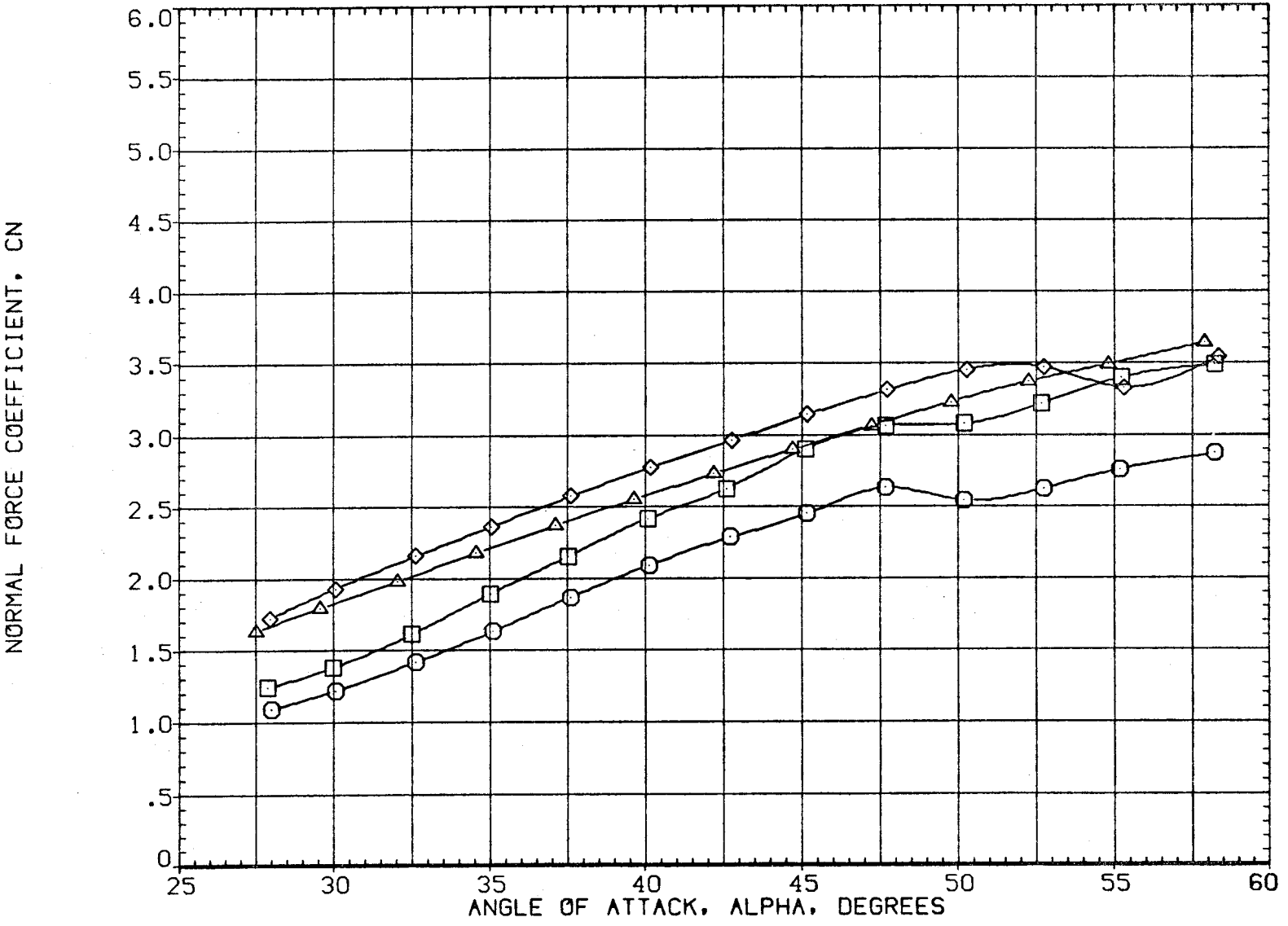

FIG.10 L/D=3.5 PARABOLOID, EFFECT OF MACH NUMBER

SYMBOL	MACH		PARAMETRIC VALUES		
○	.600	BETA	.000	R	.750
□	.795				
◇	1.497				
△	1.981				

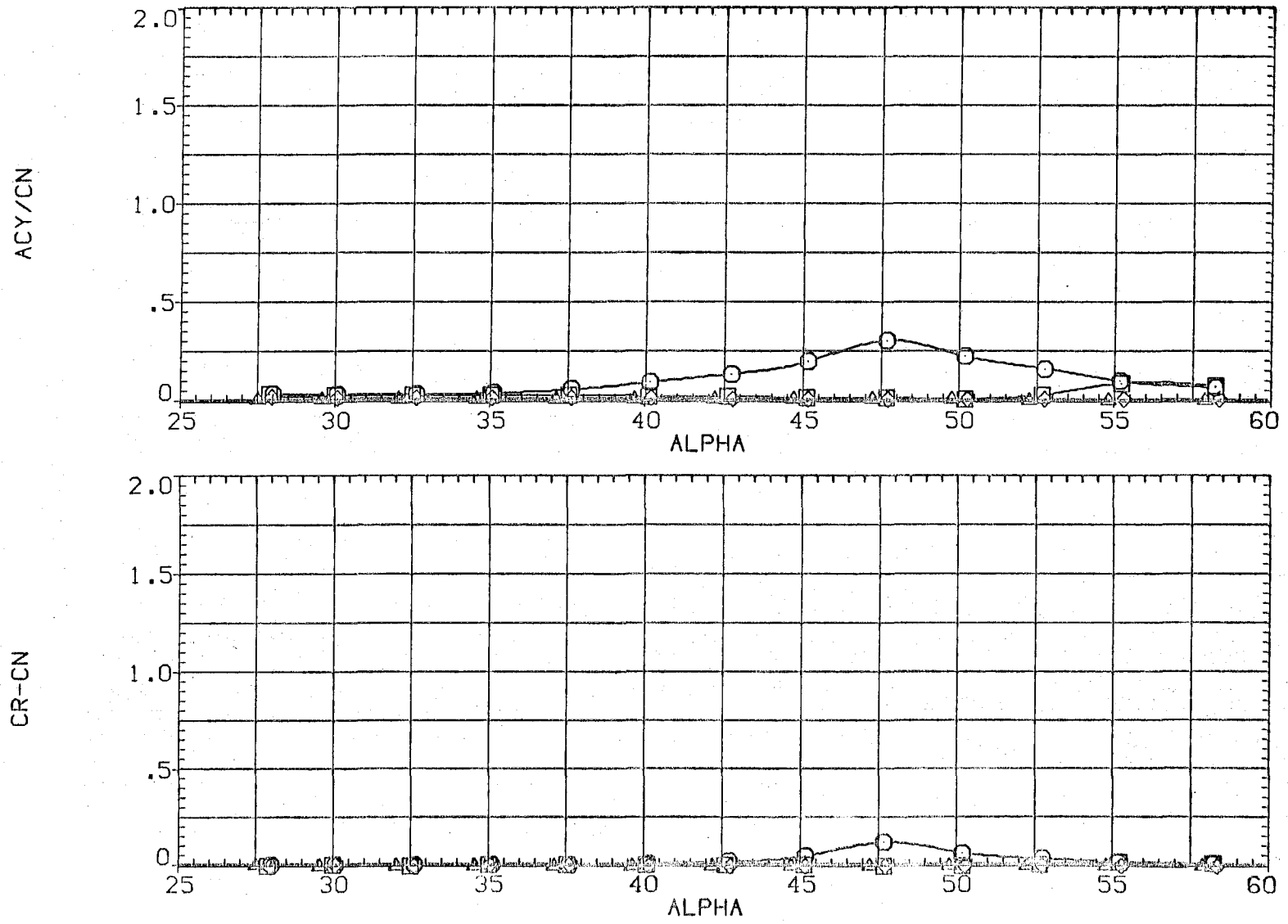

FIG.10 L/D=3.5 PARABOLOID, EFFECT OF MACH NUMBER

SYMBOL	MACH		PARAMETRIC VALUES		
○	.600	BETA	.000	R	.750
□	.795				
◇	1.497				
△	1.981				

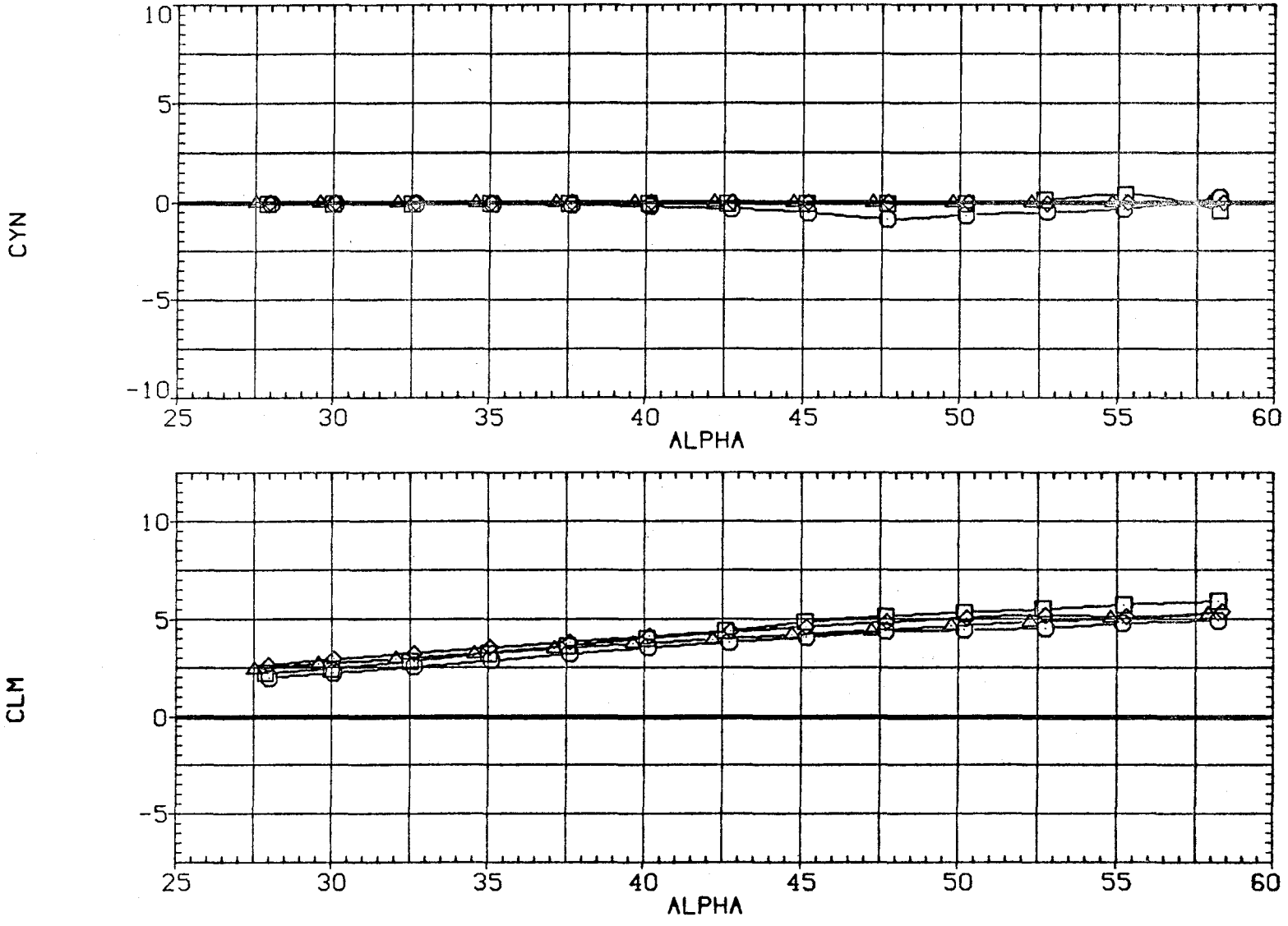

FIG.10 L/D=3.5 PARABOLOID, EFFECT OF MACH NUMBER

FP (RJDC46)

SYMBOL	MACH		PARAMETRIC VALUES		
○	.600	BETA	.000	R	.750
□	.795				
◇	1.497				
△	1.981				

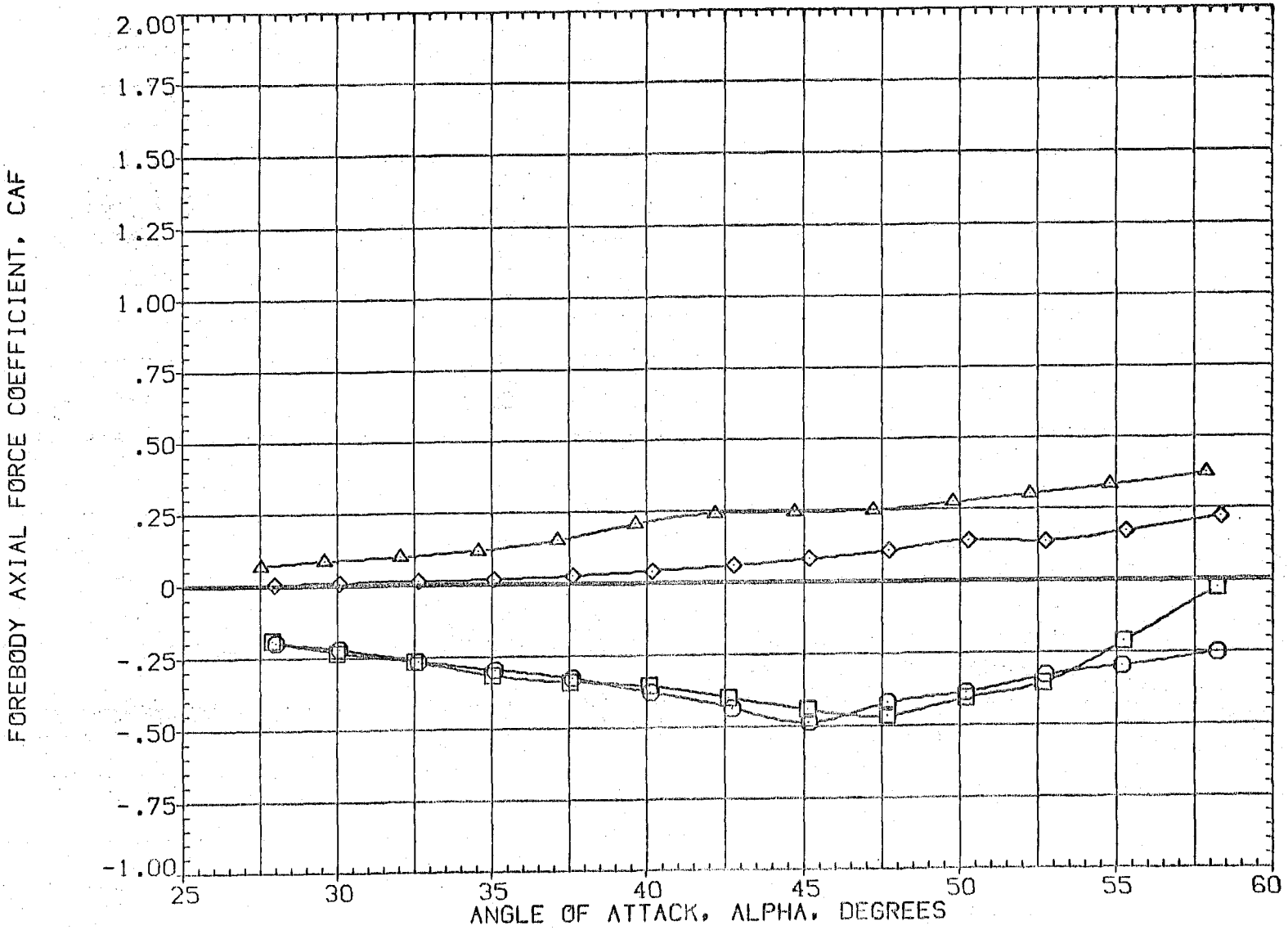

FIG.10 L/D=3.5 PARABOLOID, EFFECT OF MACH NUMBER

SYMBOL	MACH		PARAMETRIC VALUES		
○	.600	BETA	.000	R	.750
□	.795				
◇	1.497				
△	1.981				

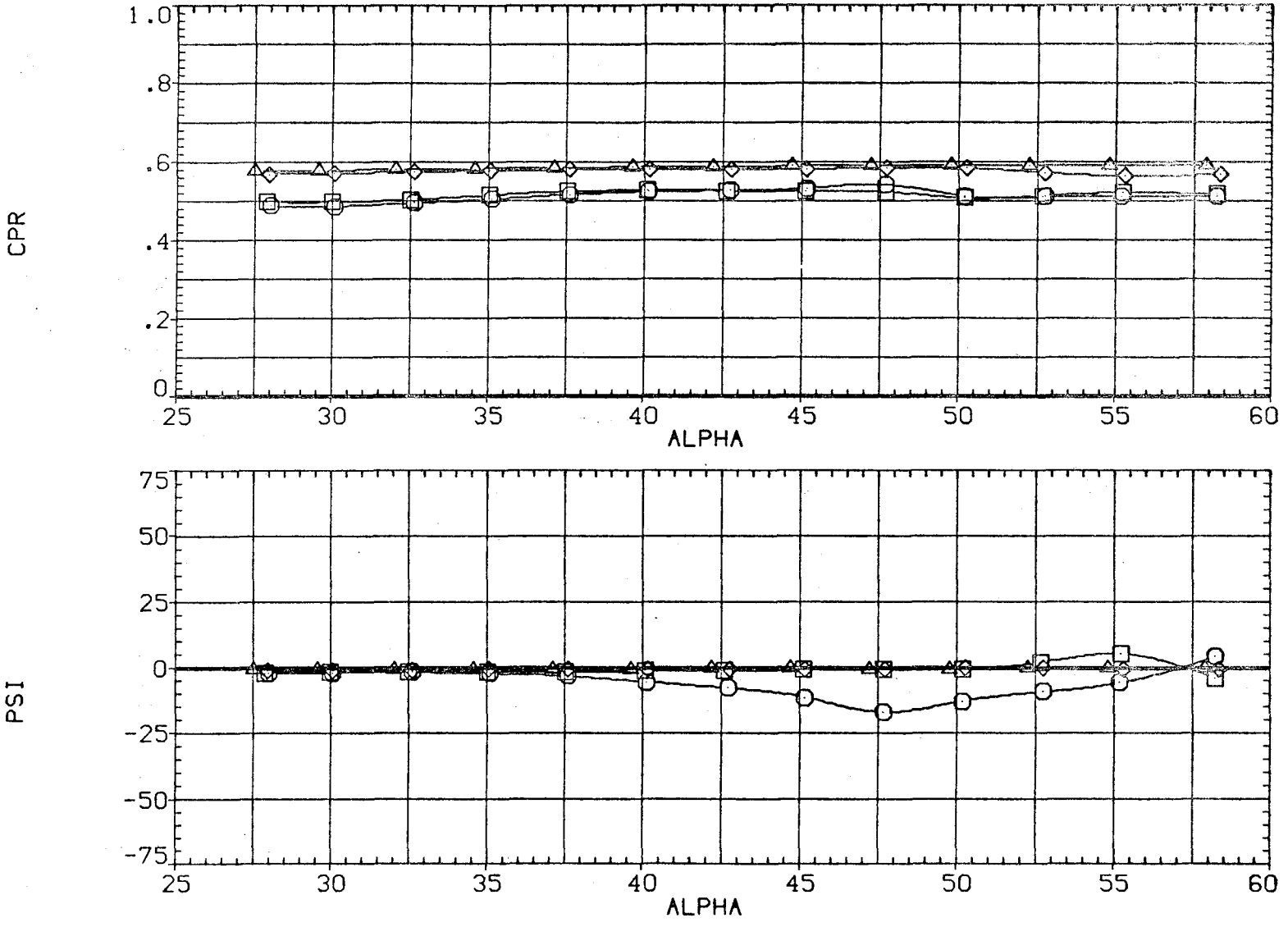

FIG.10 L/D=3.5 PARABOLOID, EFFECT OF MACH NUMBER

FP (AJDC46)

SYMBOL	MACH		PARAMETRIC VALUES		
○	.600	BETA	.000	R	.750
□	.795				
◇	1.497				
△	1.981				

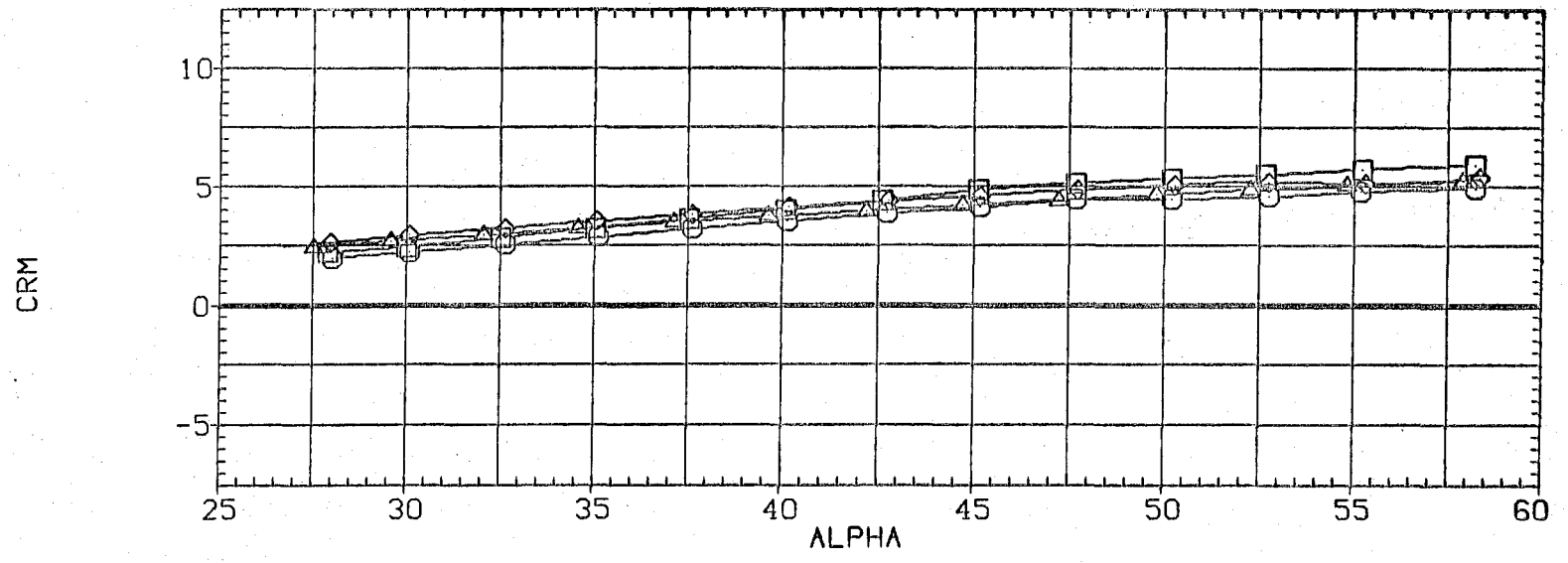

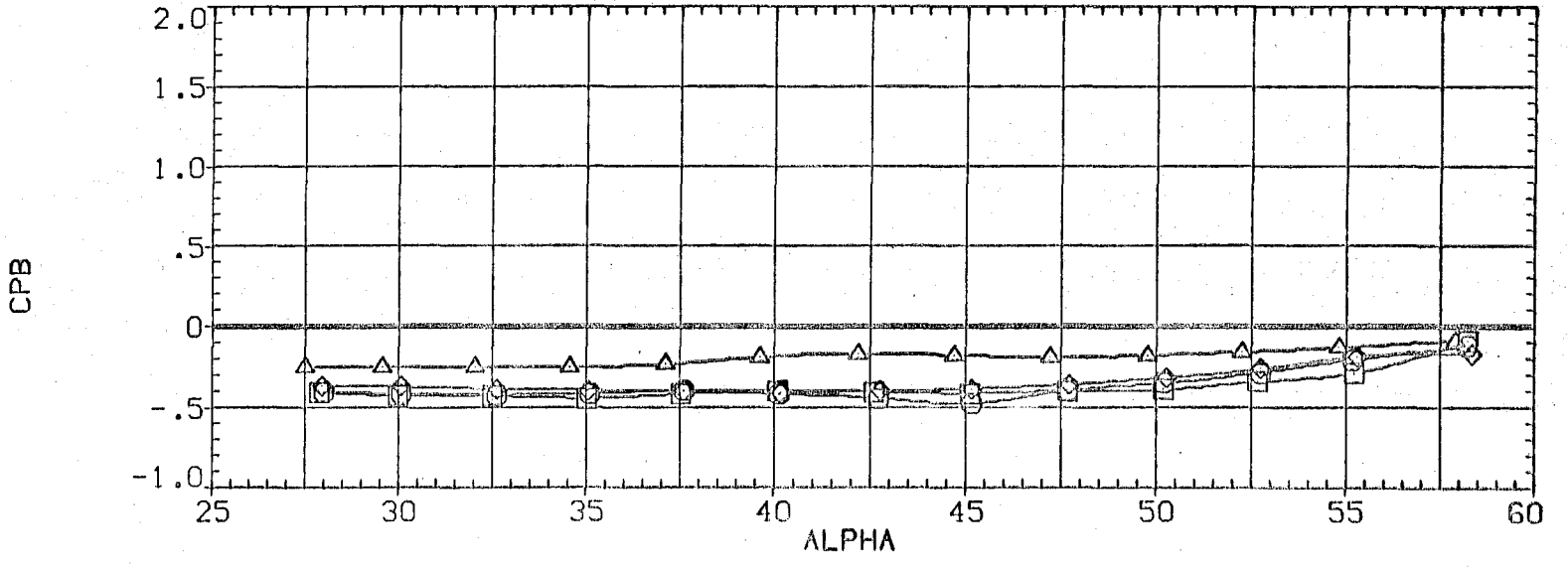

FIG.10 L/D=3.5 PARABOLOID, EFFECT OF MACH NUMBER

SYMBOL	MACH		PARAMETRIC VALUES		
○	.253	BETA	.000	R	.930
□	.599				
◇	.803				

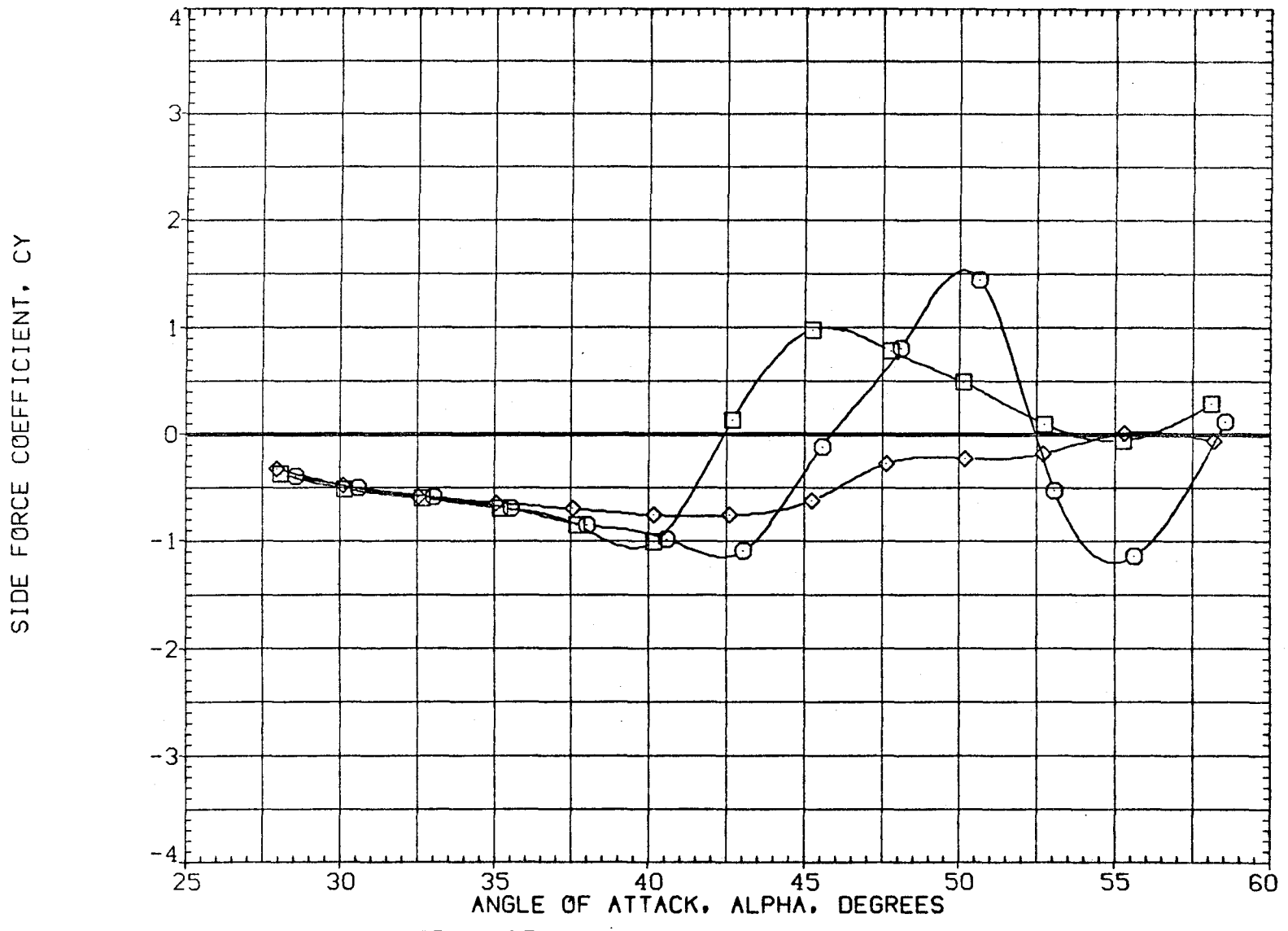

FIG.11 20 DEG. CONE, EFFECT OF MACH NUMBER, SUBSONIC

FC1 (RJDC30)

SYMBOL	MACH		PARAMETRIC VALUES		
○	.253	BETA	.000	R	.930
□	.599				
◇	.803				

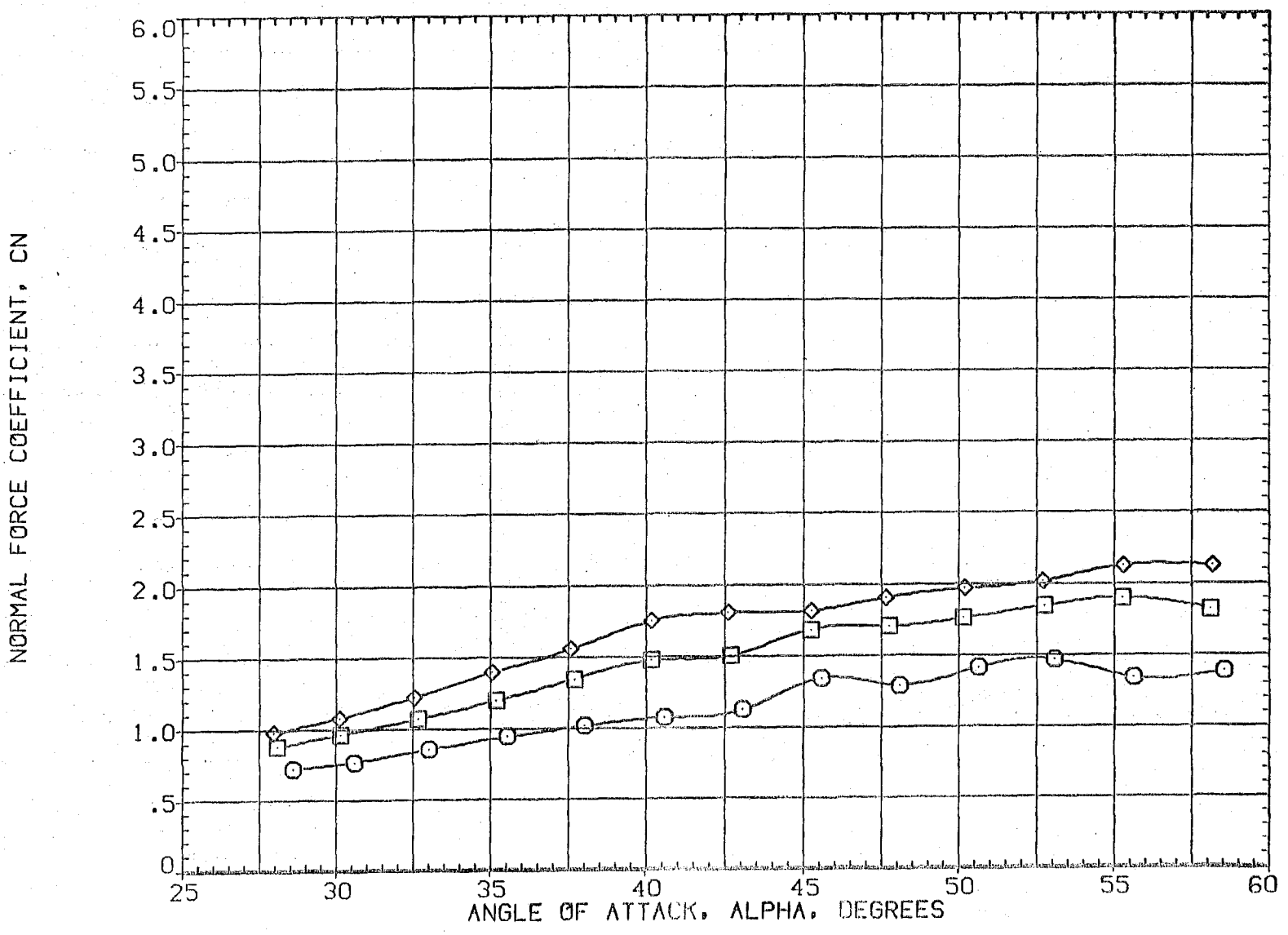

FIG.11 20 DEG. CONE, EFFECT OF MACH NUMBER, SUBSONIC

FC1 (RJDC30)

SYMBOL	MACH		PARAMETRIC VALUES		
○	.253	BETA	.000	R	.930
□	.599				
◇	.803				

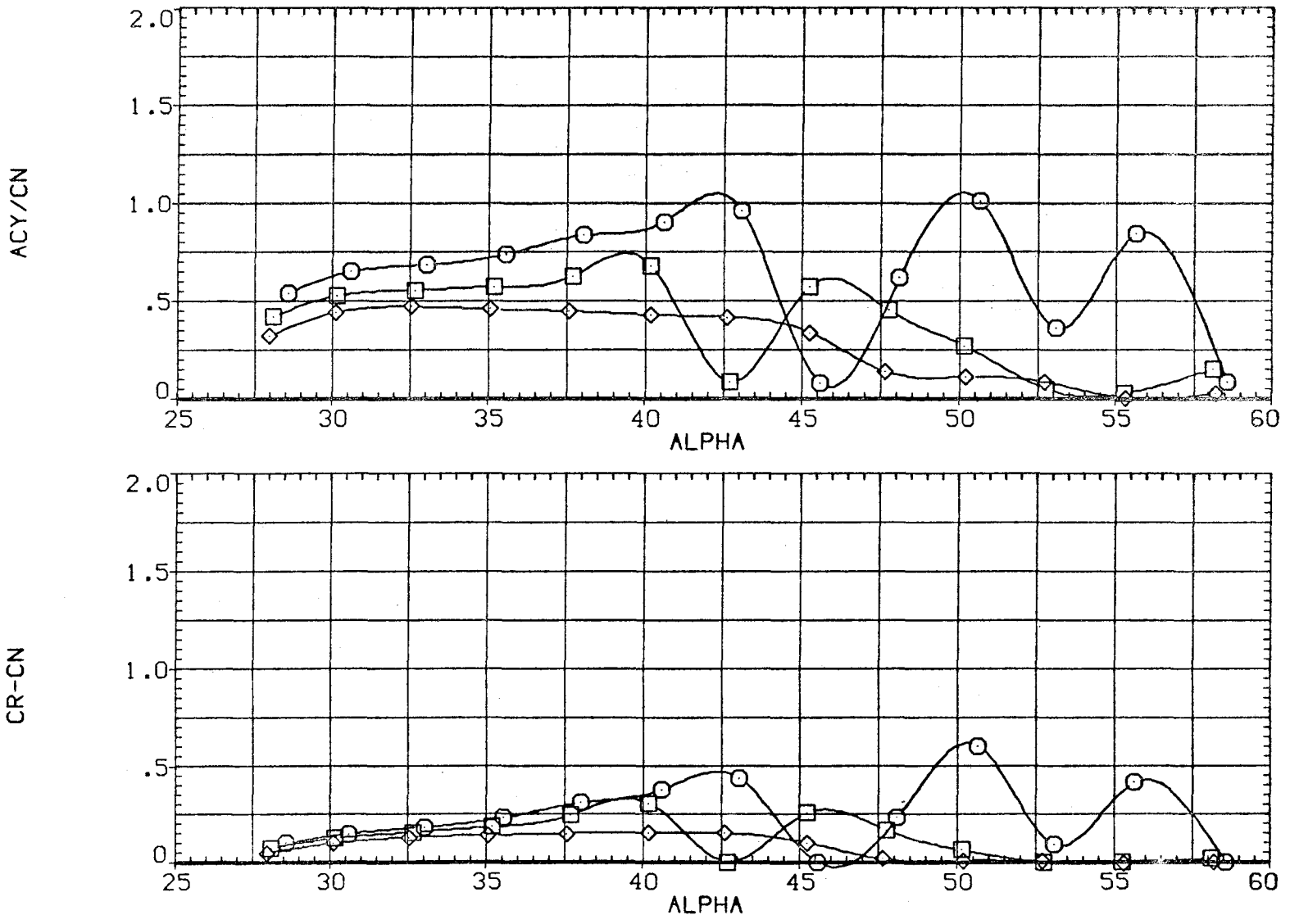

FIG.11 20 DEG. CONE, EFFECT OF MACH NUMBER, SUBSONIC

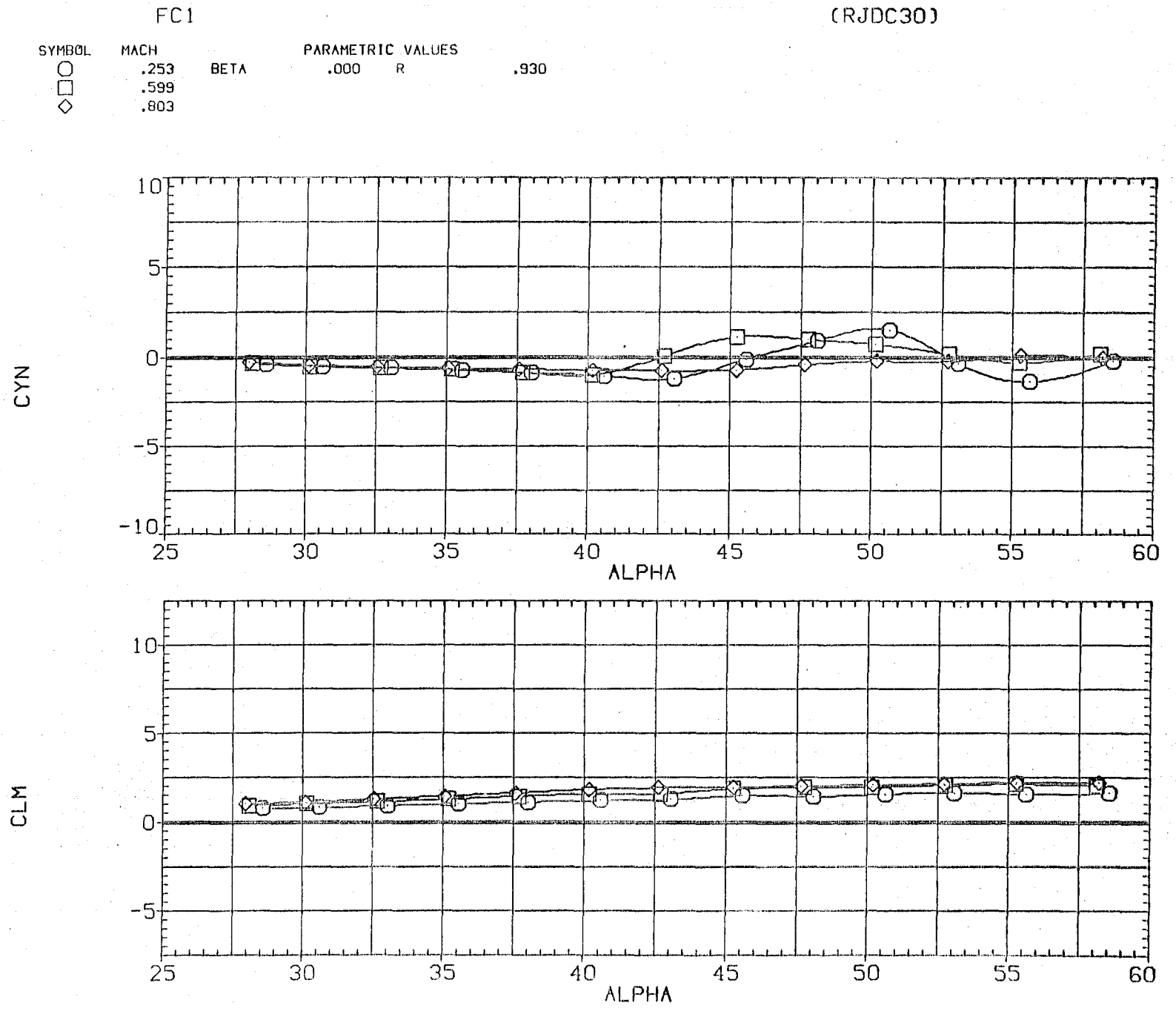

FIG.11 20 DEG. CONE, EFFECT OF MACH NUMBER, SUBSONIC

SYMBOL	MACH		PARAMETRIC VALUES		
○	.253	BETA	.000	R	.930
□	.599				
◇	.803				

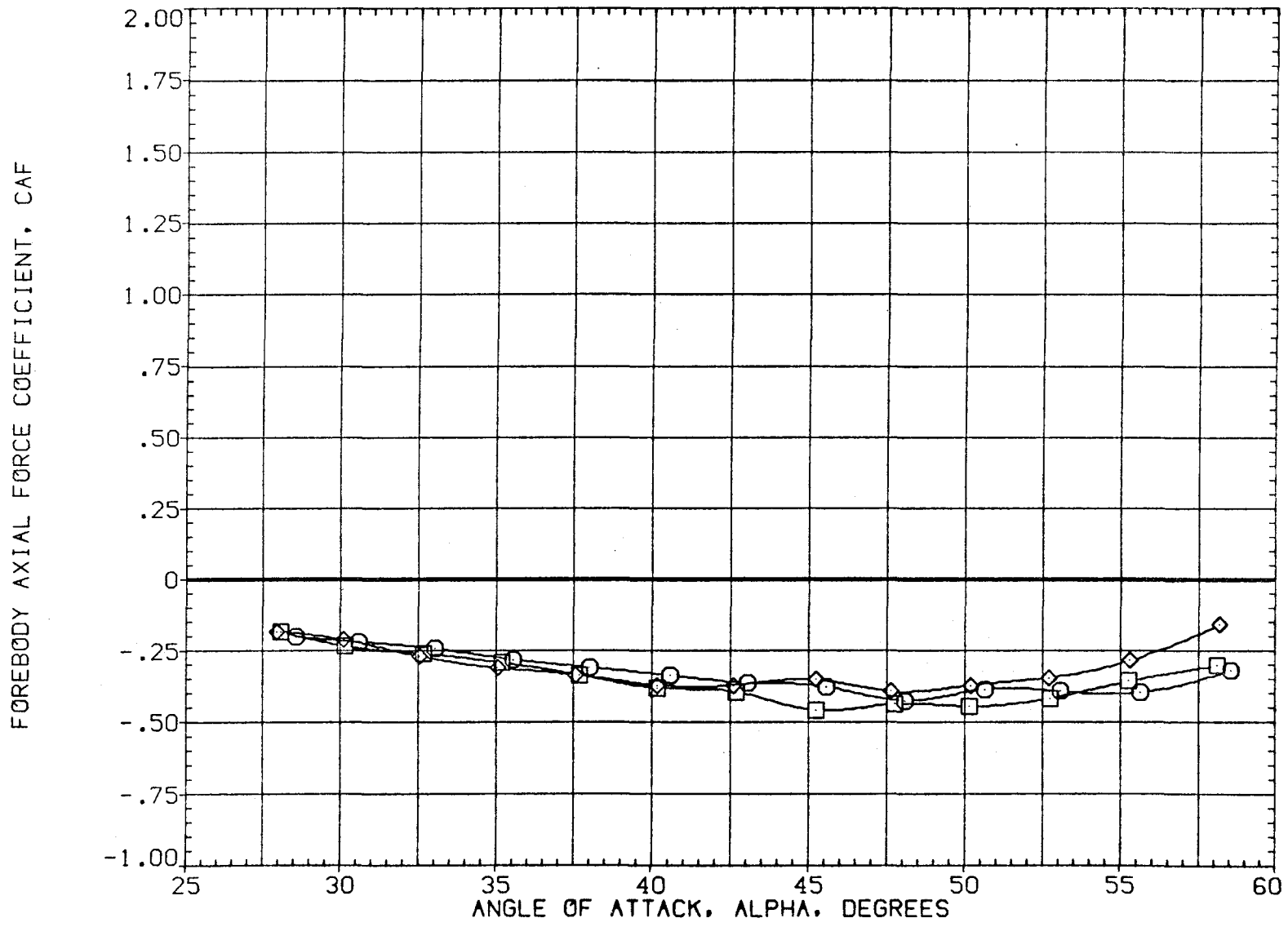

FIG.11 20 DEG. CONE, EFFECT OF MACH NUMBER, SUBSONIC

SYMBOL	MACH		PARAMETRIC VALUES		
○	.253	BETA	.000	R	.930
□	.599				
◇	.803				

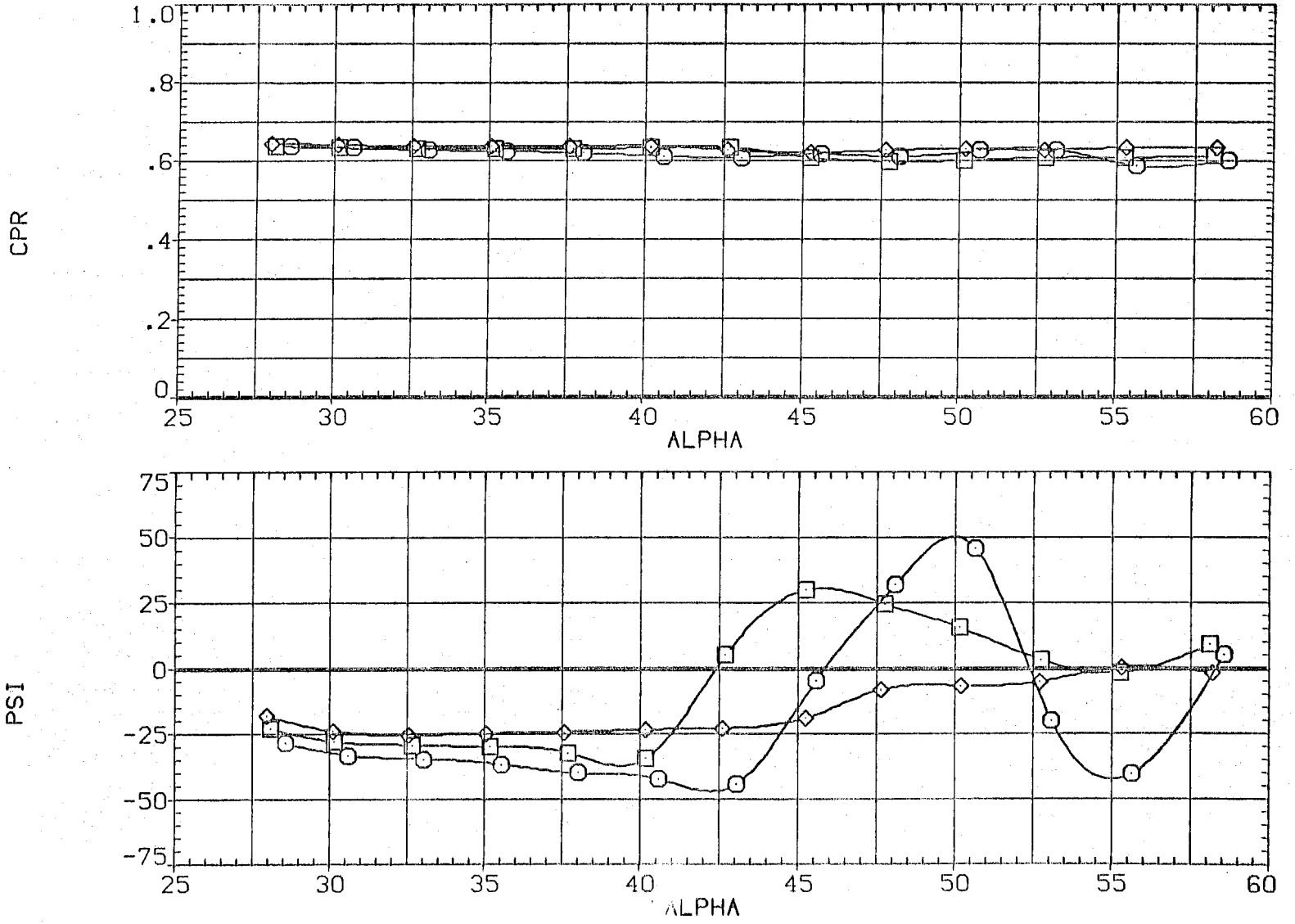

FIG.11 20 DEG. CONE, EFFECT OF MACH NUMBER, SUBSONIC

FC1 (AJDC30)

SYMBOL	MACH		PARAMETRIC VALUES		
○	.253	BETA	.000	R	.930
□	.599				
◇	.803				

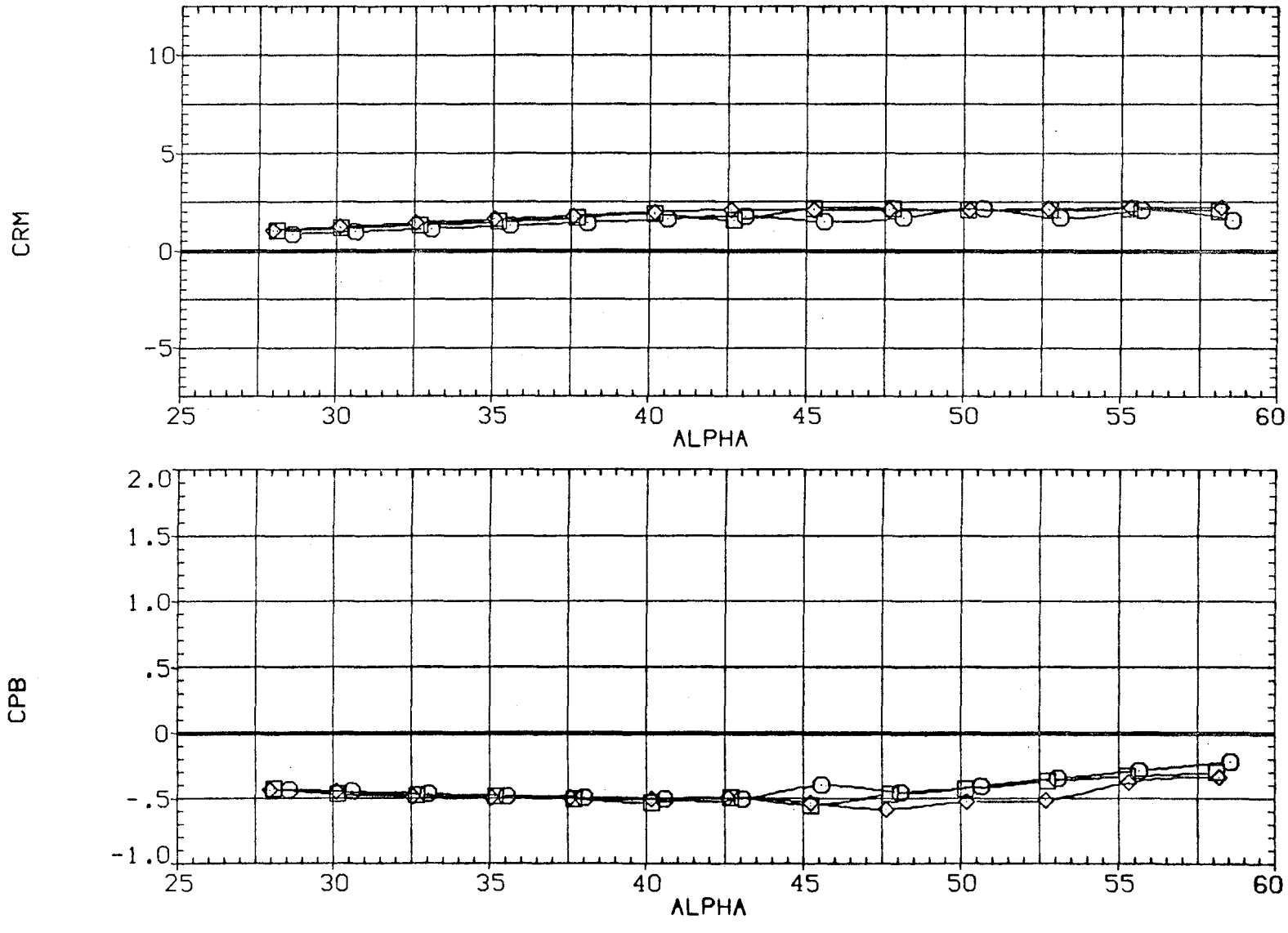

FIG.11 20 DEG. CONE, EFFECT OF MACH NUMBER, SUBSONIC

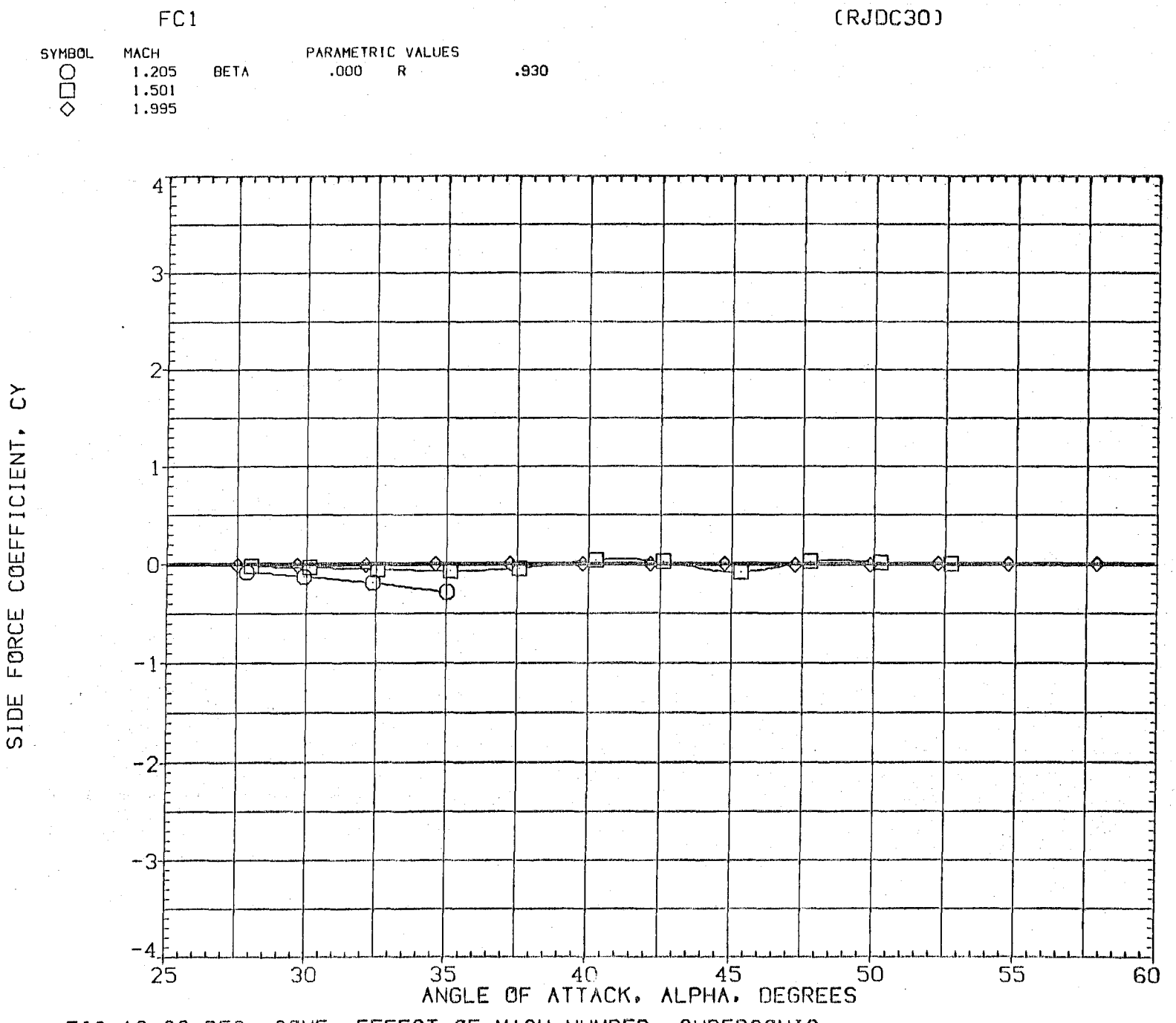

FIG.12 20 DEG. CONE, EFFECT OF MACH NUMBER, SUPERSONIC

SYMBOL	MACH		PARAMETRIC VALUES		
○	1.205	BETA	.000	R	.930
□	1.501				
◇	1.995				

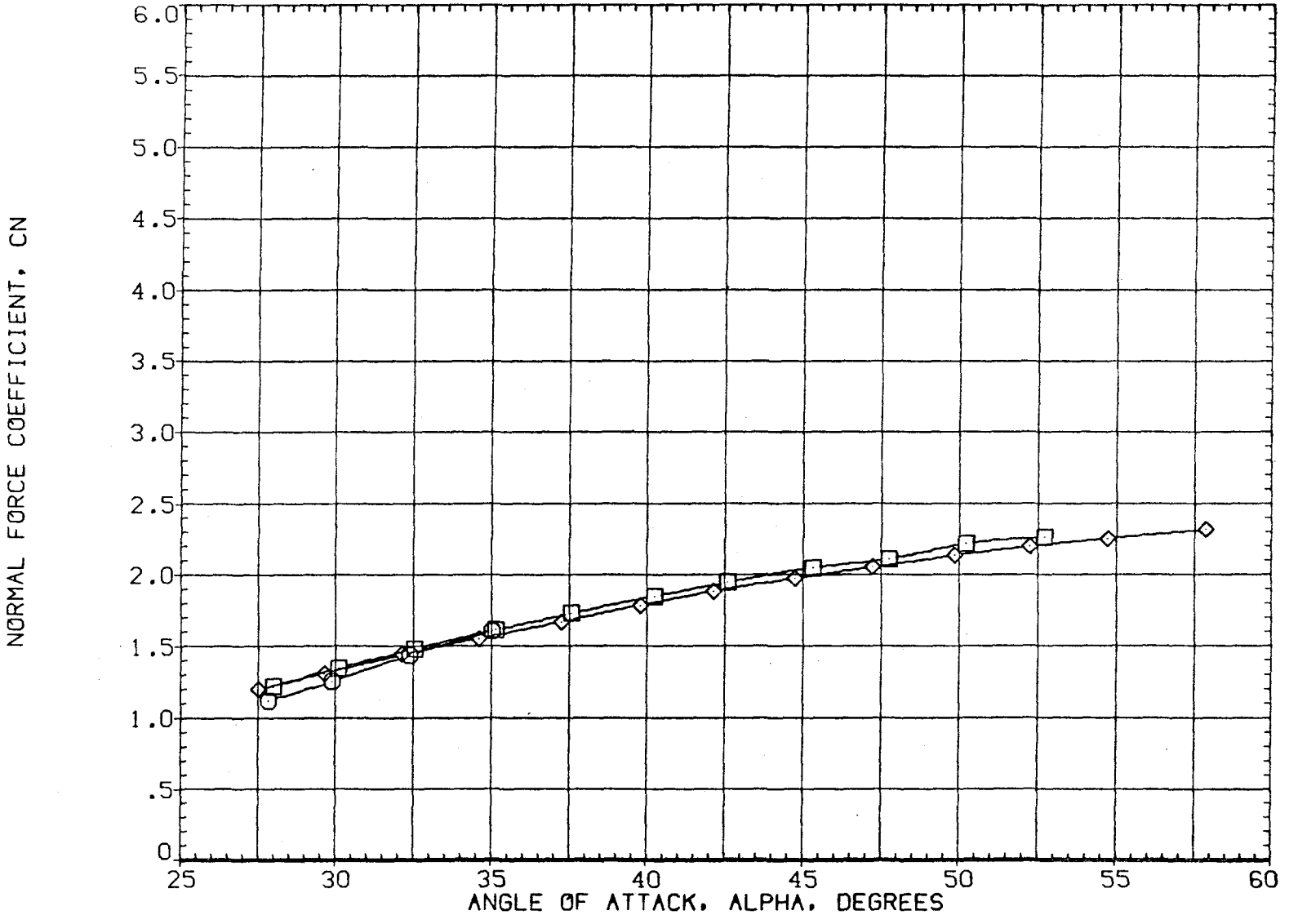

FIG.12 20 DEG. CONE, EFFECT OF MACH NUMBER, SUPERSONIC

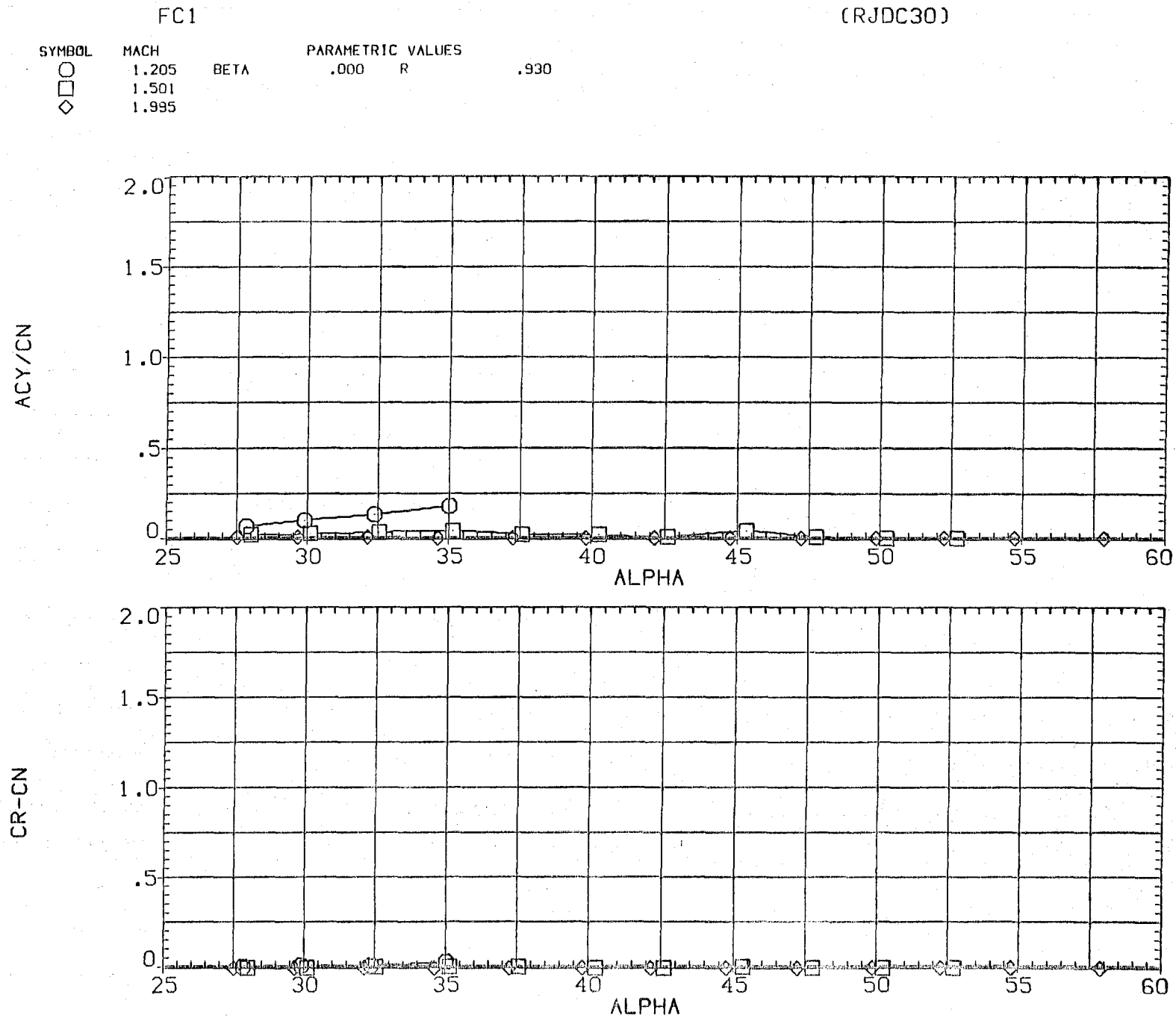

FIG.12 20 DEG. CONE, EFFECT OF MACH NUMBER, SUPERSONIC

FC1 (RJDC30)

SYMBOL	MACH		PARAMETRIC VALUES		
○	1.205	BETA	.000	R	.930
□	1.501				
◇	1.995				

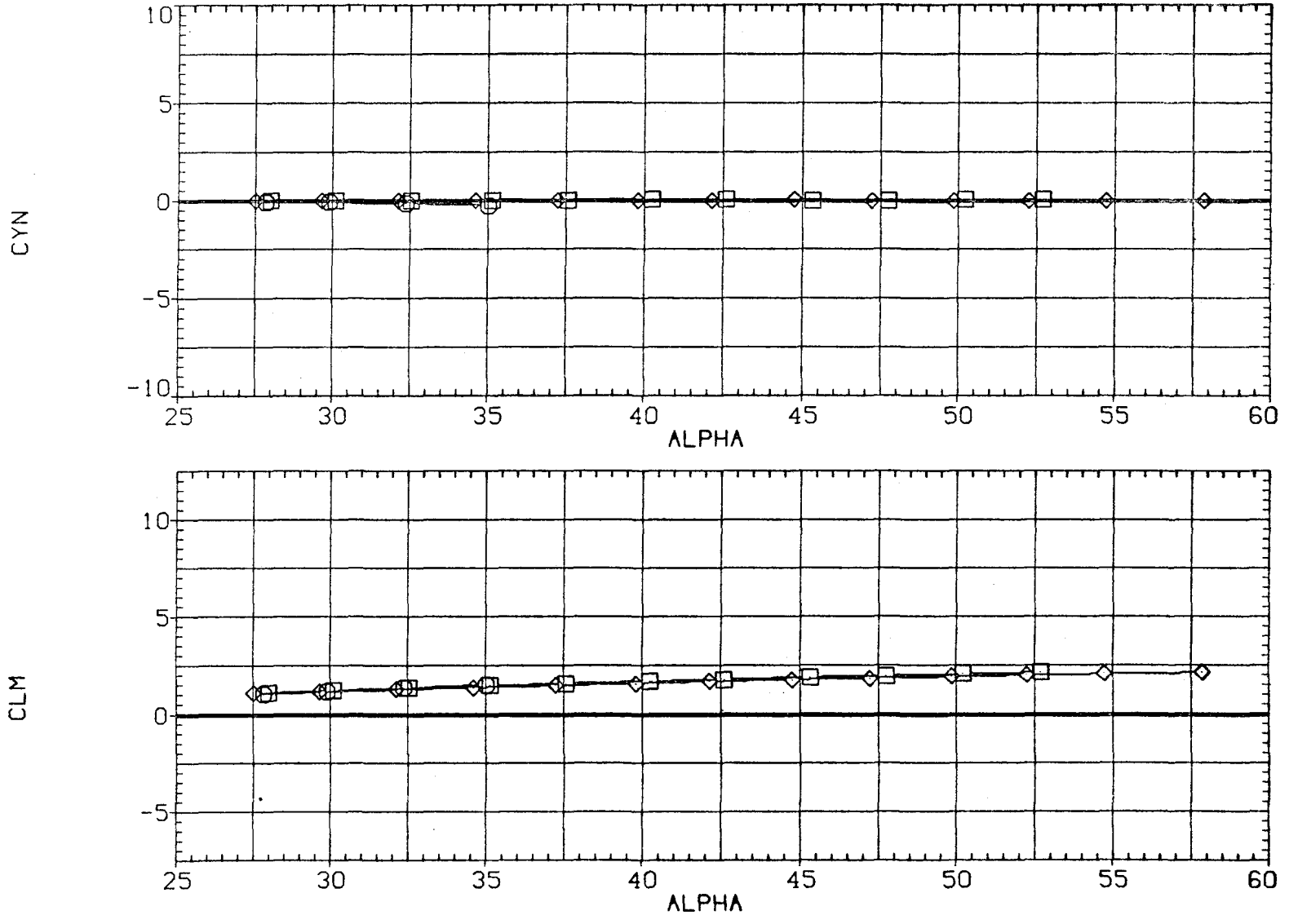

FIG.12 20 DEG. CONE, EFFECT OF MACH NUMBER, SUPERSONIC

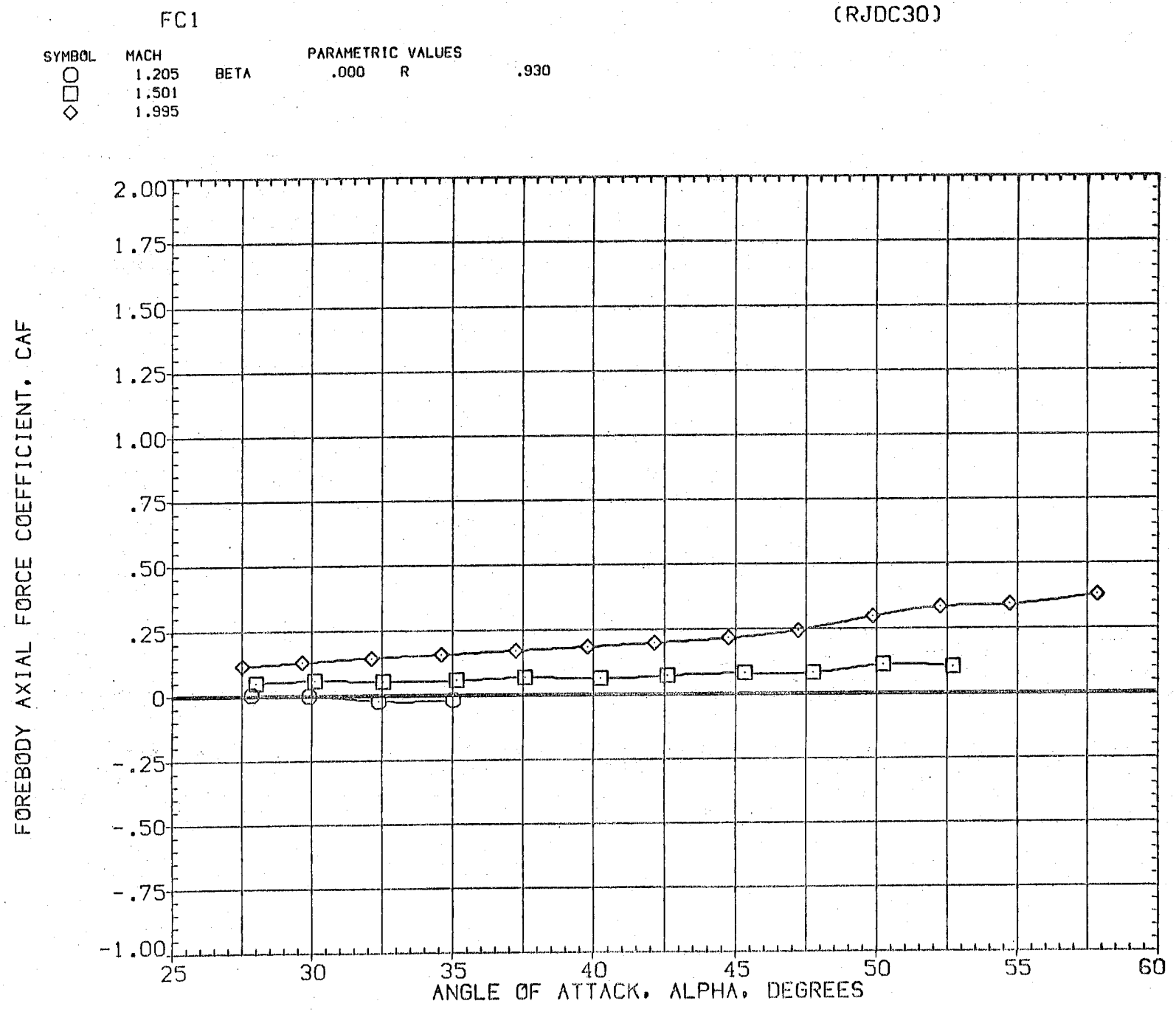

FIG.12 20 DEG. CONE, EFFECT OF MACH NUMBER, SUPERSONIC

FC1 (AJDC30)

SYMBOL	MACH		PARAMETRIC VALUES		
○	1.205	BETA	.000	R	.930
□	1.501				
◇	1.995				

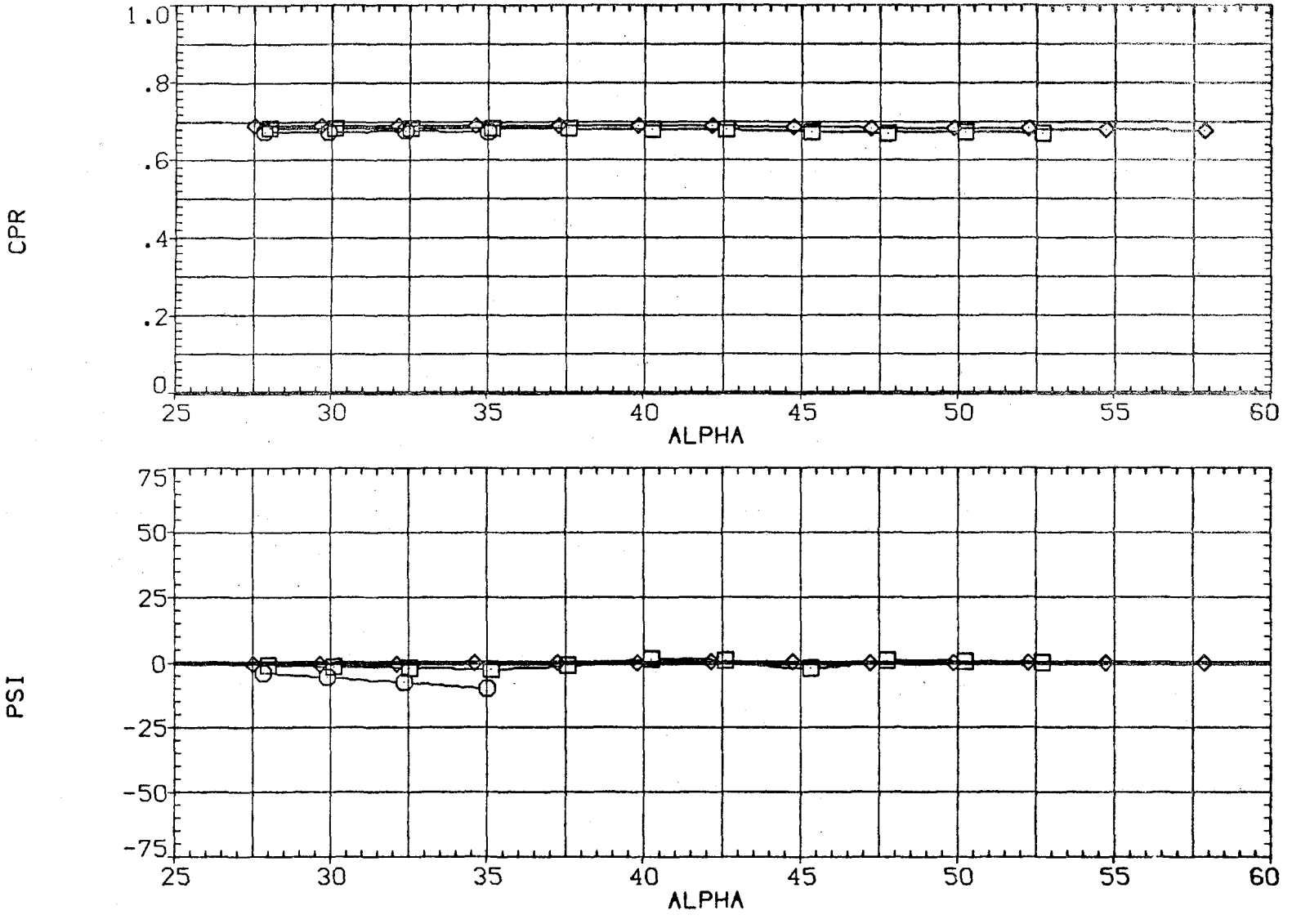

FIG.12 20 DEG. CONE, EFFECT OF MACH NUMBER, SUPERSONIC

FC1 (AJDC30)

SYMBOL	MACH		PARAMETRIC VALUES		
○	1.205	BETA	.000	R	.930
□	1.501				
◇	1.995				

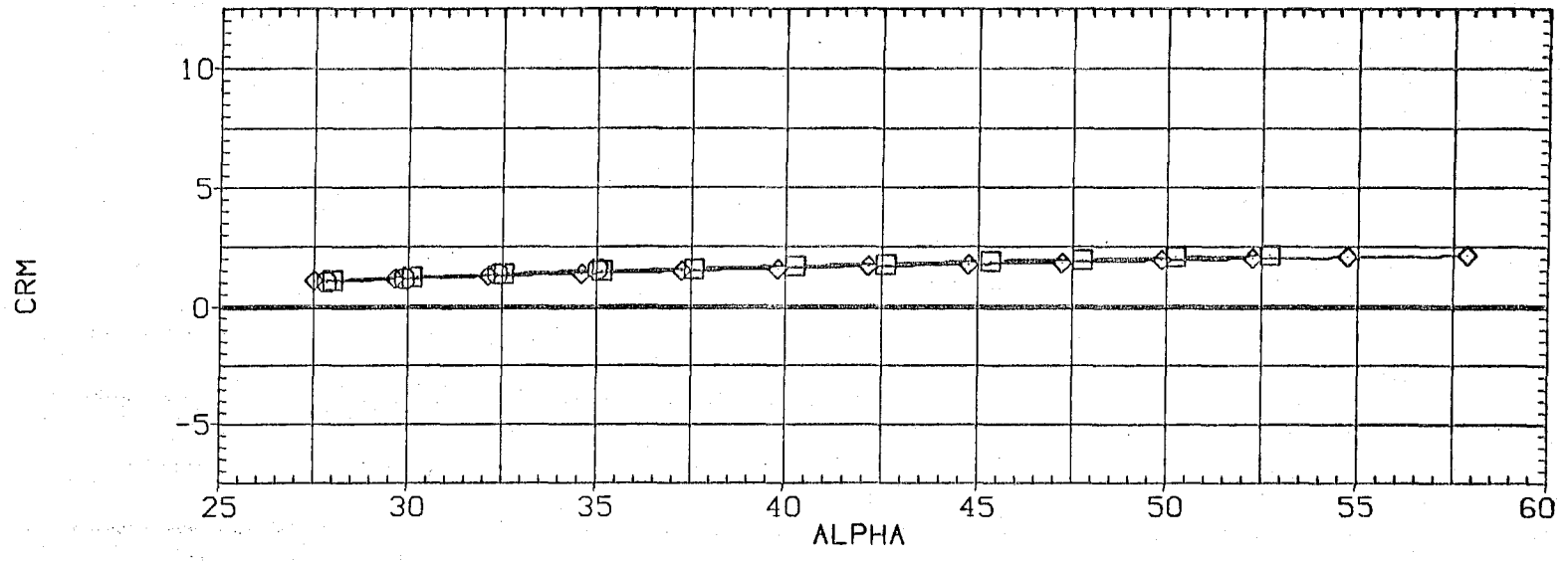

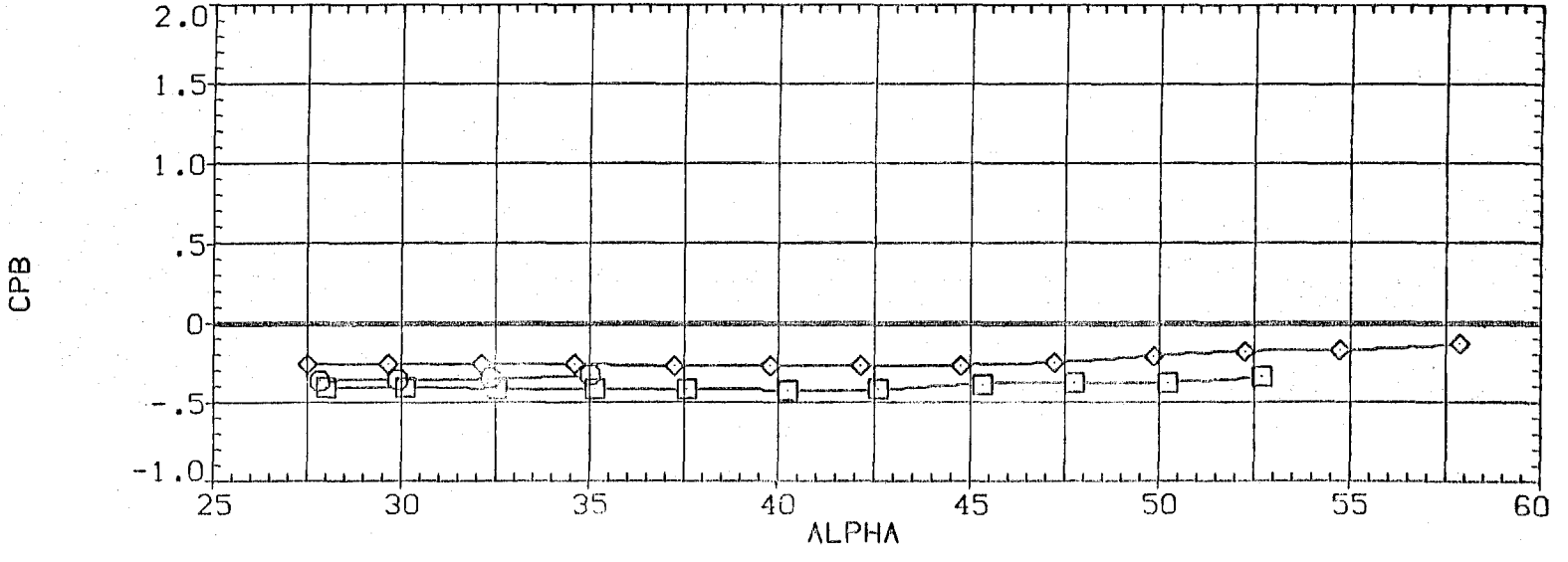

FIG.12 20 DEG. CONE, EFFECT OF MACH NUMBER, SUPERSONIC

DATA SET	SYMBOL	CONFIGURATION DESCRIPTION	R	BETA
(RJDC30)	○	FC1	.930	.000
(RJDC31)	□	FC1	2.160	.000

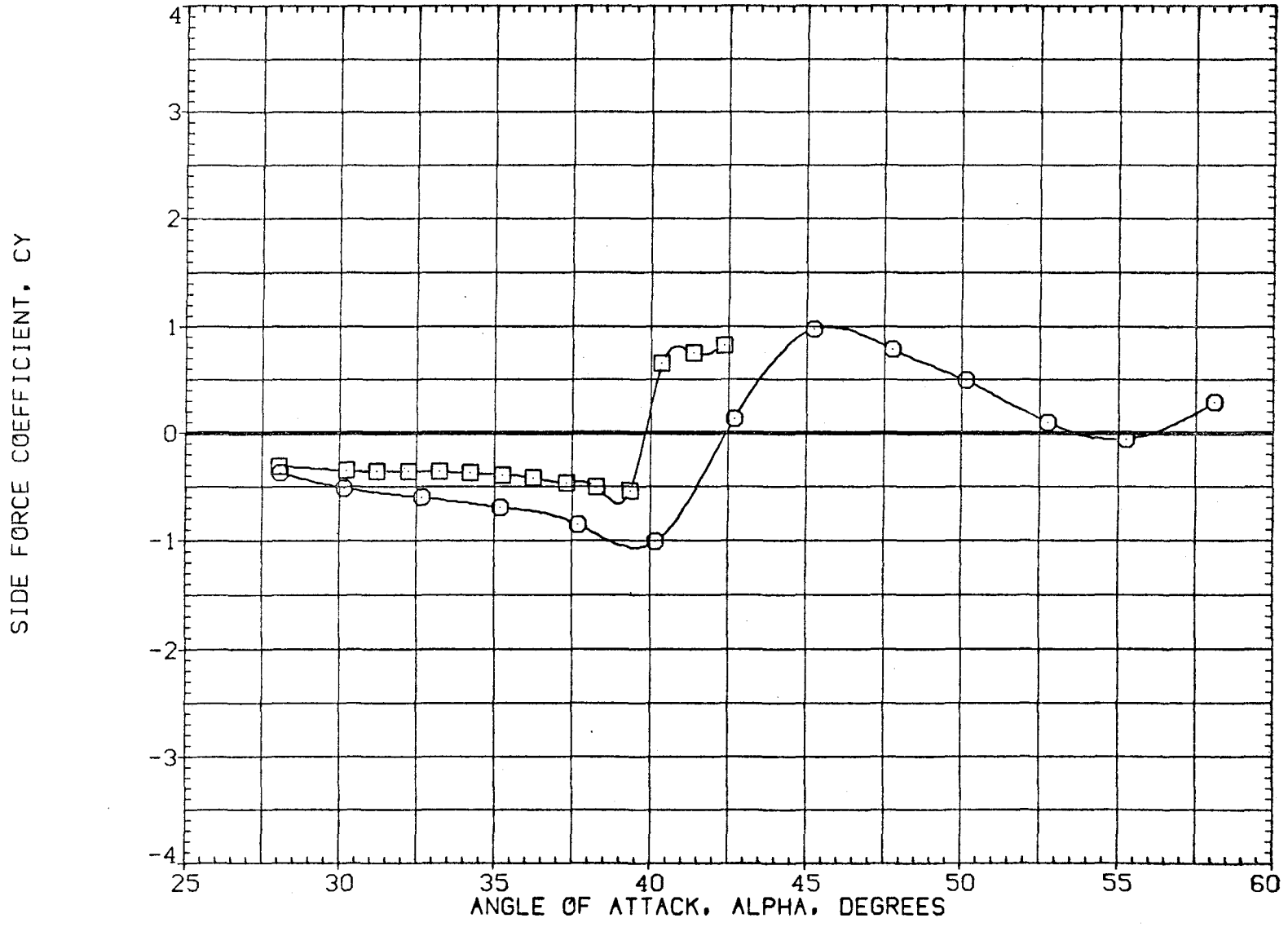

FIG.13 20 DEG. CONE, EFFECT OF REYNOLDS NUMBER

(A)MACH = .60

DATA SET	SYMBOL	CONFIGURATION DESCRIPTION	R	BETA
(RJDC30)	○	FC1	.930	.000
(RJDC31)	□	FC1	2.160	.000

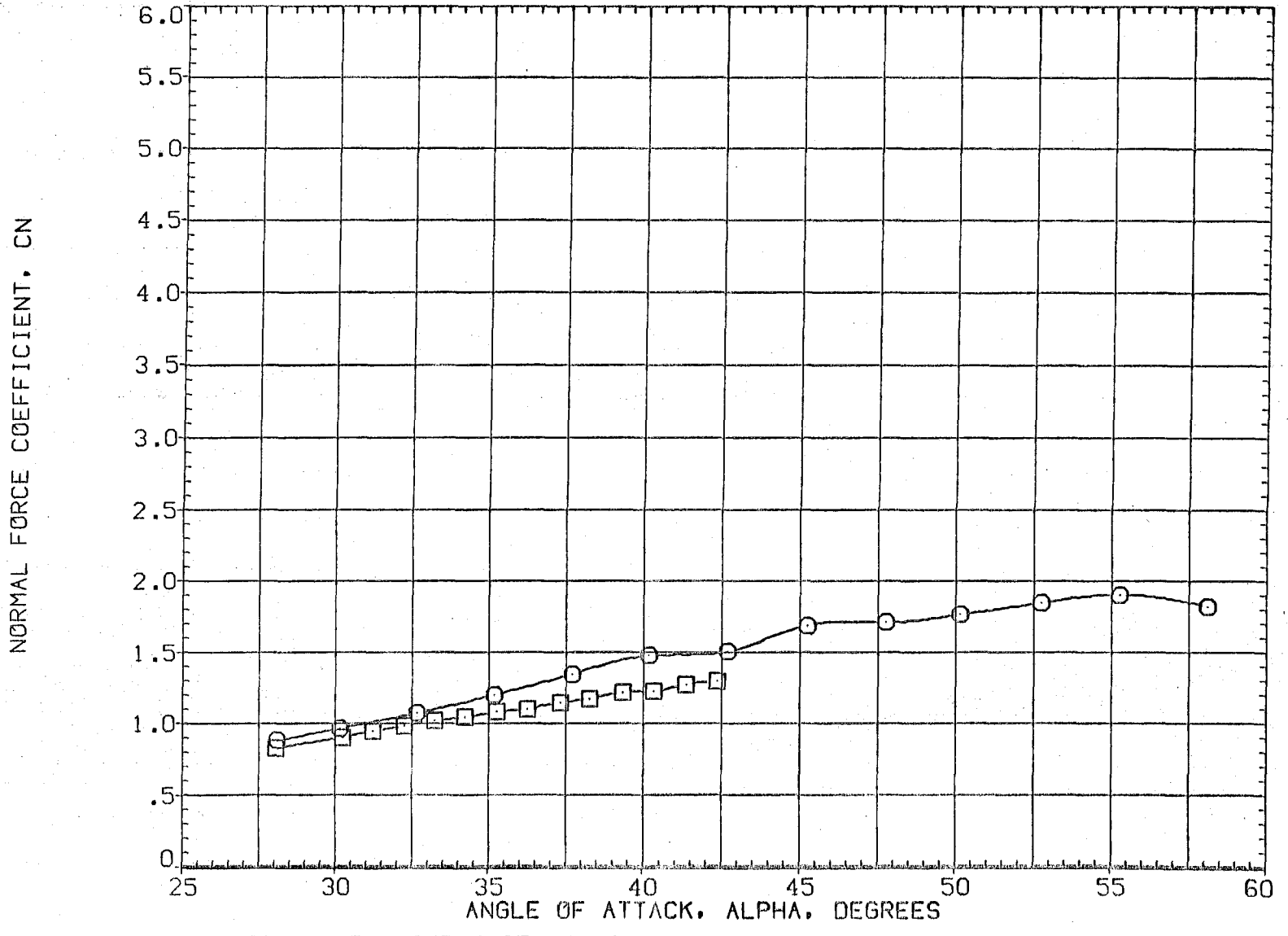

FIG.13 20 DEG. CONE, EFFECT OF REYNOLDS NUMBER

(A)MACH = .60

DATA SET	SYMBOL	CONFIGURATION DESCRIPTION	R	BETA
(RJDC30)	○	FC1	.930	.000
(RJDC31)	□	FC1	2.160	.000

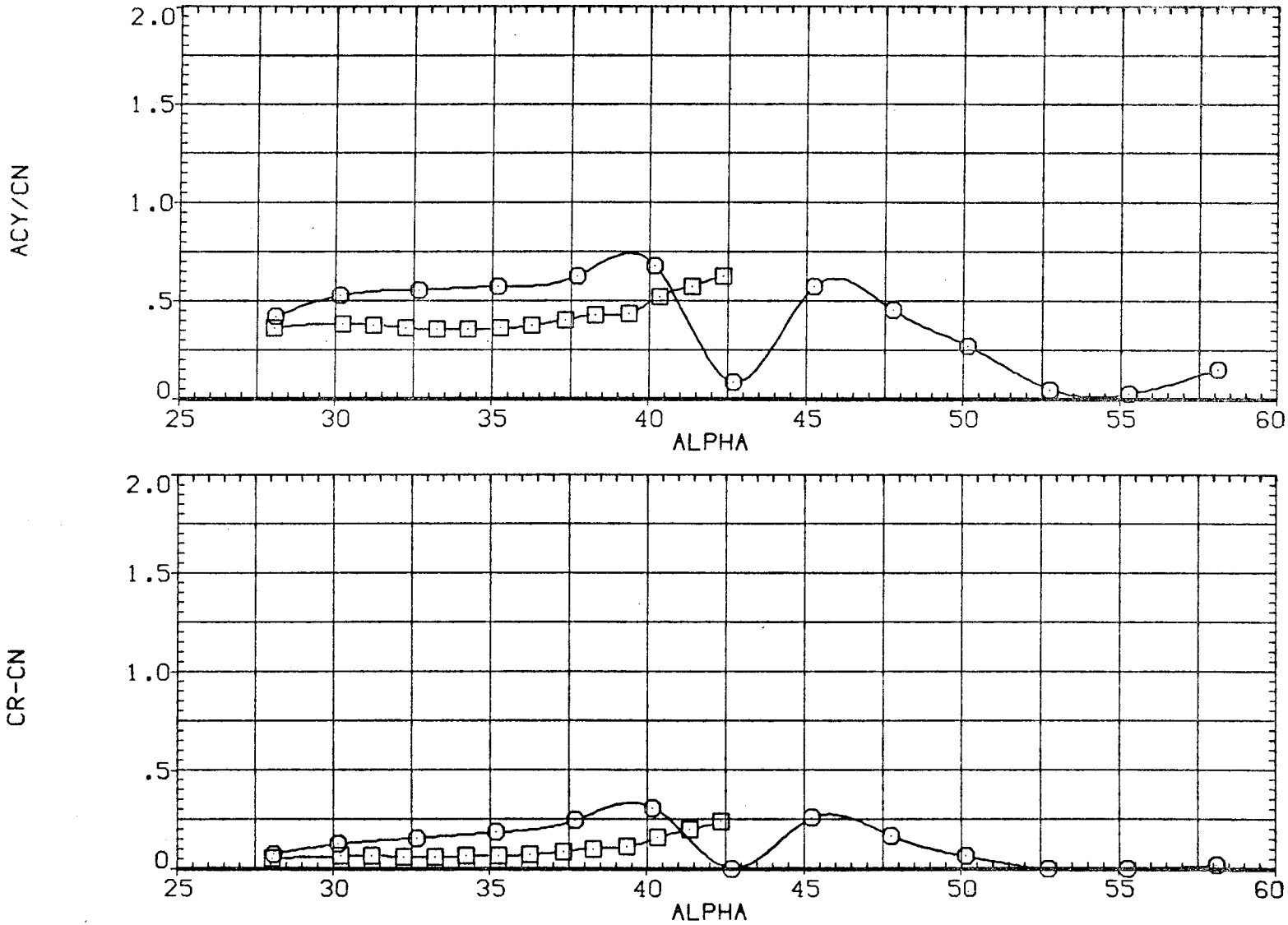

FIG.13 20 DEG. CONE, EFFECT OF REYNOLDS NUMBER

(A)MACH = .60

DATA SET	SYMBOL	CONFIGURATION DESCRIPTION	R	BETA
(RJDC30)	○	FC1	.930	.000
(RJDC31)	□	FC1	2.160	.000

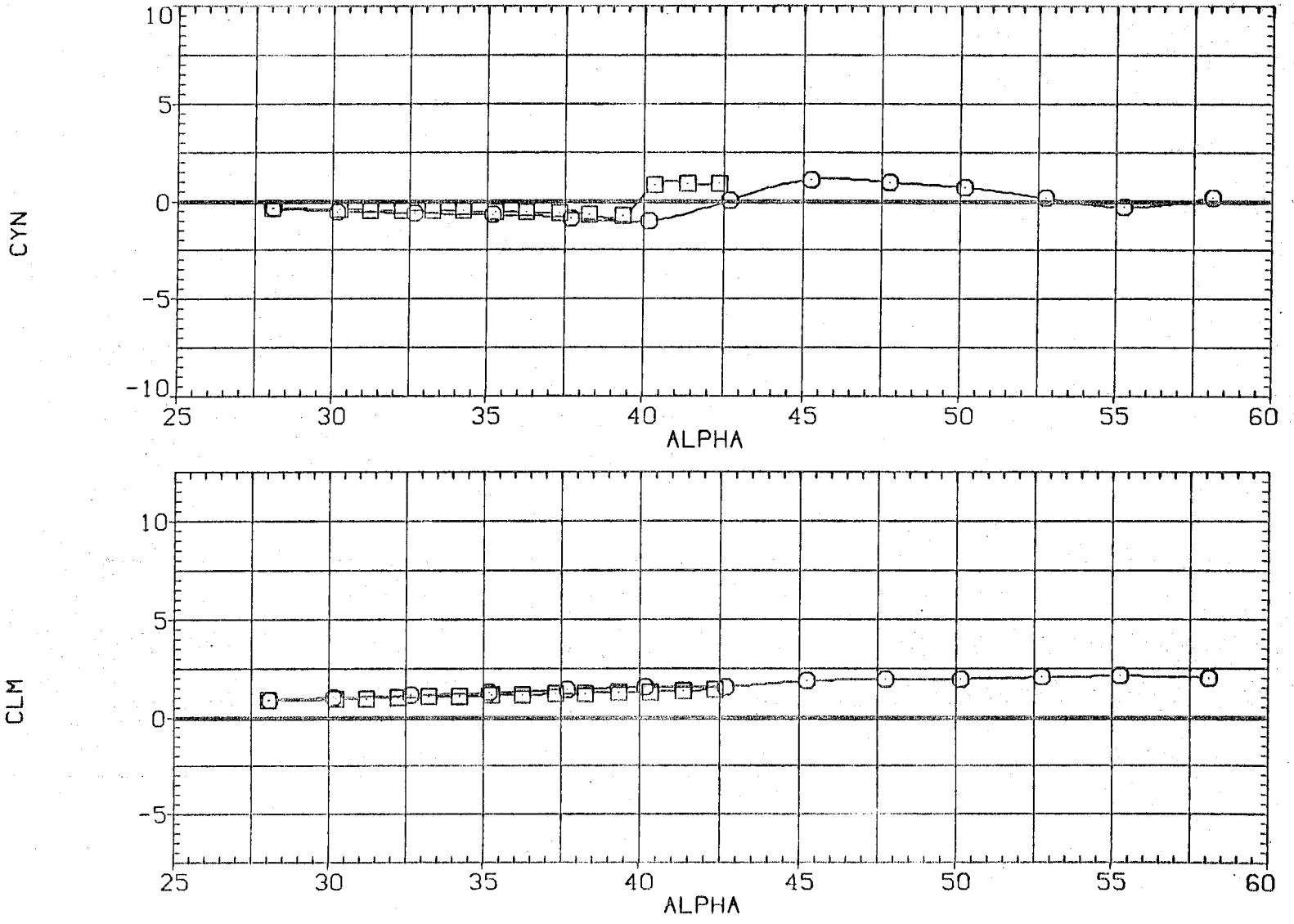

FIG.13 20 DEG. CONE, EFFECT OF REYNOLDS NUMBER

(A)MACH = .60

DATA SET SYMBOL	CONFIGURATION DESCRIPTION	R	BETA
(RJDC30) ○	FC1	.930	.000
(RJDC31) □	FC1	2.160	.000

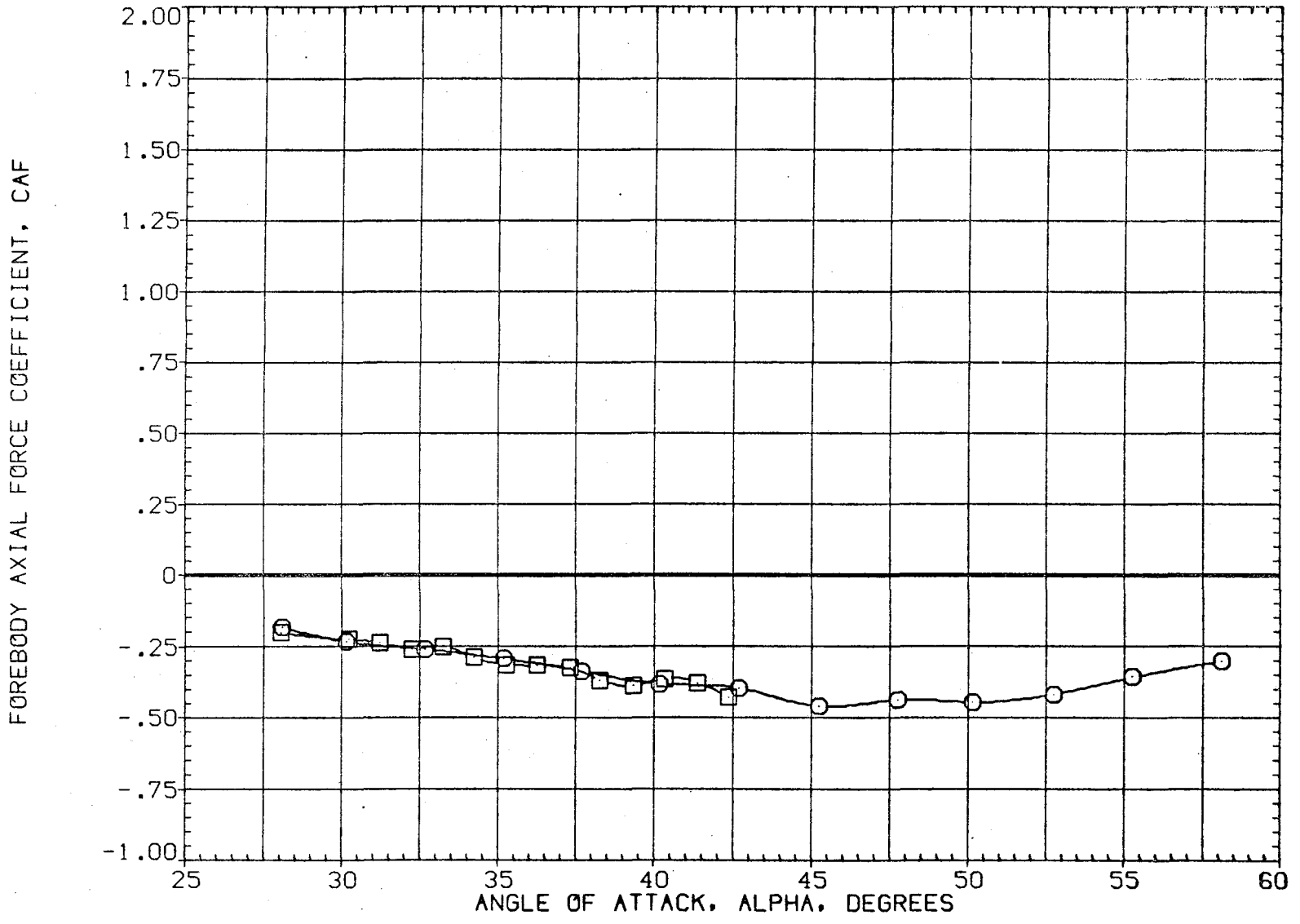

FIG.13 20 DEG. CONE, EFFECT OF REYNOLDS NUMBER

(A)MACH = .60

DATA SET	SYMBOL	CONFIGURATION DESCRIPTION	R	BETA
(AJDC30)	○	FC1	.930	.000
(AJDC31)	□	FC1	2.160	.000

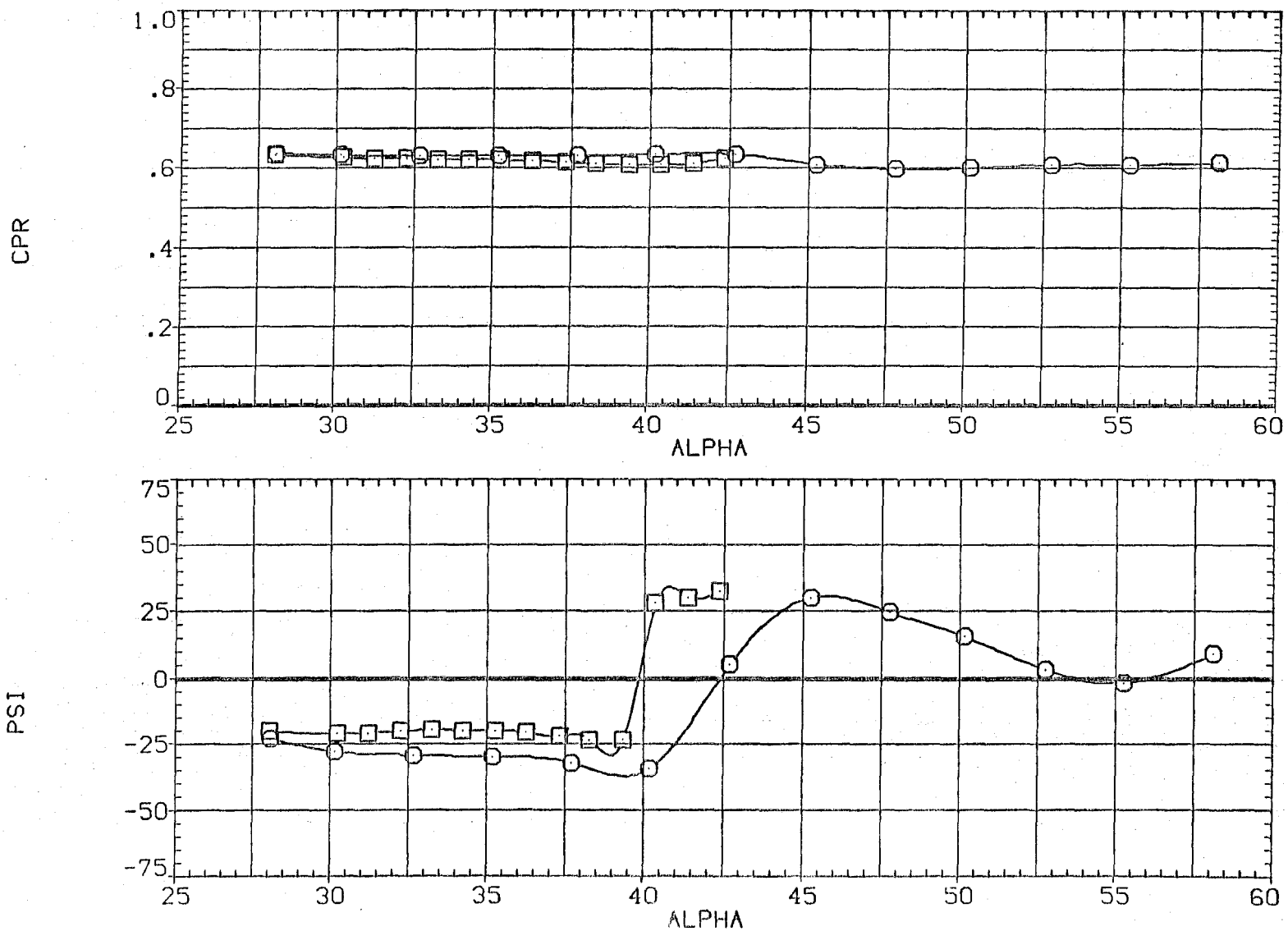

FIG.13 20 DEG. CONE, EFFECT OF REYNOLDS NUMBER

(A)MACH = .60

DATA SET	SYMBOL	CONFIGURATION DESCRIPTION	R	BETA
(AJDC30)	○	FC1	.930	.000
(AJDC31)	□	FC1	2.160	.000

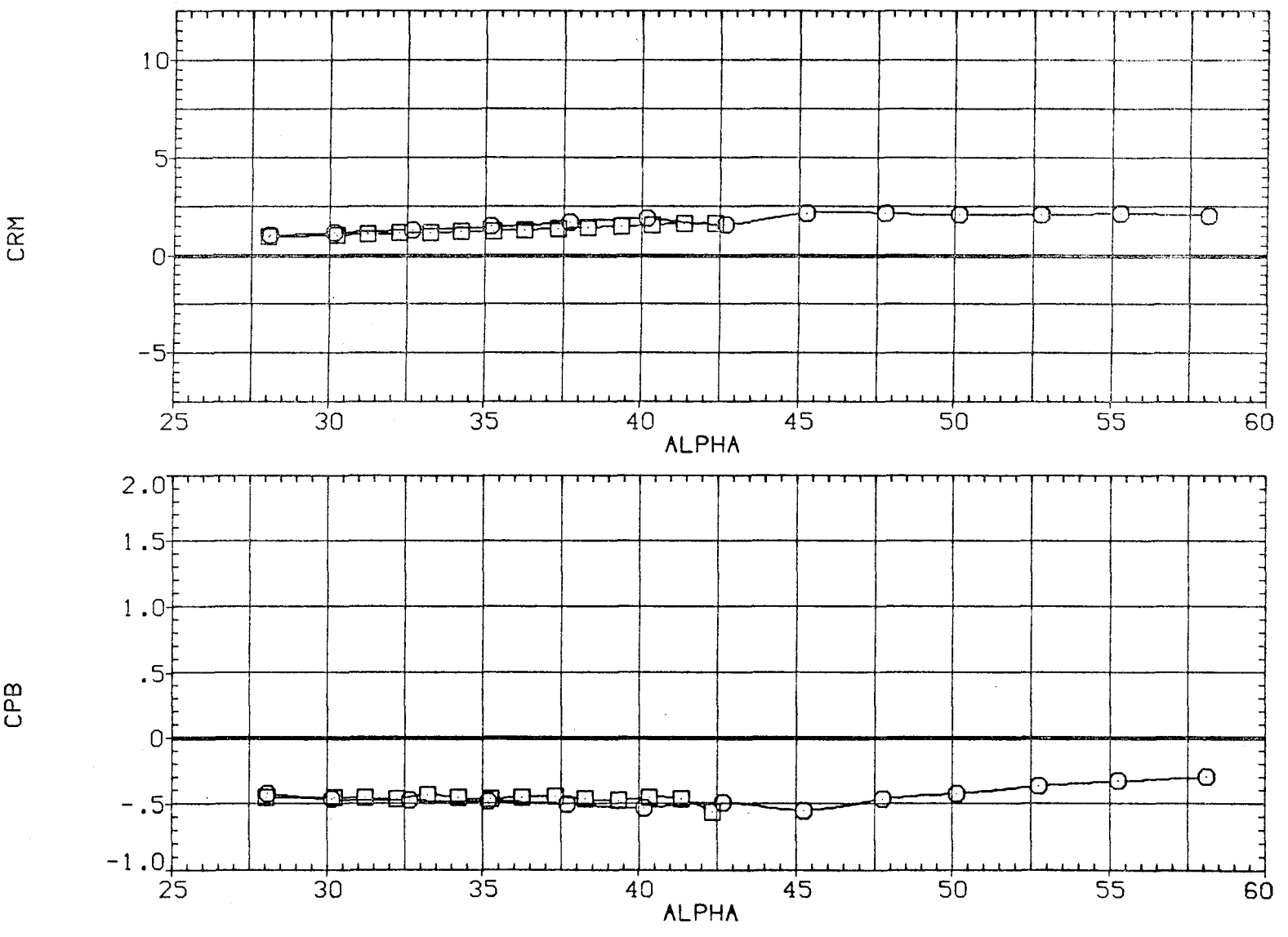

FIG.13 20 DEG. CONE, EFFECT OF REYNOLDS NUMBER

(A)MACH = .60

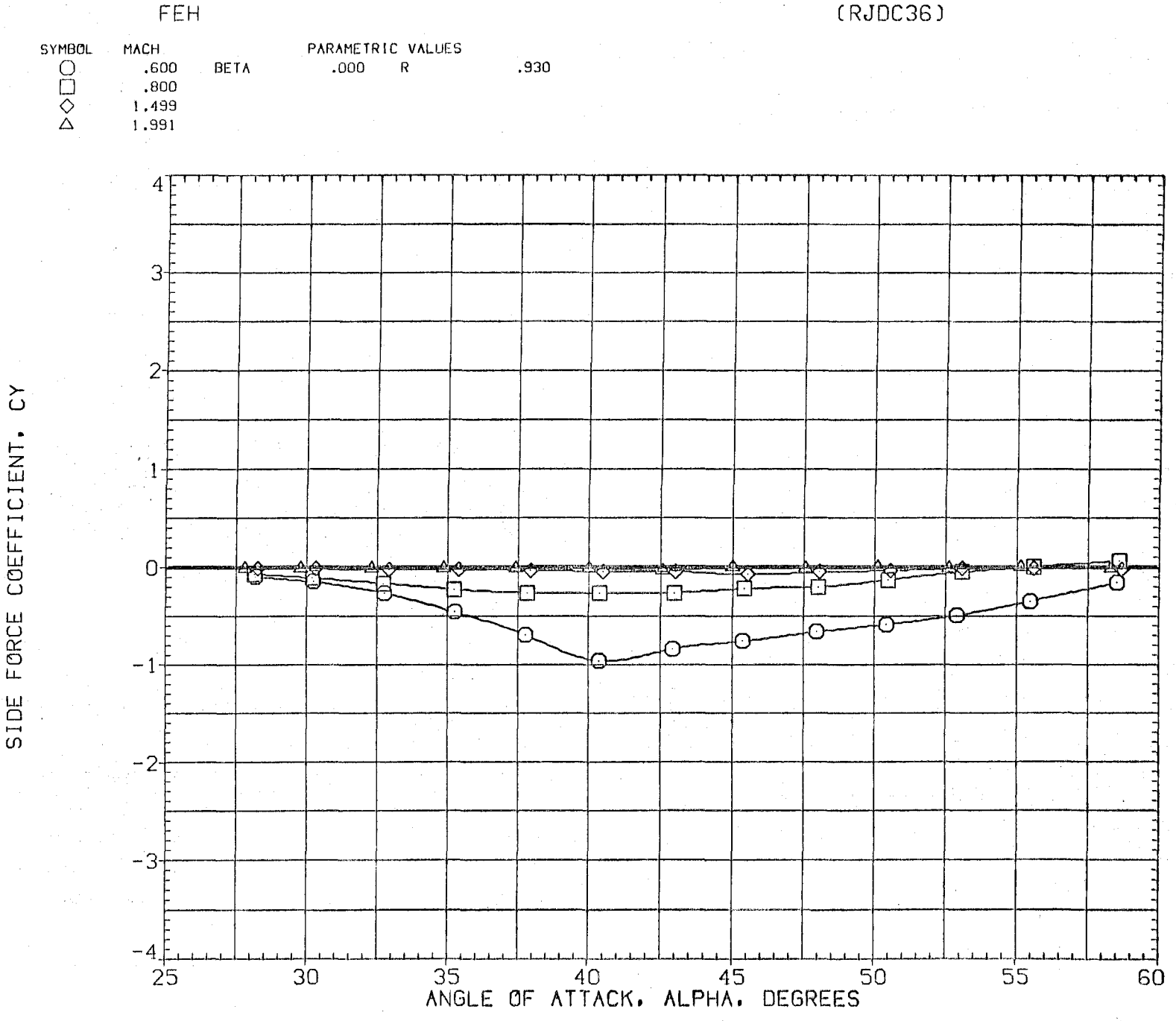

FIG.14 L/D=3.5 ELLIP. TAN. OGIVE, MAJOR AXIS HOR., EFFECT OF MACH NUMBER

SYMBOL	MACH		PARAMETRIC VALUES		
○	.600	BETA	.000	R	.930
□	.800				
◇	1.499				
△	1.991				

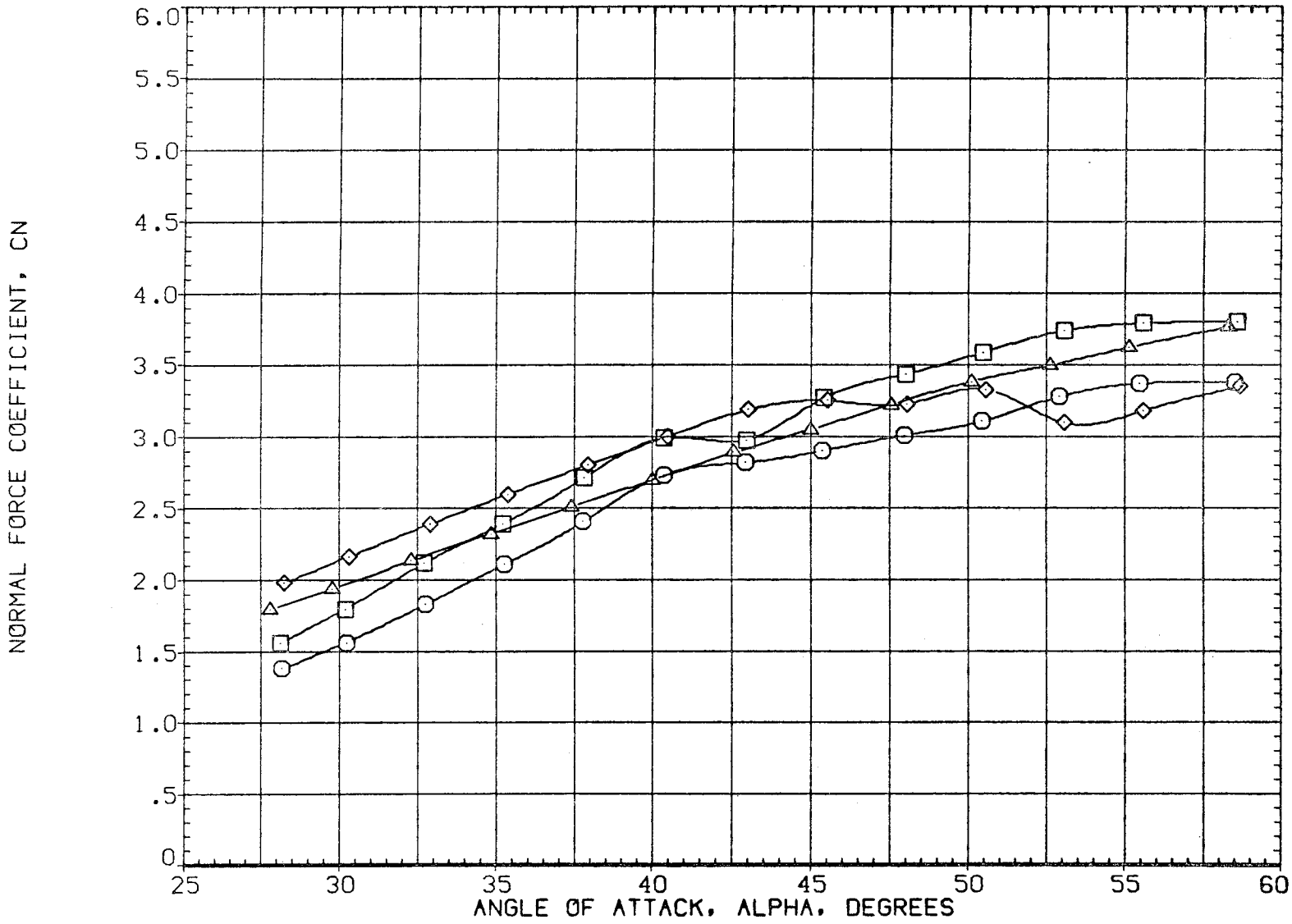

FIG.14 L/D=3.5 ELLIP. TAN. OGIVE, MAJOR AXIS HOR., EFFECT OF MACH NUMBER

SYMBOL	MACH		PARAMETRIC VALUES		
○	.600	BETA	.000	R	.930
□	.800				
◇	1.499				
△	1.991				

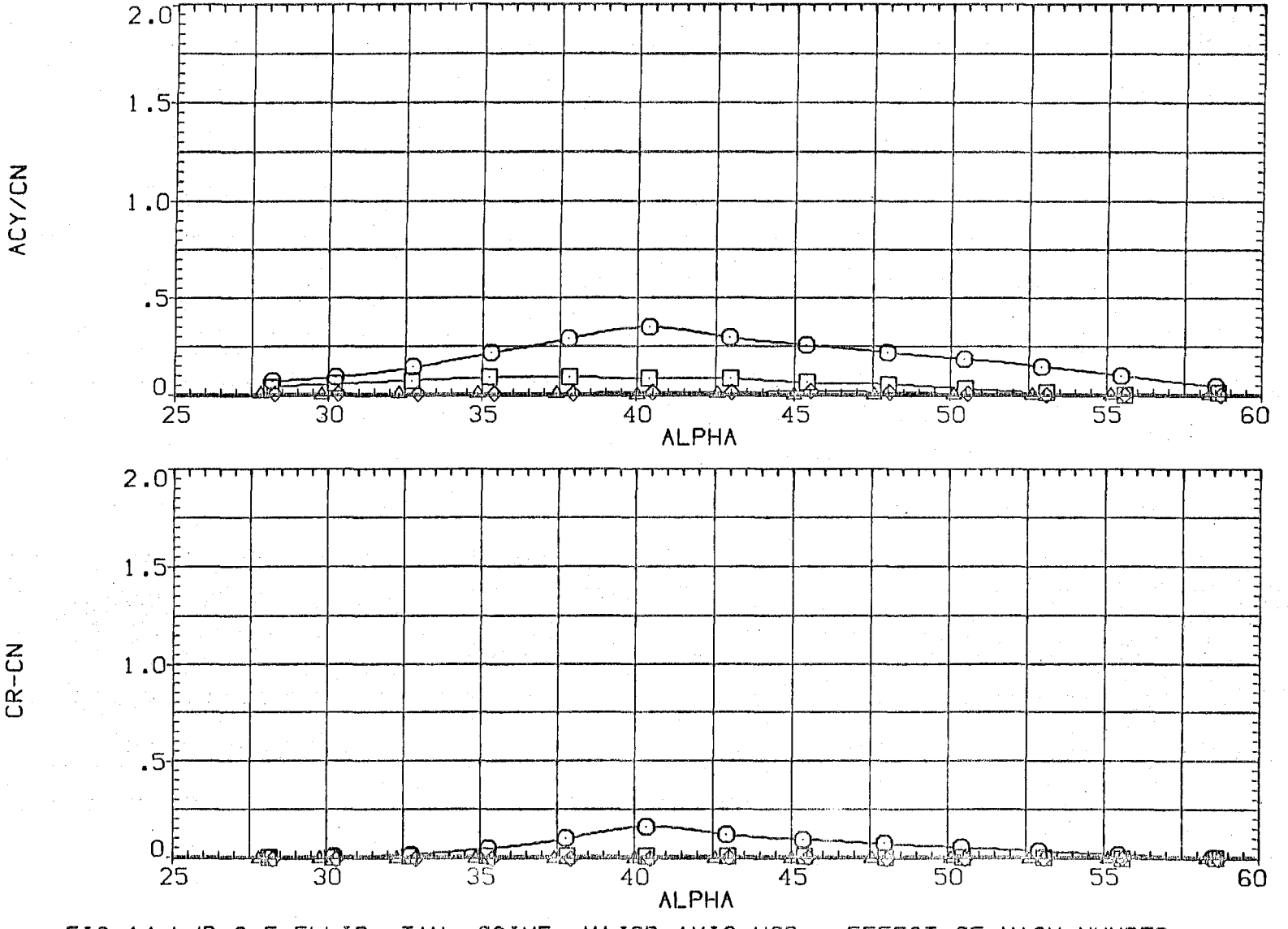

FIG.14 L/D=3.5 ELLIP. TAN. OGIVE, MAJOR AXIS HOR., EFFECT OF MACH NUMBER

SYMBOL	MACH		PARAMETRIC VALUES		
○	.600	BETA	.000	R	.930
□	.800				
◇	1.499				
△	1.991				

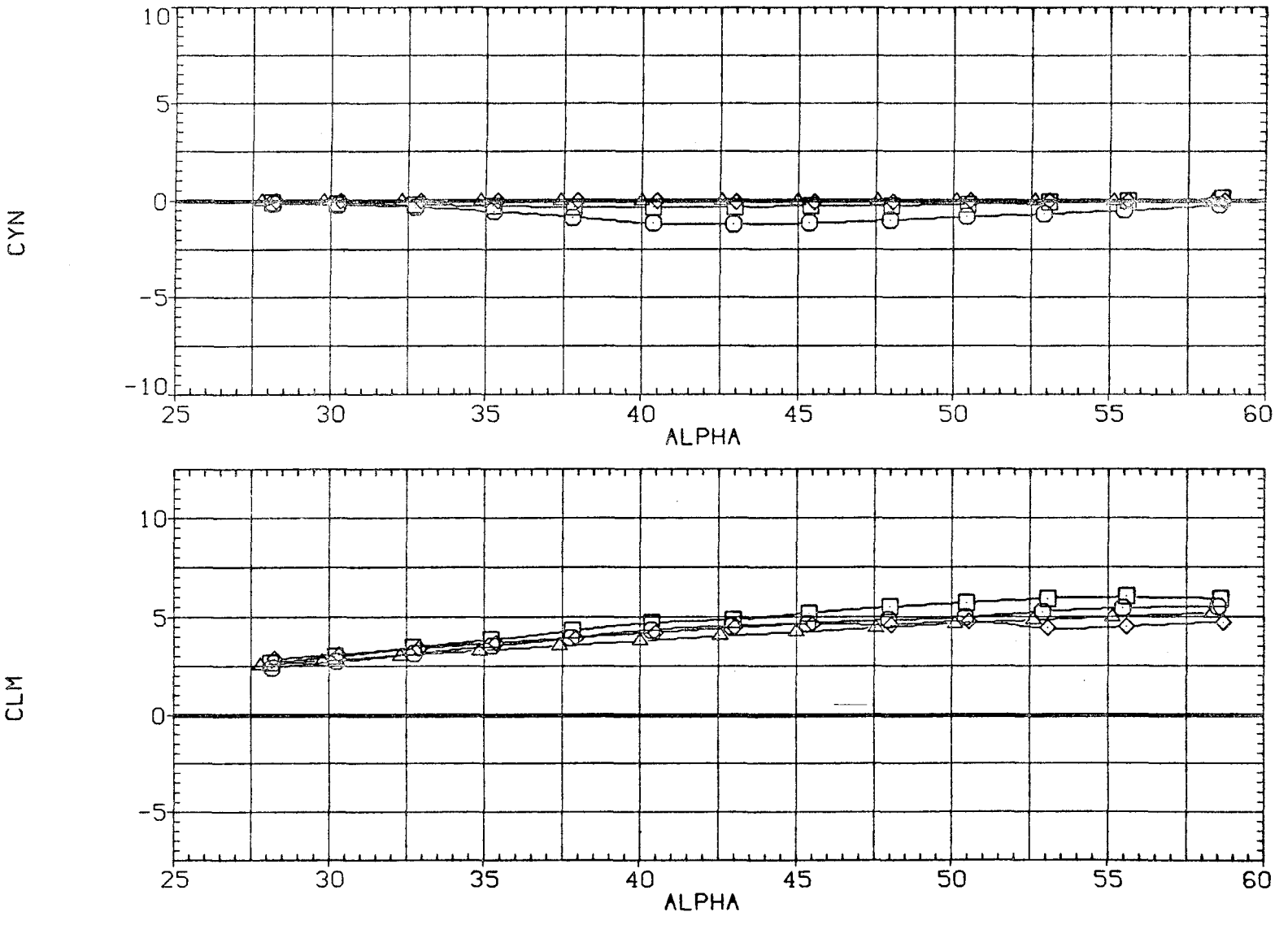

FIG.14 L/D=3.5 ELLIP. TAN. OGIVE, MAJOR AXIS HOR., EFFECT OF MACH NUMBER

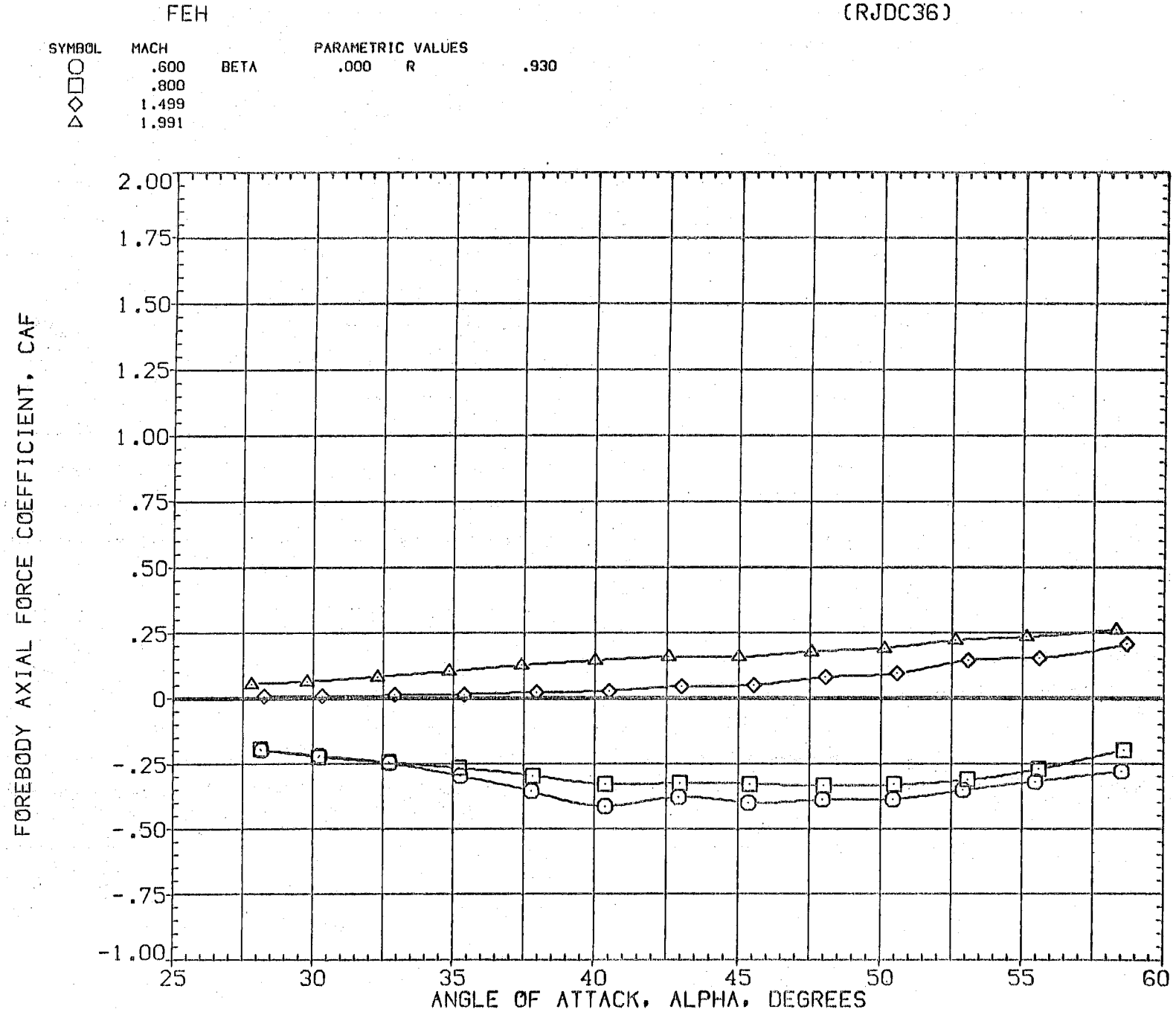

FIG.14 L/D=3.5 ELLIP. TAN. OGIVE, MAJOR AXIS HOR., EFFECT OF MACH NUMBER

SYMBOL	MACH		PARAMETRIC VALUES		
○	.600	BETA	.000	R	.930
□	.800				
◇	1.499				
△	1.991				

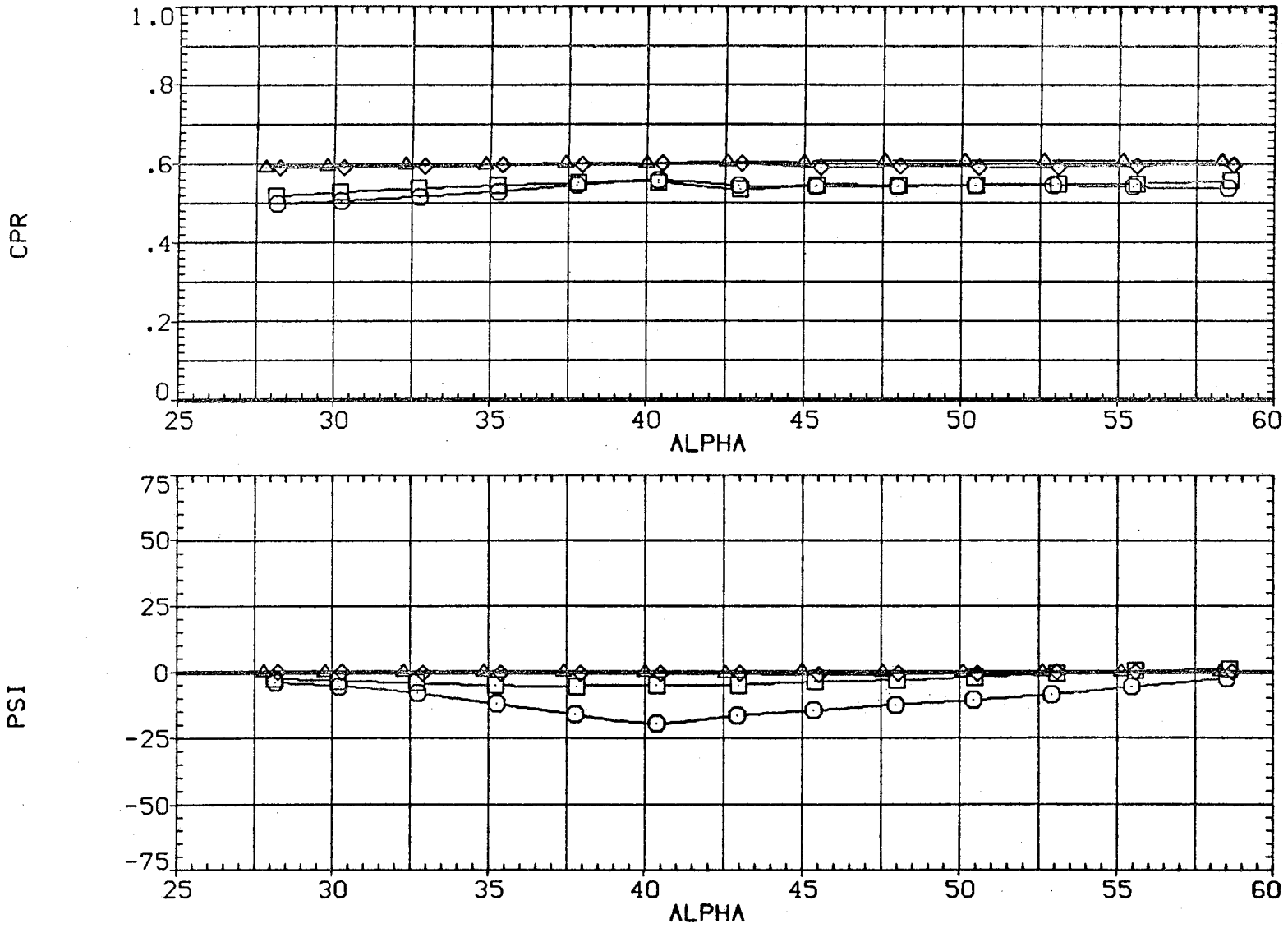

FIG.14 L/D=3.5 ELLIP. TAN. OGIVE, MAJOR AXIS HOR., EFFECT OF MACH NUMBER

SYMBOL	MACH		PARAMETRIC VALUES		
○	.600	BETA	.000	R	.930
□	.800				
◇	1.499				
△	1.991				

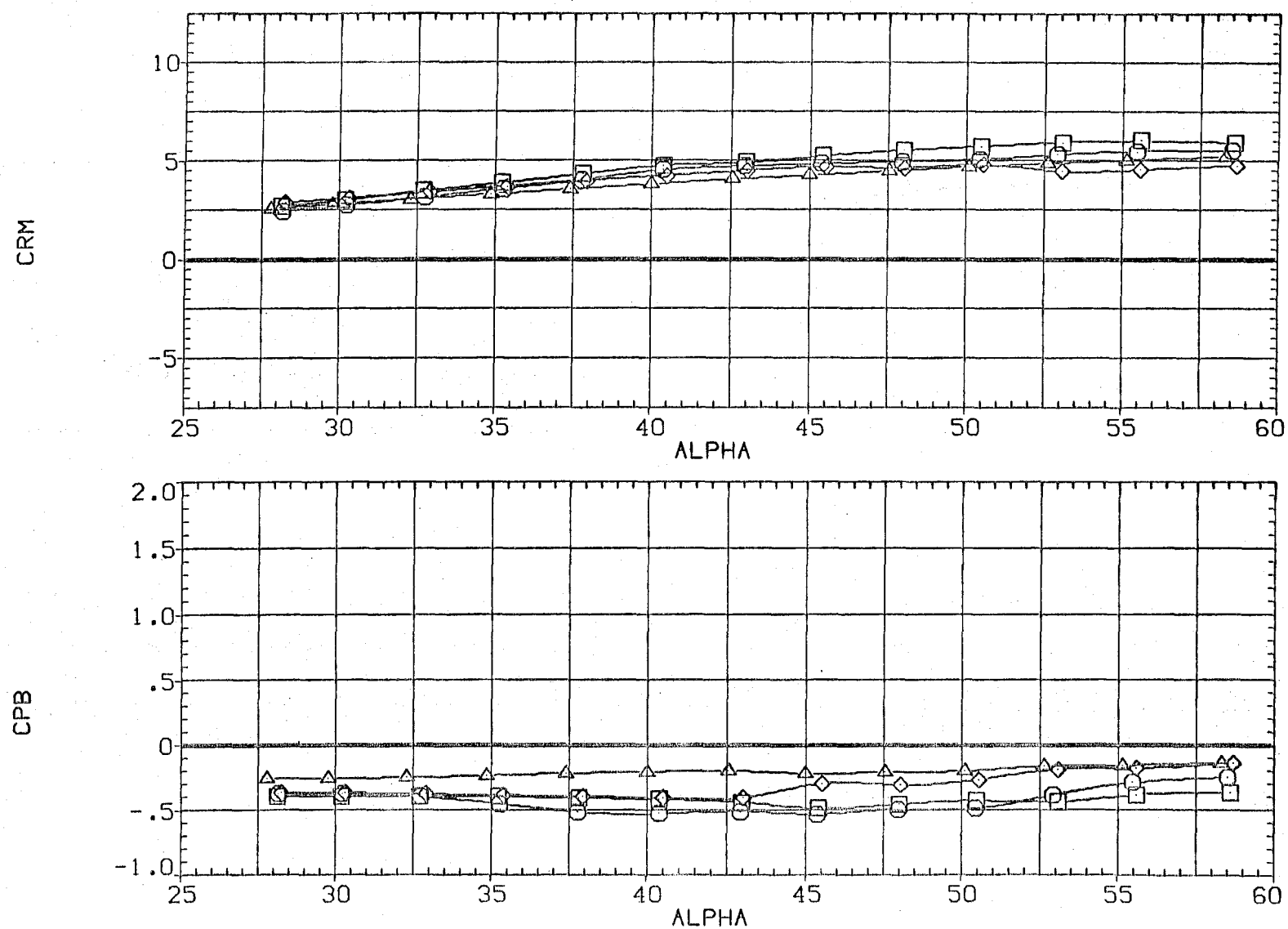

FIG.14 L/D=3.5 ELLIP. TAN. OGIVE, MAJOR AXIS HOR., EFFECT OF MACH NUMBER

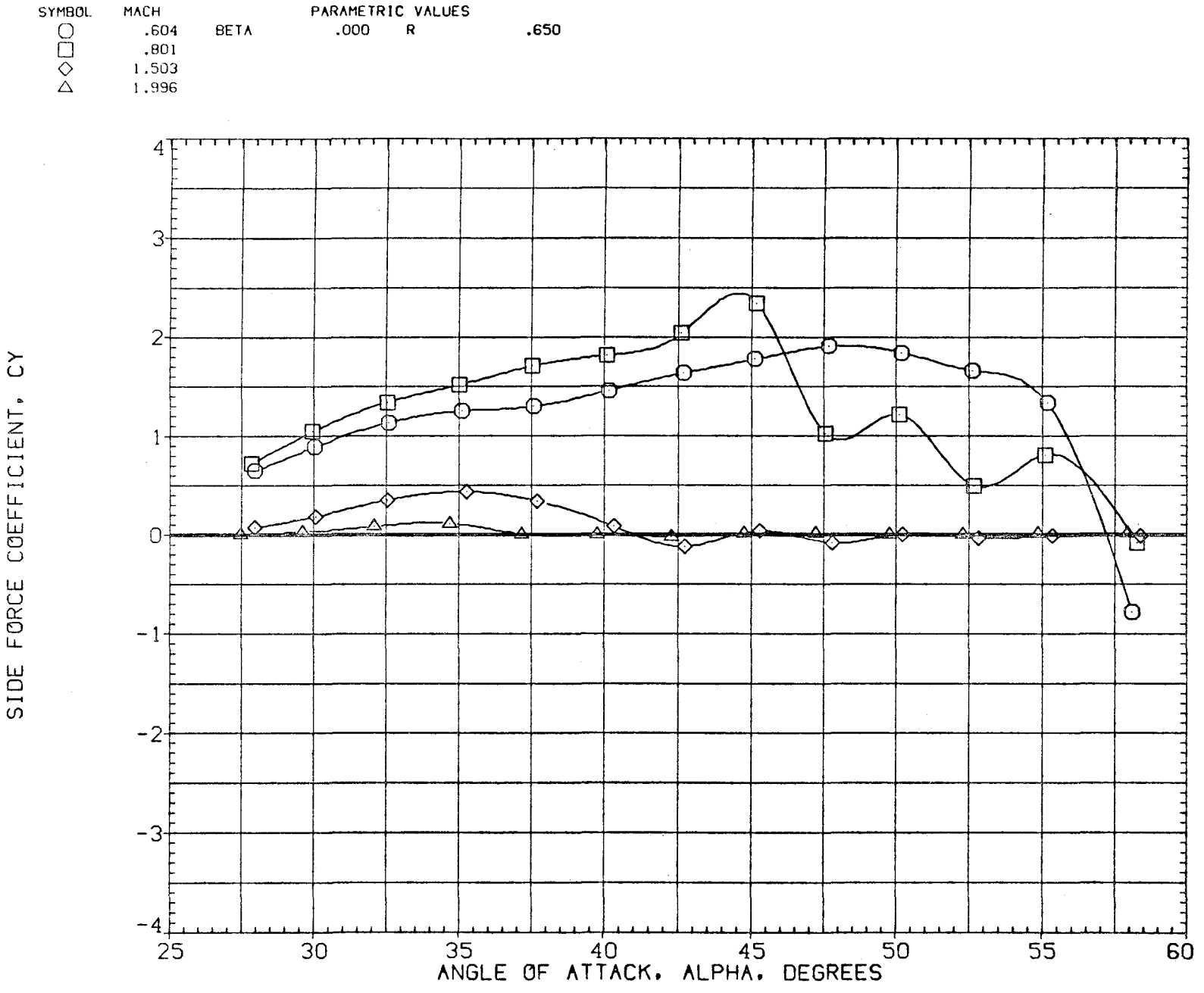

FIG.15 L/D=5 ELLIP. TAN. OGIVE, MAJOR AXIS VERT., EFFECT OF MACH NUMBER

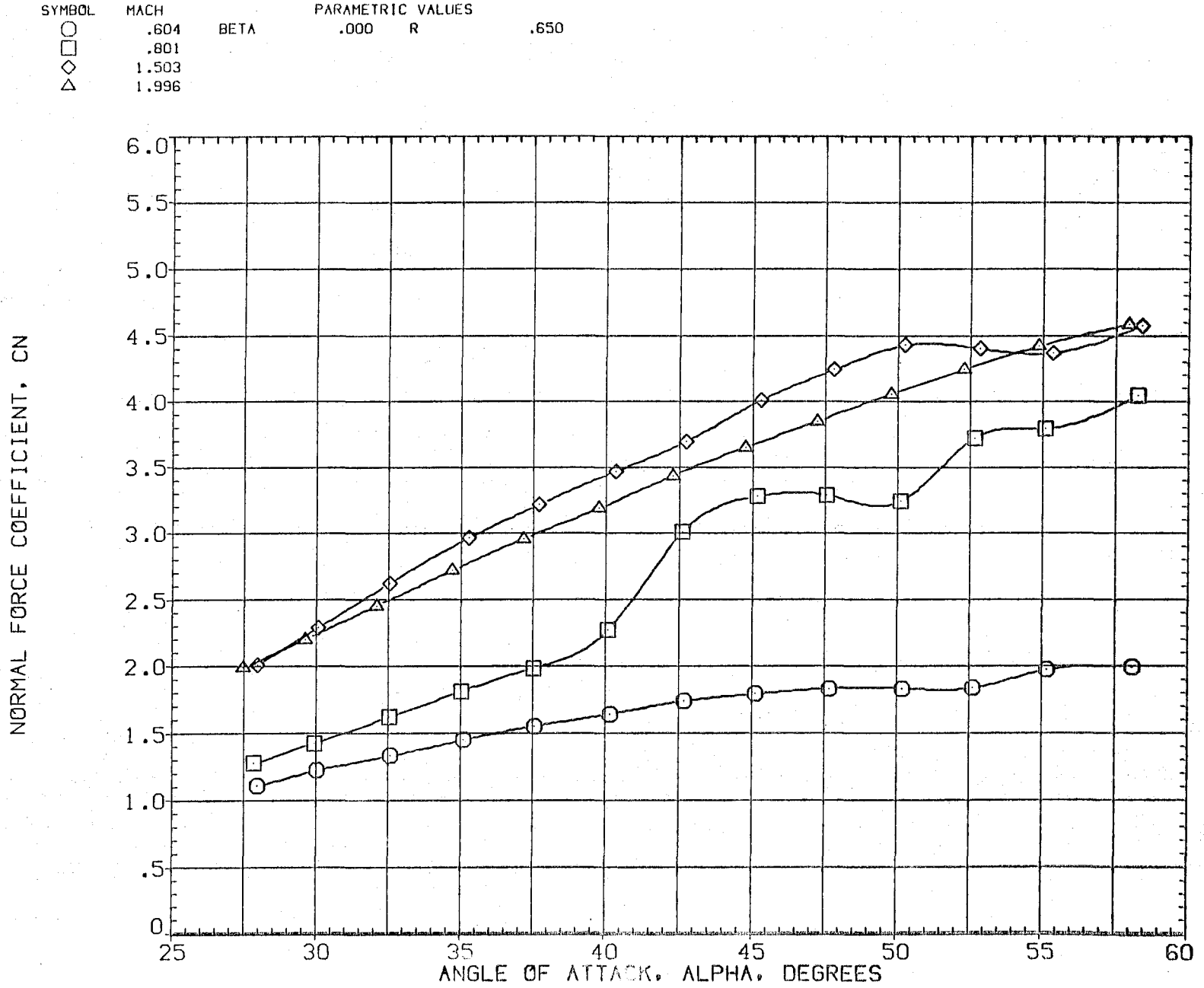

FIG.15 L/D=5 ELLIP. TAN. OGIVE, MAJOR AXIS VERT., EFFECT OF MACH NUMBER

SYMBOL	MACH		PARAMETRIC VALUES		
○	.604	BETA	.000	R	.650
□	.801				
◇	1.503				
△	1.996				

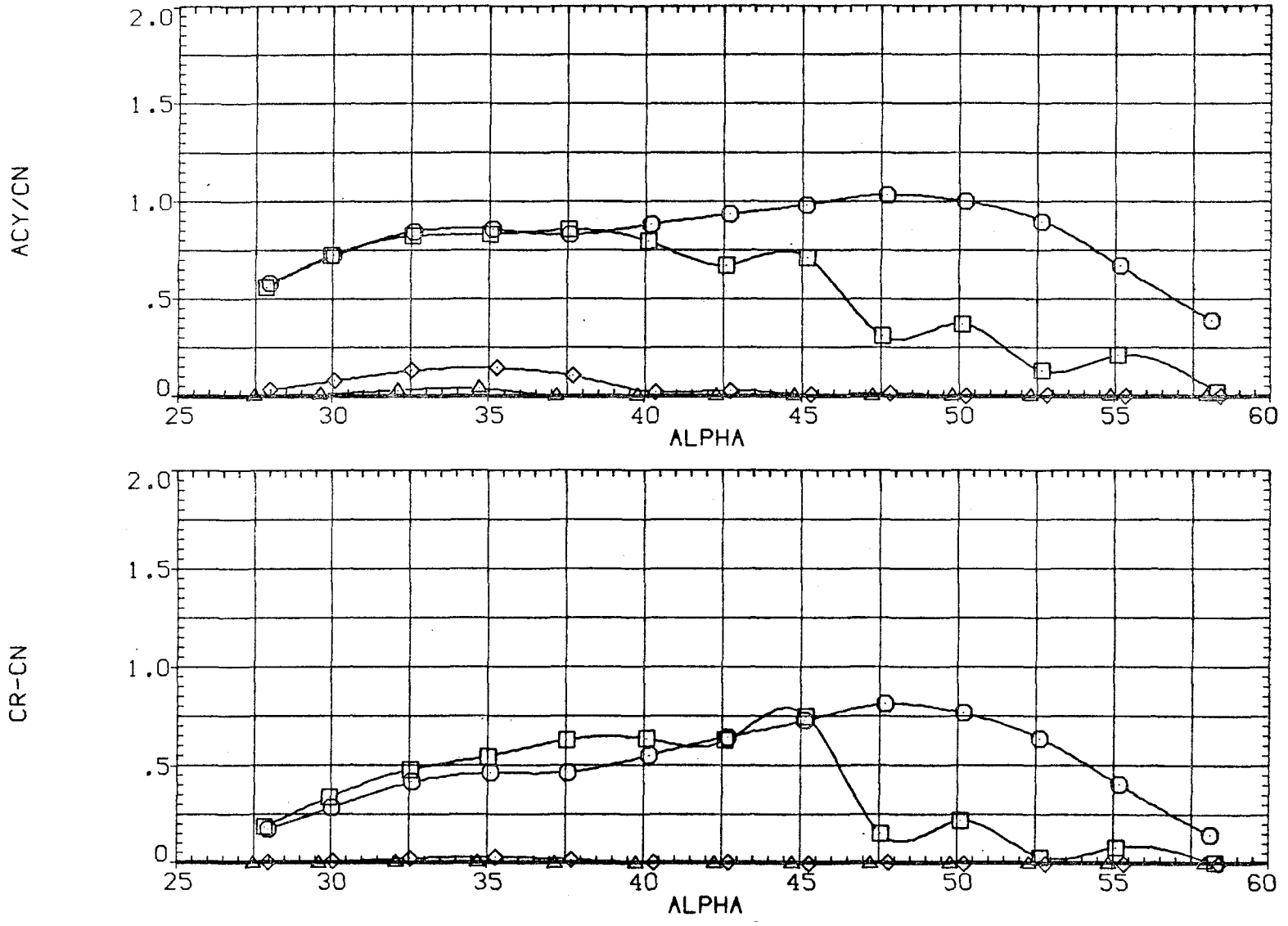

FIG.15 L/D=5 ELLIP. TAN. OGIVE, MAJOR AXIS VERT., EFFECT OF MACH NUMBER

SYMBOL	MACH		PARAMETRIC VALUES		
○	.604	BETA	.000	R	.650
□	.801				
◇	1.503				
△	1.996				

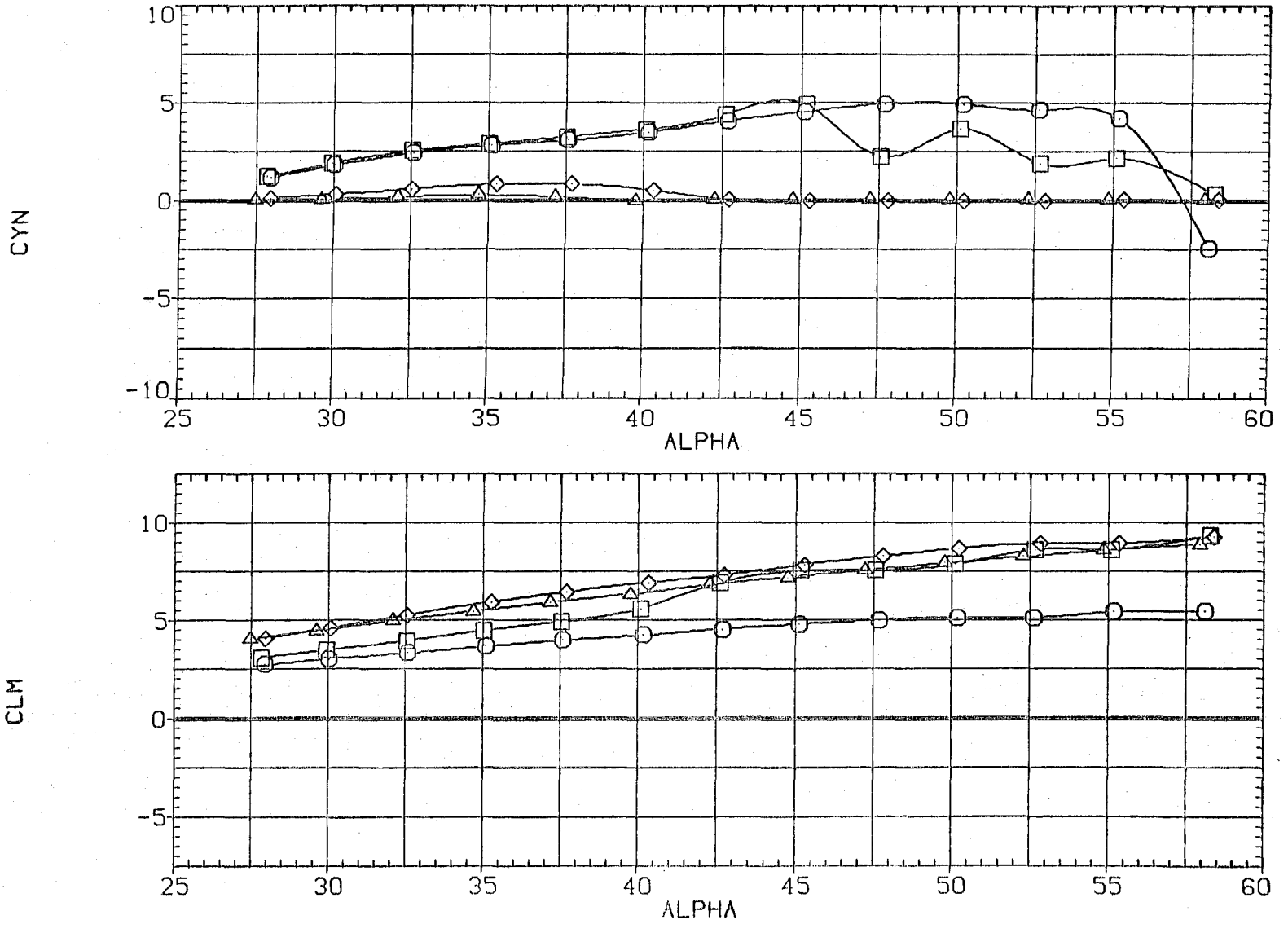

FIG.15 L/D=5 ELLIP. TAN. OGIVE, MAJOR AXIS VERT., EFFECT OF MACH NUMBER

FEV (RJDC38)

SYMBOL	MACH		PARAMETRIC VALUES		
○	.604	BETA	.000	R	.650
□	.801				
◇	1.503				
△	1.996				

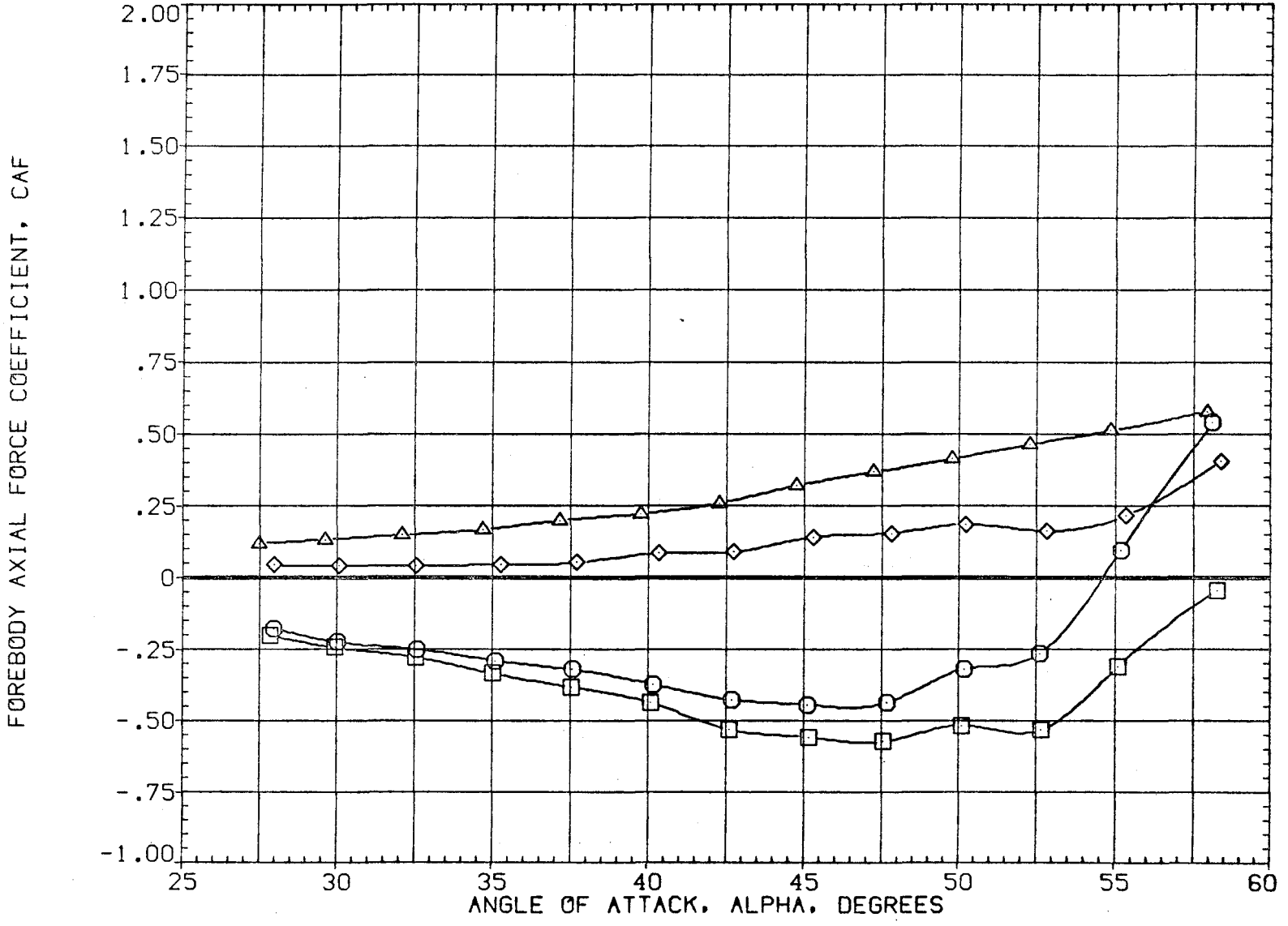

FIG.15 L/D=5 ELLIP. TAN. OGIVE, MAJOR AXIS VERT., EFFECT OF MACH NUMBER

FEV (AJDC38)

SYMBOL	MACH		PARAMETRIC VALUES		
○	.604	BETA	.000	R	.650
□	.801				
◇	1.503				
△	1.996				

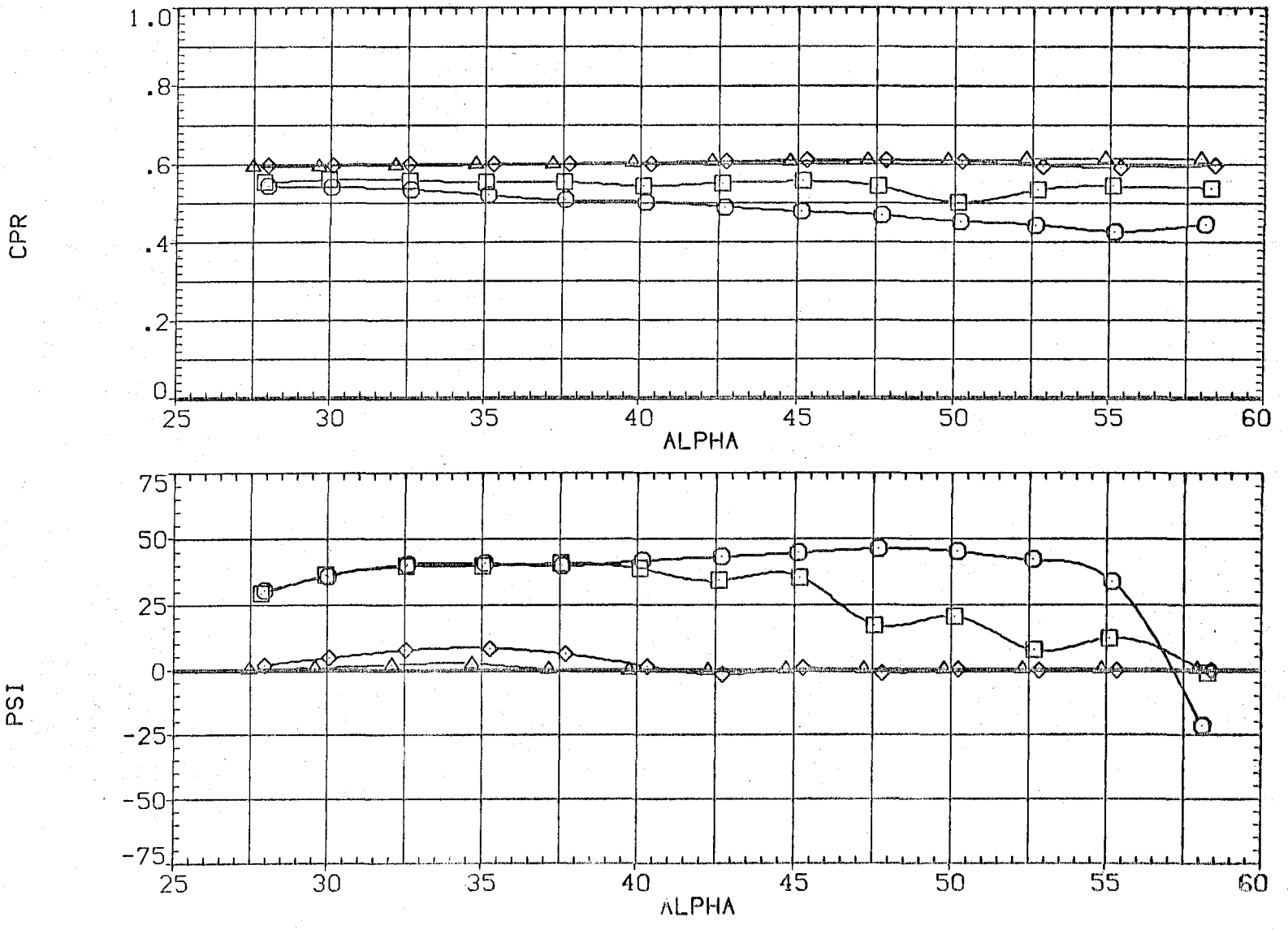

FIG.15 L/D=5 ELLIP. TAN. OGIVE, MAJOR AXIS VERT., EFFECT OF MACH NUMBER

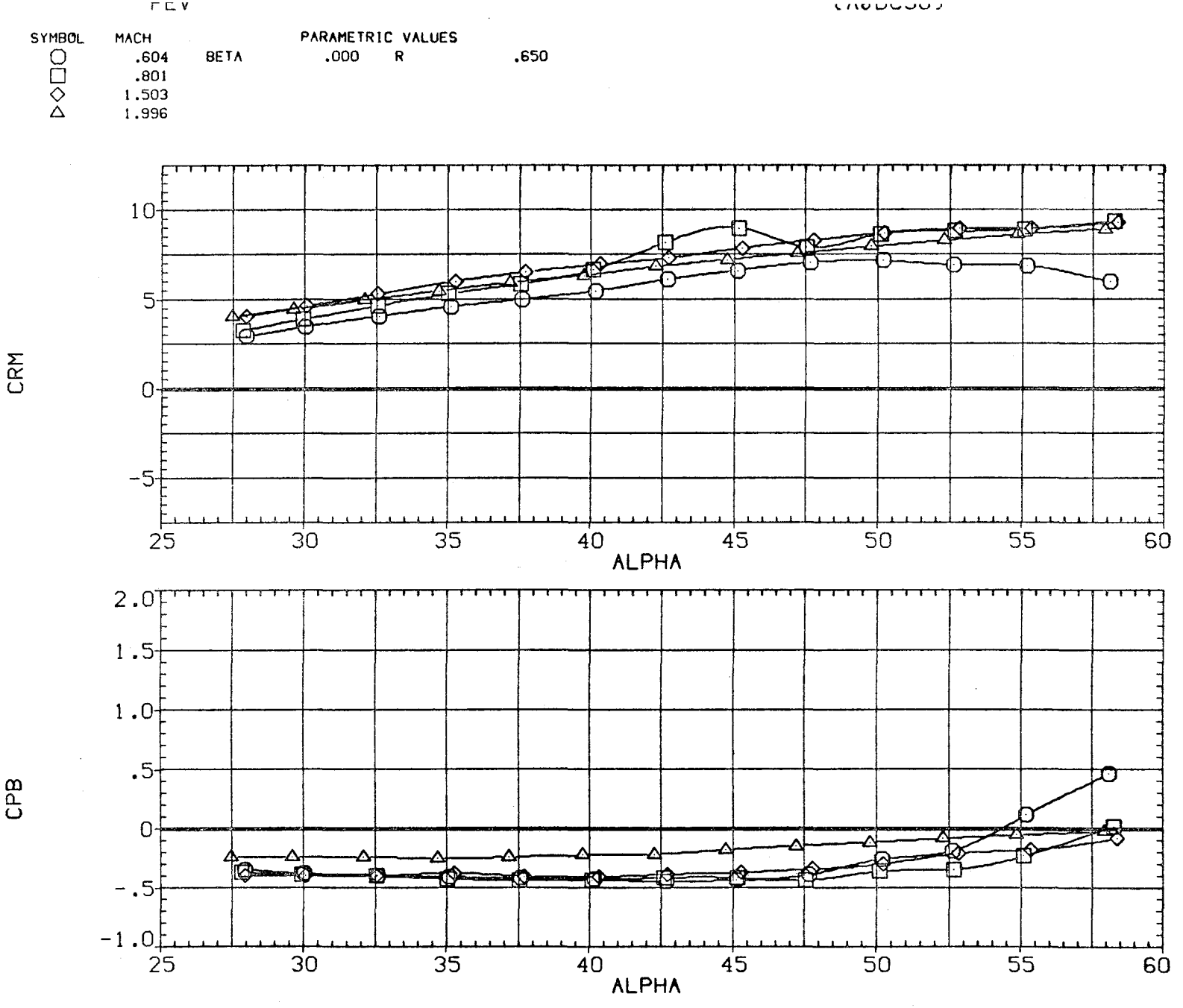

FIG.15 L/D=5 ELLIP. TAN. OGIVE, MAJOR AXIS VERT., EFFECT OF MACH NUMBER